Process Synthesis for Antibiotic Recovery by Microfiltration from *Saccharopolyspora erythraea* Fermentations

A thesis submitted to the University of London

For the degree of

DOCTOR OF PHILOSOPHY

By

Jim Davies

The Advanced Centre for Biochemical Engineering

Department of Biochemical Engineering

University College London

Torrington Place

London

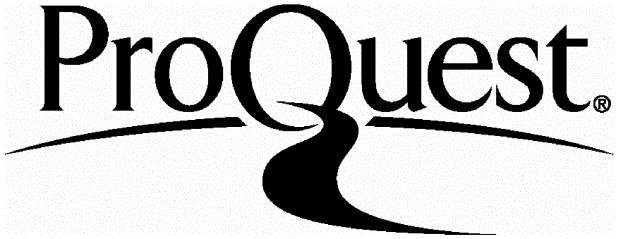

Abstract

The causes of the interactions between fermentation and microfiltration were first examined experimentally by investigating erythromycin production using two different media. Soluble complex media (SCM) broths reached maximum erythromycin concentrations more rapidly (64.2 ± 0.3 h) than the less expensive and therefore industrially preferred oil based media (OBM) broths (176 ± 15 h) but also attained lower titres (241 ± 55 $g.L^{-1}$ compared to 617 ± 104 $g.L^{-1}$). The OBM broths showed oxygen limitation due to the high apparent viscosity. Both broths were found to be shear thinning and exhibited different time dependant rheological profiles which could impact on the performance of the subsequent microfiltration operation.

The microfiltration performance of the two broths was subsequently examined using a flat sheet membrane system (area = 60 – 120 cm^2). This small-scale unit allowed the determination of flux and transmission profiles as a function of fermentation time and for membrane operation over a range of transmembrane pressures and crossflow velocities. The OBM broths were quicker to blind the membrane, achieved lower values of steady state permeate flux, which decreased over fermentation time as apparent viscosity increased. SCM broths showed no time dependant variation in steady state permeate flux. Transmission of product was higher in SCM (96.4 ± 1.6 %) than OBM broths (89.6 ± 1.4 %). This was attributed to the high solids content of the OBM broth in the form of the undissolved soya flour. The mass transfer of erythromycin across the membrane was similar in both cases (SCM: 1.47 ± 0.28 x 10^{-6} $kg.m^{-2}.s^{-1}$, OBM: 1.38 ± 0.20 x

10^{-6} $kg.m^{-2}.s^{-1}$) due to the differences between erythromycin titre and permeate flux. For the SCM broths image analysis was also used to determine if there was a relationship between bacterial morphology and microfiltration performance. No such relationship could be adequately determined. In OBM broths image analysis was used to predict the biomass concentration.

Modelling of the process using on- and off-line measurements, combined with scale-down methodologies, allows unit operations to be rapidly assessed and optimised, thus reducing product lead times through the development process. The performance of the microfiltration step was successfully predicted using a simple gel polarisation model which was reliable within a fermentation ± 9.5 % and a model modified to take account of operation at pressure below cTMP ± 6.2%. This allowed prediction of steady state permeate flux at the harvest time and the critical transmembrane pressure.

Acknowledgements

It's a difficult task to thank all the people that have helped me through this, and give them the recognition that they deserve. I would firstly like to thank Ruth for putting up with me especially during the write-up and my parents and siblings for all their support.

Gary Lye, for the tremendous effort that he has put into the project and for helping to turn a mountain into a mole-hill. Frank Baganz for all his input and Andy Ison for starting me off.

I would also like to thank the team on the MSc pilot plant week; Jon Postlethwaite, Rhys Morris, Andy Booth, Nick Murrell and all the students, next time we'll make sure nobody is allergic to erythromycin. All the technical support that was of such a high standard, immense help and a great laugh, from Clive Osborne, Billy Doyle, Ian Buchanan, Alison Clayton. Also Martin Town and the boys, and Martyn Vale and crew. Charles Christie at Millipore for all the information and help.

A special thank-you to Nick Murrell and Ronan O'Kennedy for all the advice, put downs and 'numbers'. The folk at GSK Beckenham for taking the 'edge off' over the writing up period.

To one, to all, SMB, you know who you are!

Table of Contents

List of Figures

List of Tables

Glossary

ν	kinematic viscosity ($m^2.s^{-1}$)
ω	angular velocity of centrifuge bowl ($rad.s^{-1}$) from Stoke's Law
ρ	density ($kg.m^{-3}$)
ε	energy dissipation rate per unit mass ($W.kg^{-1}$)
ϕ	erythromycin transmission (%)
γ	shear rate (s^{-1})
ι	shear stress (Pa)
μ	viscosity of the liquid ($kg.m^{-1}.s^{-1}$)
μ_a	apparent viscosity ($kg.m^{-1}.s^{-1}$)
ρ_f	liquid density ($kg.m^{-3}$) from Stoke's Law
ρ_p	particle density ($kg.m^{-3}$) from Stoke's Law
ACP	acyl carrier protein
AT	acyltransferase
b	is the channel height of the flow path through the crossflow filtration device (m)
BL	branch length (μm)
BSA	bovine serum albumin
CA	clump area (μm^2)
C_b	concentration of material in the feed stream (% weight per volume)
CER	carbon dioxide evolution rate ($mmol.L^{-1}.h^{-1}$)
CFF	crossflow filtration
cTMP	critical transmembrane pressure (Pa)
C_w	concentration of material at the membrane surface (% weight per volume)
D	diffusion coefficient ($m^2.s^{-1}$)
DCWT	dry cell weight ($g.L^{-1}$)
DEB	6-deoxyethronolide B
DEBS	6-deoxyethronolide B synthase
DH	dehydatase
D_i	impeller diameter (m)
DOT	dissolved oxygen tension (%)

d_p	diameter of particle (m) from Stoke's Law
E	modulus of elasticity of hyphae ($N.m^{-2}$)
EA	Erythromycin A
ED	electrodialysis
EFD	enhanced flow device
ER	enoyl reductase
eryA	gene(s) responsible for erythromycin A synthesis
f	initial permeate flux extrapolated from flux decay ($L.m^{-2}.h^{-1}$)
g	rate of flux decay during fouling (h^{-1})
GMO	genetically modified organism
HL	total hyphal length (μm)
HPLC	high pressure liquid chromatography
H_T	liquid height in vessel (m)
J	flux of the permeate ($L.m^{-2}.h^{-1}$)
K	consistency index (dimensionless)
k	mass transfer coefficient ($kg.m^{-3}.s^{-1}$)
k_b	Boltzman constant (dimensionless)
k_{eryth}	erythromycin partition coefficient, concentration in oil/concentration in aqueous solution (dimensionless)
k_La	Mass transfer coefficient (s^{-1})
K_p	proportionality constant (dimensionless)
KR	β-ketoacyl-ACP reductase
KS	ketoacyl-ACP-synthase
k_s	impeller shear rate constant (dimensionless)
L	length of microfiltration channel (m)
MA	mycelial area (μm^2)
MF	microfiltration
ML	main hyphal length (μm)
n	flow behaviour index (dimensionless)
N	number of hyphal units (dimensionless)
N_i	impeller speed (s^{-1})
NT	number of tips (dimensionless)
OA	total area (μm^2)

OB	minor axis (μm)
OBM	oil-based medium
OC	circularity (dimensionless)
OD	projected area (μm^2)
OL	major axis (μm)
ORF	
OUR	oxygen uptake rate ($mmol.L^{-1}.h^{-1}$)
p	probability significance level (dimensionless)
P1	inlet pressure (Pa)
P2	outlet pressure (Pa)
P3	permeate pressure (Pa)
PEG	polyethylene glycol
PPG	poly-propylene glycol (antifoam)
Q	volumetric flowrate ($m^3.s^{-1}$)
Q_g	gas flow rate ($m^3.s^{-1}$)
r	radius of centrifuge bowl (m) from Stoke's Law
R^2	the square of the Pearson product moment correlation coefficient (dimensionless)
R_b	resistance caused by pore blocking (s)
R_c	cake resistance (s)
Re	Reynold's number (dimensionless)
R_m	membrane resistance (s)
RO	reverse osmosis water
RO	reverse osmosis
r_p	radius of diffusing particle (m)
RQ	respiratory quotient (= OUR/CER) (dimensionless)
RSO	rape seed oil
R_t	total hydrodynamic resistance (s)
RVDF	rotary drum vacuum filtration
SCM	soluble complex medium
S_F	critical strain energy (J)
ssJ	steady state permeate flux ($L.m^{-2}.h^{-1}$)
ssJ	steady state permeate flux ($L.m^{-2}.s^{-1}$)

t	time (s)
t_c	circulation time (s)
TE	thioesterase-cyclase
TFF	tangential flow filtration
TKL	tri-ketide lactone
TMP	transmembrane pressure (Pa)
U	crossflow velocity ($m.s^{-1}$)
u_c	settling velocity ($m.s^{-1}$) from Stoke's Law
UF	ultrafiltration
V_f	phase volume ratio (= V_{oil}/V_{aq}) (dimensionless)
V_r	Volume ratio (volume of oil/ volume of aueous phase) (dimensionless)
vvm	volume of air per volume of medium per minute (min^{-1})
w	width of microfiltration channel (m)
x_a	concentration of a in aqueous phase when equilibrium is reached during liquid/liquid extraction ($g.L^{-1}$)
y_a	concentration of a in organic phase when equilibrium is reached during liquid/liquid extraction ($g.L^{-1}$)

1 Introduction

1.1 The Organism

1.1.1 Actinomycetes

The *Actinomycetes* are irregularly shaped Gram-positive bacteria. Their morphology is complex and growth can occur in one of two ways, single celled and mycelial (Stanier *et al.* 1987). There has been some debate as to their classification, but they are regarded as prokaryotes even though they are thought of as distinct from other bacteria (Goodfellow *et al.* 1983). Single-celled microbes, such as *Micrococcus sp.*, form discrete units which reproduce by means of budding and fission. Mycelia, however, are formed by the growth of finger-like strands called hyphae. Hyphae extend by elongation and branching, the latter occurring at regular intervals along the length of the strand. These hyphal units combine to form a mycelium, which in certain organisms (in submerged culture) can form macroscopic accumulations called pellets (Bader 1986).

1.1.1.1 Streptomycetes

Streptomyces is the most commonly described genus of the *Actinomycetes*, probably due to their industrial importance. They have proved to be a rich source of antibiotics, vitamins, enzymes and enzyme inhibitors (Goodfellow and Cross 1983). Approximately 60 % of microbially produced antibiotics are produced by *Streptomyces* species (Queener and Day 1986). The ability of this group of organisms to secrete proteins into the surrounding medium also makes them an attractive host for the production of foreign proteins (Wallace *et al.* 1992), as this

would remove the need to disrupt the cells prior to product isolation. Most *Streptomycetes* produce a non-fragmenting, branched substrate mycelium, which form aerial spores on solid media (Locci and Sharples 1983). In liquid culture it has been reported that hyphae have a diameter of 0.5-1.5 μm and can reach lengths of approximately 10,000 μm (Prosser and Trough, 1991).

1.1.1.2 Saccharopolyspora erythraea

Although *Saccharopolyspora erythraea*, the organism used in this work, was originally named *Streptomyces erythreus*, it has since been reclassified (Labeda 1987). The culture conditions are, however, similar to those of *Streptomyces sp.* and work done on this genus has points of relevance. There have been a number of studies of erythromycin production in *S. erythraea* due to it's economic significance. Factors affecting the repression of erythromycin production (Escalante *et al.* 1982; Clark *et al.* 1995), growth rate and production (Trilli *et al.* 1987) have been considered. The genetics behind erythromycin biosynthesis (Caffrey *et al.* 1992) and reprogramming the genetic pathway to produce novel products have been investigated (Donadio *et al.* 1993; Cane *et al.* 1995; Cortes *et al.* 1995), as well as the changes that genetic manipulation has on bioprocessing (Vargas-Mora 1997; Postlethwaite, 1999; Mirjalili *et al.* 1999). Determining erythromycin production in terms of the morphology of the mycelia of the organism has also been studied (Heydarian *et al.* 1996; Martin and Bushell 1996; Sarra *et al.* 1996; Bushell *et al.* 1997; Heydarian *et al.* 1999).

1.1.2 Erythromycin Biosynthesis

The main antibiotic produced by *S. erythraea* is erythromycin. Erythromycin is part of the macrolide group of antibiotics (Reid *et al.* 1992), this term describes antibiotics produced by *Streptomyces sp.* which contain a macrocyclic lactone ring linked with amino sugars through glycosidic bonds. The lactone ring is comprised of small three-carbon units called ketides.

The metabolism and genetics of polyketide production of the macrolide ring have come under scrutiny recently since it has also been noted that many of the natural compounds that display antibiotic properties have a polyketide-derived skeleton (Donadio *et al.* 1993). The production of the polyketide backbone has been shown to be closely related to fatty acid biosynthesis (Neusil and Hostalek 1986; Wakil 1989; Summers *et al.* 1995). Weber *et al.* (1989) showed that the erythromycin biosynthetic genes were clustered in the vicinity of the erythromycin resistance gene. Many research groups have carried out investigations into the genetics of the synthesis of this antibiotic, until the complete enzymatic pathway and the genes related to them had been mapped (Caffrey *et al.* 1992). The results of this research is the map of the genetic regulation of the enzymes involved in the pathway shown in Figure 1.1.

The erythromycin aglycone consists of the core macrolide ring without any sugar residues, to which two mono-saccharides are added (Figure 1.2). The synthesis of the aglycone is split into three genes each coding for a multi-enzyme complex 6-Deoxyethronolide B synthase (DEBS). These are also subdivided into modules, leaving a total of six modules, each of which carry out a condensation cycle that adds a three – carbon unit to the chain.

The production of antibiotics and other secondary metabolites is considered to be a response to nutrient limitation (Bu'Lock 1974; Bushell 1983). However, it has been reported in previous studies with other antibiotics, that changing strain and/or medium components can reverse the relationship between growth and productivity of secondary metabolites (Matsumura *et al.* 1978; Kuenzi 1980; Clark *et al.* 1995; Martin and Bushell 1996). In all the studies it has been noted that the antibiotic production begins as the growth slows and stationary phase begins. The biosynthetic pathway to erythromycins is shown in Figure 1.2.

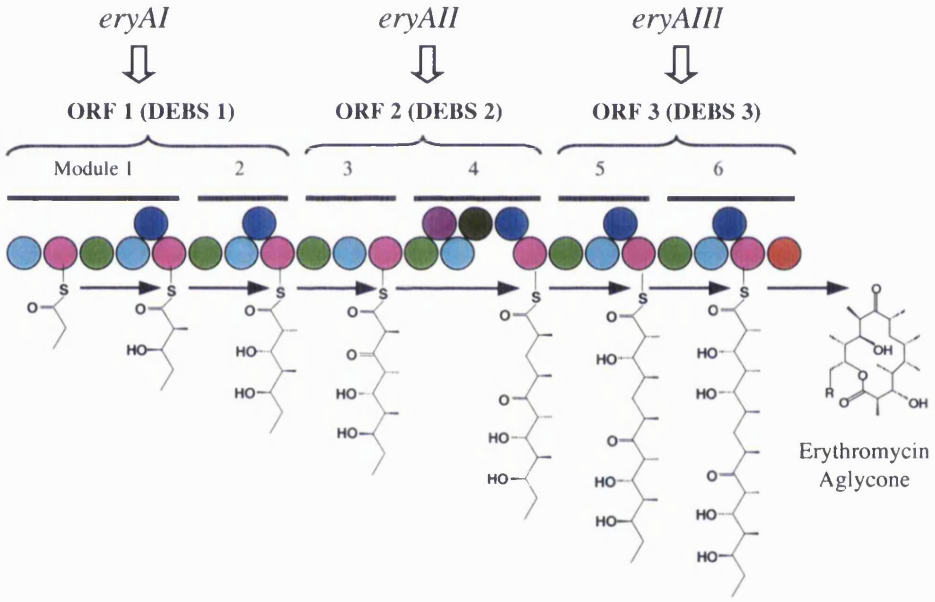

Figure 1.1. A summary of the enzymes in the synthesis of the erythromycin aglycone 6-Deoxyethronolide B (DEB) ● - Acyltransferase (AT), ● - Acyl carrier protein (ACP), ● - β-ketoacyl-ACP synthase (KS), ● - β-ketoacyl-ACP reductase (KR), ● - Dehydratase (DH), ● - Enoyl reductase (ER), ● - Thioesterase-cyclase (TE).

Erythromycin A is the main product of the fermentation (~70 %), but there are three other main forms, which are intermediates in the biosynthetic pathway; these are called erythromycins B, C and D respectively. They differ at three sites on the molecule, denoted by R, R' and R'', as shown in Figure 1.3.

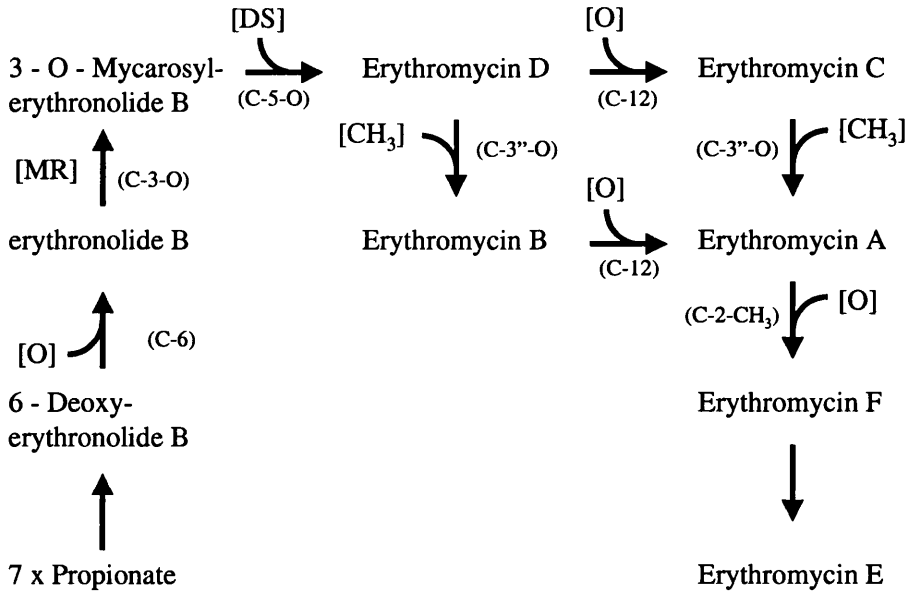

Figure 1.2. The biosynthetic pathway of erythromycin.

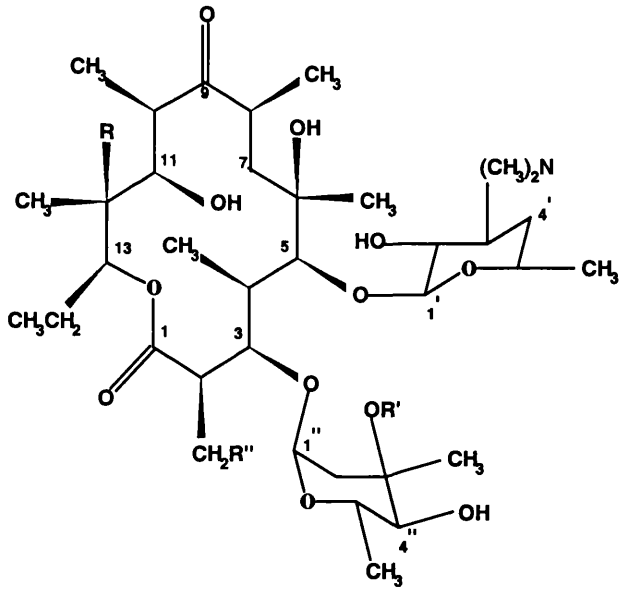

Erythromycin	Molecular Formula	Molecular Weight	R	R'	R''
A	$C_{37}H_{67}NO_{13}$	734	OH	CH_3	H
B	$C_{37}H_{67}NO_{12}$	718	H	CH_3	H
C	$C_{36}H_{65}NO_{13}$	720	H	H	H
D	$C_{37}H_{67}NO_{14}$	750	OH	CH_3	OH

Figure 1.3. Structure of the various forms of erythromycin (from Carrington 1996).

Erythromycin inhibits protein synthesis as a result of its binding with the 50s ribosome subunit (Reid *et al.* 1992). The steps of transpeptidation and translocation in protein synthesis are therefore blocked. It is an important

antibiotic both in humans and animals. Erythromycin A is active against Gram-positive bacteria, some Gram-negative bacteria and pathogenic spirochetes. It can be used clinically where there is an allergy to penicillin and or amoxycillin as it has a similar antibacterial spectrum. It is also the drug of choice for *Legionella pneumophilia* and is used for chest infections (Reid *et al.* 1992).

1.1.3 Novel Polyketide Antibiotics: Metabolic Engineering of *S. erythraea* and Process Implications

The genetics of the synthetic pathway of erythromycin has been well studied (as covered in Section 1.1.2). In recent years there have been many investigations into genetic manipulation of these pathways (Kao *et al.* 1994; McDaniel *et al.* 1995; Alvarez *et al.* 1996). *Streptomyces* have attracted such attention as hosts for recombinant antibiotics for a number of reasons. Many compounds showing antibacterial, antihelminthic, antitumour and immunosuppressive activities contain a polyketide-derived skeleton (Donadio *et* al. 1993), this increases the chance that any recombinant molecule may also have such properties. Streptomycetes are also able to secrete secondary metabolites and heterologous proteins into the medium (Wallace *et al.* 1992).

Changing the sequence of steps in the production of the macrolide aglycone of erythromycin; 6-deoxyerythronolide B (DEB), has led to the production of novel polyketides of predicted structure, (Donadio *et al.* 1991; Donadio *et al.* 1993; Cortes *et al.* 1995). It has been widely reported that since there are distinct enzyme systems within each synthesis step there is the potential that by modifying a single step only the corresponding transformation will be affected, leaving a wide scope for variation in the reprogramming of polyketide synthesis.

Triketide lactone (TKL) is a molecule produced by changing the enzymatic sequence of erythromycin synthesis (Cortes *et al.* 1995). The thioesterase-cyclase (TE) enzyme that normally cyclises the full length chain to DEB has been moved from the end of module six to the end of module two (at the end of DEBS 1) see Figure 1.4. Although the TKL produced does not exhibit antimicrobial properties, the strain that produces it has been chosen as a test of how genetic engineering affects the production and processing of *S. erythraea*.

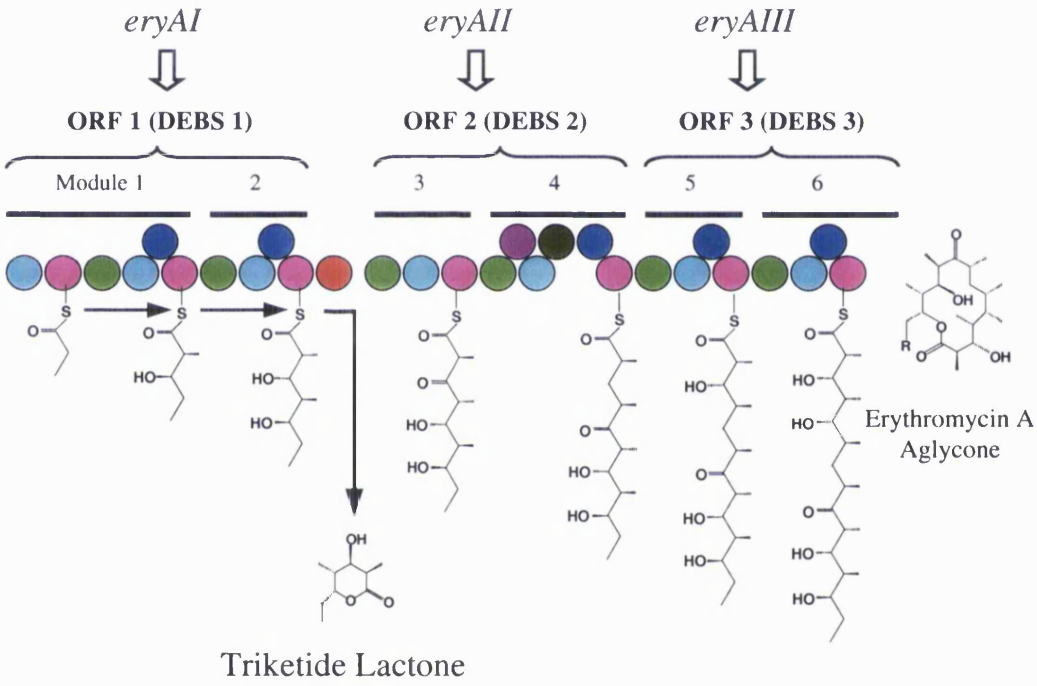

Figure 1.4. Production of TKL by repositioning of the Thioesterase-cyclase (TE) enzyme, (from Cortes *et al.* 1995) ● - Acyltransferase (AT), ● - Acyl carrier protein (ACP), ● - β-ketoacyl-ACP synthase (KS), ● - β-ketoacyl-ACP reductase (KR), ● - Dehydratase (DH), ● - Enoyl reductase (ER), ● - Thioesterase-cyclase (TE).

It has been shown that in other organisms, such as *E. coli* and *Sacc. cerevisiae* (Birnbaum and Bailey 1991; Danash *et al.* 1991; Sato *et al.* 1994), that manipulation of the genetic structure can affect the cell characteristics. There are few studies on how recombinant *S. erythraea* strains react when processed.

Donadio *et al.* (1993) found that for their novel polyketide, $\Delta^{6,7}$-anhydroerythromycin C, concentrations approximately 5 times lower than that of erythromycin A in the parent strain, and that it showed approximately 200-500 times lower bioactivity. When considered from a process engineering viewpoint this leads to larger volumes to produce, since higher doses will be required and lower titres of product which would affect the method of fine purification. Although this is just an example molecule, changes in expression are possibly only one of the factors that will affect the manufacture of new drugs.

In the TKL producing strain of *S. erythraea*, described by Cortes *et al.* (1995), an investigation has been carried out into the effects of altering the genetics of an organism on the growth of the organism and expression of the product using an industrially based medium (Mirjalili *et al.* 1999). The study found that the TKL strain showed reduced product titres; 1089 $mg.L^{-1}$ (*wt* strain) and 150 $mg.L^{-1}$ (TKL strain) and the specific rate of oil utilisation was also reduced in the recombinant strain; 3500 $[(g\ oil)/(kg.m^{-1}.s^{-1})]$ (*wt* strain) compared to 1250 $[(g\ oil)/(kg.m^{-1}.s^{-1})]$ (TKL strain). These variations will affect both the fermentation and vessel turnaround time and also will require optimisation of the new process. Downstream processes such as primary biomass removal and liquid-liquid extraction for product purification, will also be affected by biomass viscosity changes, product titres and product chemistry.

For small changes in a secondary metabolite pathway, it has been shown that this can cause profound effects on the growth profiles and nutrient utilisation of the fermentation which will in itself then affect the purification of any novel anti-microbial compound to be produced. It is indeed possible that each fresh change in

the genetic reprogramming of *S. erythraea* will require totally new process synthesis and optimisation. With the time to market of primary importance for profit maximisation and the need for speed in combating ever more resistant bacteria the ability to rapidly optimise processes will be necessary. The process interactions between steps of manufacture need to be more firmly understood in order to reduce the number of variables investigated and also the range over which those variables need to be examined. Combining these parameters with the capability of direct linear scale-down whereby operations at bench scale can then be used to predict full scale processes will lead to the fastest and most cost effective ways of designing and validating new operations for pharmaceutical grade biologics.

1.1.4 Fermentation

Streptomyces fermentations are carried out at large scale, vessels can reach 300 m^3 (Bader 1986). Large fermenters encounter mixing limitations due to their size which cause regions of heterogeneity within the culture broth. This can lead to areas of low oxygen, variable temperatures and pH ranges which in *S. erythraea* cultures may lead to damage to cells and/or the reduction in the production of erythromycin. Mixing efficiency is a function of the apparent viscosity of the fermentation broth (Doran 1995). In this section the broth rheology, hyphal morphology and it's measurement using image analysis along with the composition of the media are discussed.

1.1.4.1 Broth Rheology

There are two rheological categories under which liquids and suspensions can be grouped, these are Newtonian and non-Newtonian fluids. For Newtonian fluids the viscosity, a measurement of the internal resistance to flow, is independent of the shear rate applied (Atkinson and Mavituna 1991). Non-Newtonian fluids, however, have viscosities that are dependant on the shear rate applied to the system; viscosity can either increase or decrease depending on the shear rate. A problem associated with the measurement of viscosity, is the time dependence of the measurement. Metz *et al.* (1979) described this phenomenon and suggested a time of 5 seconds after changing the shear rate to take the measurements. The effect of the type of measuring device used should also be considered since several reviews have shown disagreements between the values of viscosity found by different measurement techniques (Bjorkman 1987; Allen and Robinson 1990). These variances can be due to "slip effects", settling of the suspension, or breakage of the solids (Karsheva *et al.* 1997). Warren *et al* (1995) found that for three different species of *Actinomycetes* including *S. erythraea*, viscosity measurements were consistent between two different instruments; a cup and bob viscometer and an impeller viscometer.

Considering the problems of reproducibility when studying biological systems, it becomes difficult to predict how small changes in the fermentation will affect processes downstream where the rheological properties of the broth are important. There are four main models which have been developed to describe the rheological behaviour of fermentation broths (Karsheva *et al.* 1997), these are the Newtonian, Power Law, Bingham plastic and Casson plastic models as shown in Figure 1.5. Researchers have found different rheological models to be more accurate

depending on species, strain and medium (Bjökman 1987; Allen and Robinson 1990; Warren *et al.* 1995).

Fermentation broths of *S. erythraea* follow the Power Law model, (Heydarian *et al.* 1999) which is itself separated into two types, shear thinning (pseudoplastic) and shear thickening (dilatant). The former state is where the flow index, n, is less than 1; as shear increases the apparent viscosity decreases. Shear thickening (where n is greater than 1), is where as the shear rate increases so does the apparent viscosity. *S. erythraea* broths show adherence to the pseudoplastic Power Law.

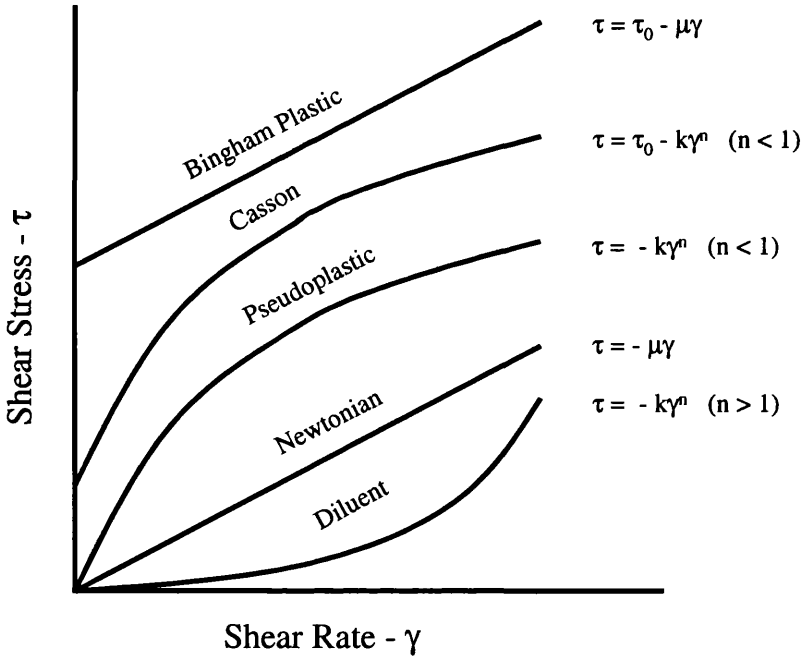

Figure 1.5. Different models for the viscosity of fluids. τ is shear stress, γ is shear rate, μ is the viscosity, k is the consistency index and n is the flow behaviour index (from Bader, 1986).

1.1.4.2 Hyphal Morphology

S. erythraea forms long mycelial strands which can be a disadvantage during the course of the fermentation. As morphology changes over the course of the

fermentation it adversely affects the mixing within a stirred tank vessel (Li *et al.* 1995), which can lead to a decrease in erythromycin concentration (Herdarian *et al.* 1996). Hyphal breakage occurs in shake flasks and fermenters resulting in fragments incapable of producing antibiotics in many filamentous bacteria, this is because secondary metabolites such as erythromycin are only formed once the hyphae reach a certain length (Heydarian *et al.* 1996, Martin and Bushell 1996). This may account for the ability to synthesise antibiotics on agar, but not in liquid culture (Pickup *et al.* 1993).

This is supported by other studies that have reported low productivity in cultures whose hyphae were highly fragmented (Shomura *et al.* 1979; Roth *et al.* 1982). Lilly *et al.* (1992) reported a good relationship between morphological changes and the rate of penicillin production by *Penicillium chrysogenum.* As is discussed in Section 1.1.3.1, broth rheology is inter-linked with morphological changes. This suggests that since morphology within the fermenter changes with time, apparent viscosity will also change as indicated in Figure 1.6 (Karsheva *et al.* 1997). Since rheology affects process performance further downstream the time at which the broth is harvested could have a profound effect on product recovery by microfiltration.

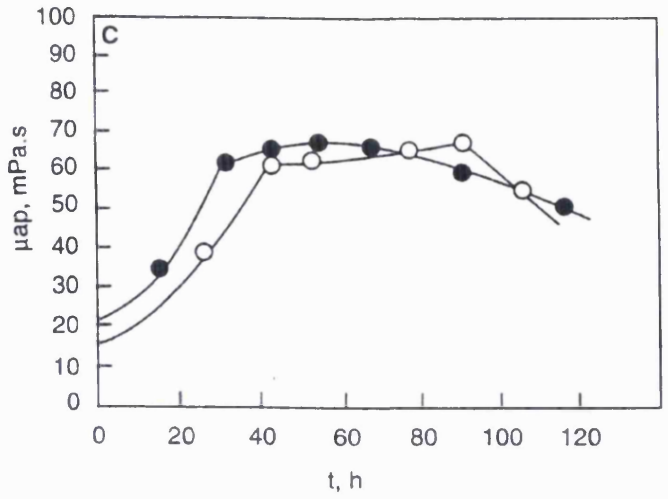

Figure 1.6. Dependence of apparent viscosity (u_{ap}) on fermentation time (t) for two fermentation runs of *Cephalosporium acremonium*, μ_a was measured at $\gamma = 27\ s^{-1}$ (from Karsheva *et al.* 1997).

1.1.4.3 Image Analysis of Fermentation Broths

The characterisation of mycelial morphology using image analysis has been well documented. Equipment and techniques have recently been reviewed by Paul and Thomas (1998). Image analysis has been widely used to study filamentous organisms in liquid culture and observe how their morphology changes with time. (Martin and Bushell 1996; Treskatis *et al.* 1997). The factors listed and described in Table 1.1 have previously been used in different studies to quantify the morphology of mycelial bacteria (Packer and Thomas 1990; Heydarian 1998a).

Martin and Bushell (1996) reported that only hyphae over 88 μm were capable of producing erythromycin and that changes in stirrer speed affected the size distribution of the hyphae in the fermenter and consequently the productivity of erythromycin. The effect of fermenter operating conditions (type and operation) on *S. erythraea* morphology, biomass and erythromycin production has also been studied (Sarra *et al.* 1996; Bushell *et al.* 1997; Heydarian 1998a). Previous work

by Sarra *et al.* (1996) showed an increase in main hyphal length (ML) with fermentation time up to 35 hours followed by a gradual decline.

Measurement	Nomen-clature	Description
Main hyphal length*	ML	The longest connected path through the cells
Branch length*	BL	Other parts of the mycelia apart from the main length
Total hyphal length*	HL	= ML + BL
Number of tips*	NT	The number of branches(growing tips)
Major axis+	OL	Maximum mycelia diameter
Minor axis+	OB	Longest distance perpendicular to the major axis
Mycelia area	MA	Projected area of the freely dispersed mycelia
Clump area	CA	Projected area of the clumped mycelia
Projected area+	OD	MA or CA
Total area+	OA	= OD + internal holes
Circularity+	OC	= (4 x π x OA)/(Perimeter)^2

Table 1.1. Morphological parameters that can be quantified by image analysis (Heydarian, 1998);* applied only for freely dispersed mycelia, + applied to both freely dispersed mycelia and mycelial clumps.

Heydarian (1998a) also showed that the power input to the fermentation via the impeller affected morphology. It was discovered that as the impeller speed increased, the major axis (OL) of the mycelia decreased, which was concluded to be due to increased shear. From this work a turbulent breakage model for filamentous bacteria was derived:

$$OL = (S_F E)\left[\frac{\rho\mu\varepsilon}{\sqrt{t_c}}\right]^{-0.15} \qquad [1.1]$$

where S_F is the critical total strain energy (J), E is the modulus of elasticity of hyphae (N.m^{-2}), ρ is the density of the broth (kg.m^{-3}), μ is the apparent viscosity of the fluid (N.m^{-2}.s), ε is the energy dissipation rate per unit mass (W.kg^{-1}) and t_c is the circulation time (s). Similar experiments with *Aspergillus oryzae* (Amanullah *et al.* 1999) and *P. chrysogenum* (Justen *et al.* 1998) have shown hyphal breakage to be a function of power input to the fermenter via the impeller.

1.1.4.4 Fermentation Media Components

The medium components of the broth are often chosen solely to maximise product yield. This is frequently considered without an understanding as to the effects of these components on processes further downstream or the effects that changing components can have on the apparent viscosity of the broth. Broths can consist of a number of phases. For example, solid media constituents, which can block membrane systems, the continuous aqueous phase which can be polarising at the membrane pores (Porter 1972; Brose *et al.* 1996) and liquid organic phases, such as oils which can cause entrapment blocking of the pores.

Oils which are added at the beginning of the fermentation are not always totally utilised by the organism (Mirjalili *et al.* 1999) and a certain concentration can remain when the broth is harvested. It is these residual oils that cause surface and entrapment blocking of microfiltration membranes. The lipids block the pores on the membrane leading to a decrease in flux. Conrad and Lee (1998) showed that 5 % (v/v) soybean oil in water lead to an order of magnitude decrease of the steady state permeate flux. Additives to the broth such as antifoams can also have an adverse affect (Liew *et al.* 1997).

1.2 Downstream Processing

1.2.1 Introduction to Downstream Processing

The recovery of material from a biological system is intricate. The complexity of the broth and the chemical and physical similarity between compounds makes separation less than straightforward. Separation of materials takes advantage of the differences between them for example size, density or solubility (Doran 1995). In

this respect the method of separation depends on the desired product. When considering an industrial system, expense and safety are also important factors (Zeman and Zydney 1996). For this reason it is imperative to consider the predicted price per unit mass of the desired compound, the purity required and the scale of the process. For example it would not be expected to use the same techniques for making non-beverage ethanol, a large scale process (2×10^{10} $kg.yr^{-1}$), where purity is relatively unimportant and the production of human growth hormone, which has an estimated requirement of less than 20 $kg.yr^{-1}$ (Shuler 1987).

Knight (1989) reported that purification costs are primarily responsible for the high selling price of biotechnology derived products and that the key to cutting these costs is to reduce the number of steps. Not only does this reduce the amount of product lost during the purification, but also the cost of developing, validating, and running the additional process steps. In order to minimise loss of product throughout a process, not only should the minimum amount of steps be used, but the step yield of each operation should be as high as possible. Figure 1.7 considers a process with up to ten steps downstream of the fermentation. Obviously the efficiency of each unit operation will vary but the figure gives an approximation for the importance of both purification effectiveness and the limitation of many steps.

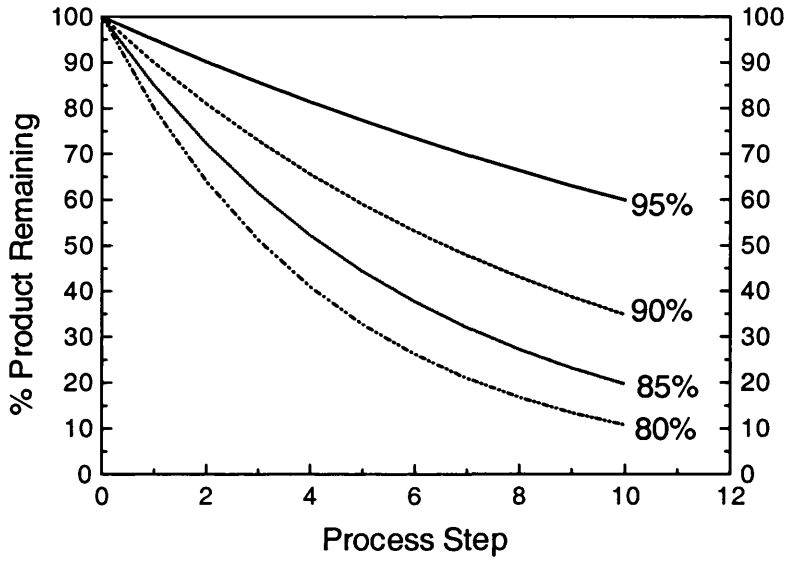

Figure 1.7. A graph of percentage product remaining against number of process steps, where 1 represents the end of fermentation and 10, the final preparation, based on an assumed step efficiencies of 80-90 %.

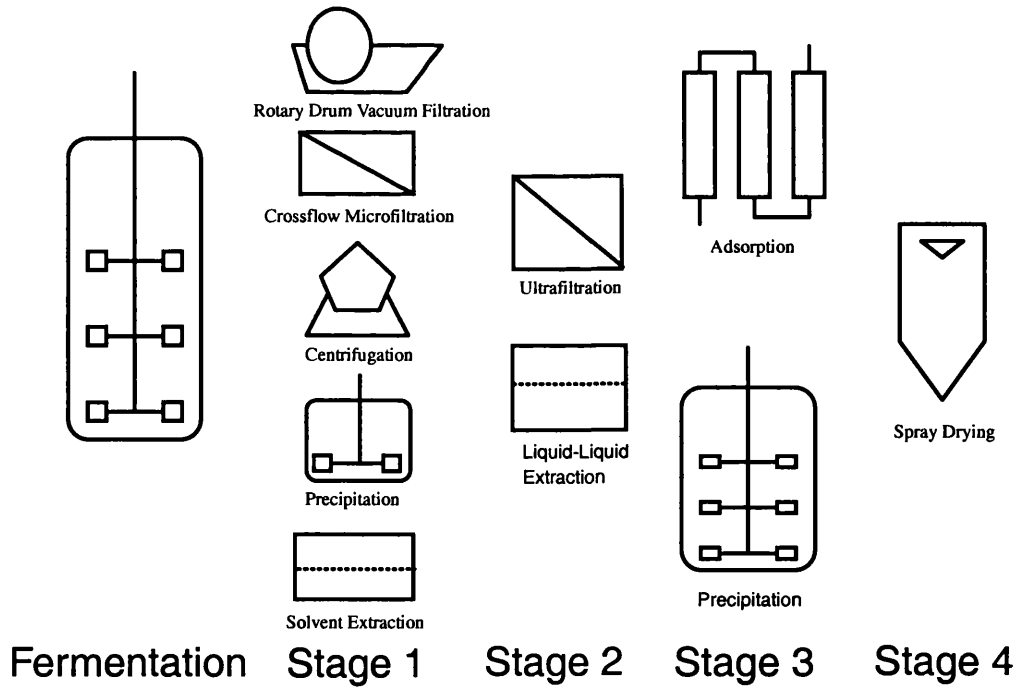

Figure 1.8. Process diagram showing the five different biomass removal options and three additional steps further downstream for erythromycin production.

Erythromycin A is an extracellular product and therefore the biomass must first be separated from the liquor before any further purification can take place. It is this

stage of the process that the current work seeks to address. Figure 1.8 shows a schematic of a typical process, the five methods of primary separation considered later in Section 1.2.2 are shown after the fermentation. The next three steps are representative of product extraction/concentration, purification and formulation respectfully. When investigating a single unit operation, the effects of processes upstream on it and downstream due to it must also be considered. This is discussed in detail with respect to fermentation and crossflow microfiltration in Section 1.4.

1.2.2 Primary Recovery Operations

Solid-liquid separation is desirable after or during a microbial fermentation for a number of different reasons. For products that are intra-cellular or periplasmic, the broth may require dewatering before lysis of the cells by mechanical or chemical means. In the case of *Saccharomyces cerevisiae* (baker's yeast) or *Fusarium graminearum* (Quorn micro-organism), the cells themselves are the desired product and must be separated from the liquor.

For extra-cellular products such as erythromycin the biomass must be removed from the liquor in order to reduce the particulate loading on unit operations further down the process. This is important for unit operations such as chromatography where solid contaminants can reduce and even stop the flow through a column (Berthold and Kempken 1994). Since biomass removal also reduces the process volume, the scale of subsequent steps can be reduced. Chromatography media and solvents, which are likely to be used further downstream, are a significant cost of the process and any reduction in the volume required to produce a standard amount of the desired compound increases the efficiency of production. The current industrially preferred method for cell removal in the purification of erythromycin is

that of rotary drum vacuum filtration (RDVF). The unit operations of centrifugation, precipitation, whole broth solvent extraction and crossflow microfiltration have also been considered to be an industrially viable alternative to RDVF. A description of these techniques is presented below and a discussion of their suitability are presented in Section 1.2.3.

1.2.2.1 Centrifugal Separation

Centrifugal separation of cell biomass fractionates the phases by means of the density difference between the liquid and solid phases of the fermentation broth. This works for natural settling under gravity as defined by Stoke's Law. Stoke's Law can be adapted for centrifugal forces by substituting the acceleration due to gravity (g) with angular acceleration $\omega^2 r$:

$$u_c = \frac{(\rho_p - \rho_f) d_p^2 \omega^2 r}{18\mu} \qquad [1.2]$$

where u_c is the settling velocity in a centrifuge ($m.s^{-1}$), ρ_p is the density of the particle ($kg.m^{-3}$), ρ_f is the density of the liquid ($kg.m^{-3}$), μ is the viscosity of the liquid (Pa.s), d_p is the diameter of the particle (m), ω is the angular velocity of the bowl ($rad.s^{-1}$), r is the radius of the bowl (m). In a centrifuge, the force exerted on the particles can be many orders of magnitude greater than that of gravity, thus increasing settling velocity to many times greater than if the suspension were allowed to separate naturally.

1.2.2.2 Precipitation

The definition of precipitation is open to interpretation though in this work it will be used as an umbrella term for flocculation, coagulation and agglomeration. Precipitation is a process by which a particle is increased in size to ease separation from the liquor. For whole cell and debris removal the term flocculation is used, this is where an agent such as polyethylene glycol (PEG) is added which accumulates the small particles into more dense aggregates. Increasing particle diameter (d_p) and density (ρ_p), increases the settling velocity (u_c) in a centrifuge according to the modified Stoke's law, as described in Equation [1.2].

Precipitation has been shown to be of benefit in the removal of cell debris and cellular contaminants after homogenisation in yeast and bacteria (Salt *et al.* 1995). The usefulness of selective precipitation in the isolation of target molecules such as nucleic acids and associated metabolising enzymes has also been demonstrated (Jendrisak 1987). A process patented in 1990 (Pfizer) describes the purification of several macrolide antibiotics including erythromycin by precipitating the free base of the antibiotic.

The extent of flocculation achieved, whether it is of the product itself or whole cells and debris, depends on the physical properties of the product. For example charge density (Lindquist and Stratton 1976; Mabire *et al.* 1984) and molecular weight (Wilde and Dexter 1972; Kitchener 1972; Gregory 1976) are two such factors. It can also depend on the properties of the solution, for example pH (Bentham 1990; Wilde and Dexter 1972; Kitchener 1972) and ionic strength (Lindstrom and Soremark 1976; Gregory 1973).

1.2.2.3 Dead-End Filtration

Dead-end filtration systems have feed streams that flow parallel to the filtrate. The broth is forced through the membrane using a difference in pressure as the driving force. As a result, material (filter cake) is deposited at the membrane surface which is then compressed by the feed stream. Flux therefore decreases over time due to the resistance to flow of the impacted material as shown in Figure 1.9. To reduce the compressibility of the filter cake a filter aid is often added. This works by maintaining the structural integrity of the cake. Diatomaceous earth (also known as Kieselguhr), made up of fossilised diatom shells, is used in many dead-end filtration processes (Bailey and Ollis 1986). By reducing cake compressibility, flux is increased, however, the biomass is contaminated by the Kieslghur.

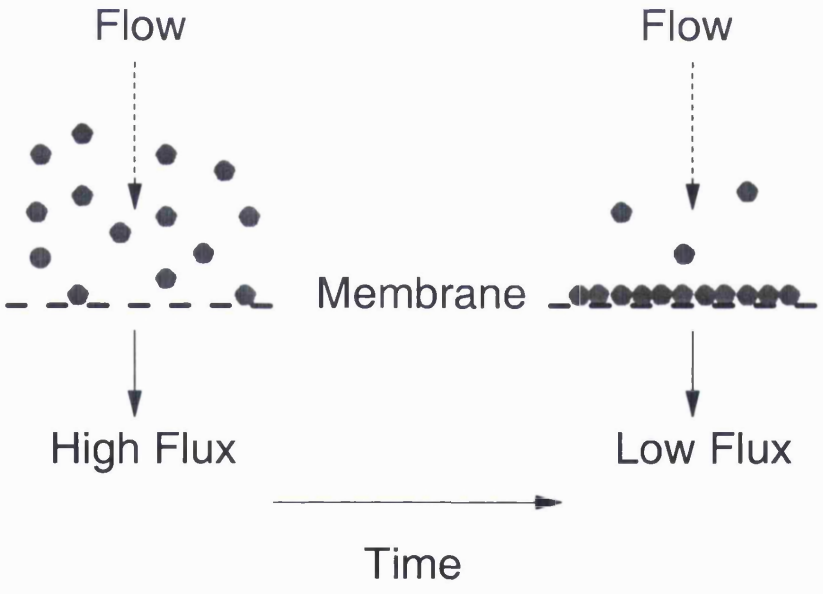

Figure 1.9. A diagrammatic representation of dead-end filtration, showing how membrane fouling decreases flux over time.

Rotary drum vacuum filtration (RDVF) is the most widely used method of dead-end filtration from antibiotic fermentation broths (Doran 1995; Zeman and Zydney 1996). In an industrial RDVF system the cake must be continuously removed.

This is achieved by the presence of a scrapper positioned just above the surface of the membrane. As the drum rotates through the broth, the solids on the membrane are removed as shown in Figure 1.10.

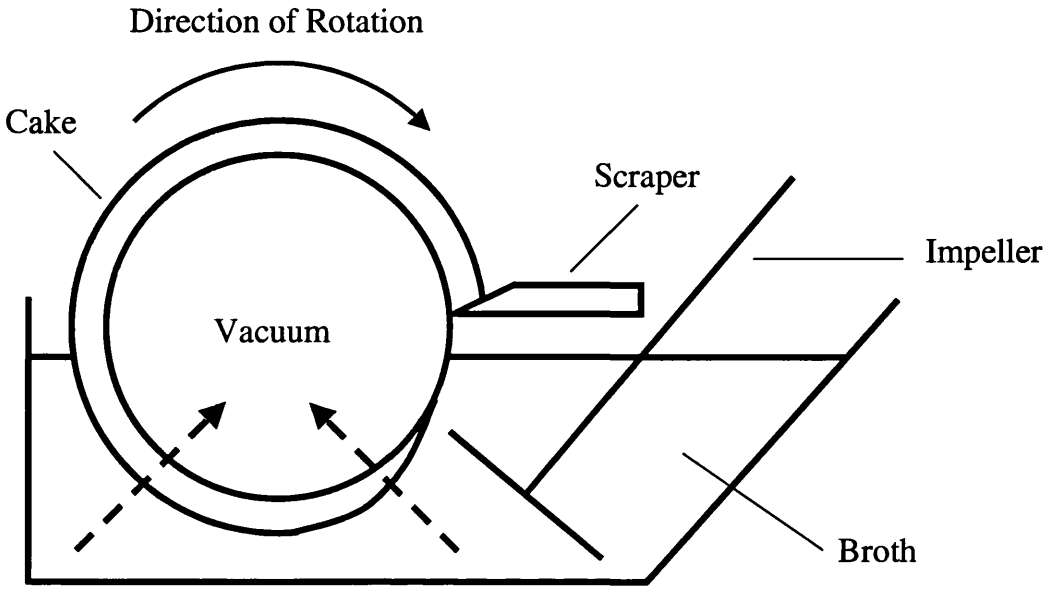

Figure 1.10. Continuous RDVF (From Brown *et al.* 1950).

1.2.2.4 Whole Broth Solvent Extraction

Solvent extraction takes advantage of the different solubilities of products under the same conditions in two immiscible solvents. If the two phases are in contact with each other then a proportion of the product will dissolve in each. The proportion in each phase is called the partition coefficient (K_{eryth}), which is defined by:

$$K_a = \frac{y_a}{x_a} \qquad [1.3]$$

Where y_a is the concentration of *a* in the organic phase ($g.L^{-1}$) and x_a is the concentration of *a* in the aqueous phase ($g.L^{-1}$). K_{eryth} is affected by temperature,

pH, ionic strength of the aqueous phase and the concentration and partition coefficients of the other solutes in the fermentation broth.

The technique has already been successfully used for the extraction of penicillin G and V and has been shown to be effective for the direct extraction of erythromycin (Brunner 1985). A typical instrument for the process is the Podbielniak centrifugal contractor. Erythromycin can be purified in this way using amyl acetate as the organic solvent. The advantage of this technique is that directly removing the product from the process stream reduces the number of steps required.

1.2.2.5 Crossflow Microfiltration

In crossflow filtration the feed stream runs across the membrane instead of parallel to it as in dead-end filtration. In this way solids are carried away from the membrane surface rather than settling on it as shown in Figure 1.11, thus reducing fouling and increasing the permeate flux. The tangential retentate stream causes shear which disrupts cake build up. The shear forces can be enhanced by introducing flow separators which promote the production of vortices (Da Costa *et al.* 1991), or by introducing air into the feed stream and therefore across the membrane which increases turbulence (Li *et al.* 1997). A further way of increasing shear at the surface of the membrane is by using a moving membrane, for example a rotating or vibrating membrane (Lee and Buckland 1995; Lee *et al.* 1996; Alex and Haughney 1998). A rotating membrane system has already been successfully used by Merck and Co. in the purification of cephamycin C (Lee *et al.* 1996). The initial problems that have previously been associated with MF i.e. fouling of the membranes with antifoam agents and cell debris have been addressed successfully

with the improvements in membrane technology (Carrington 1986); this will be discussed in greater detail in Section 1.4.

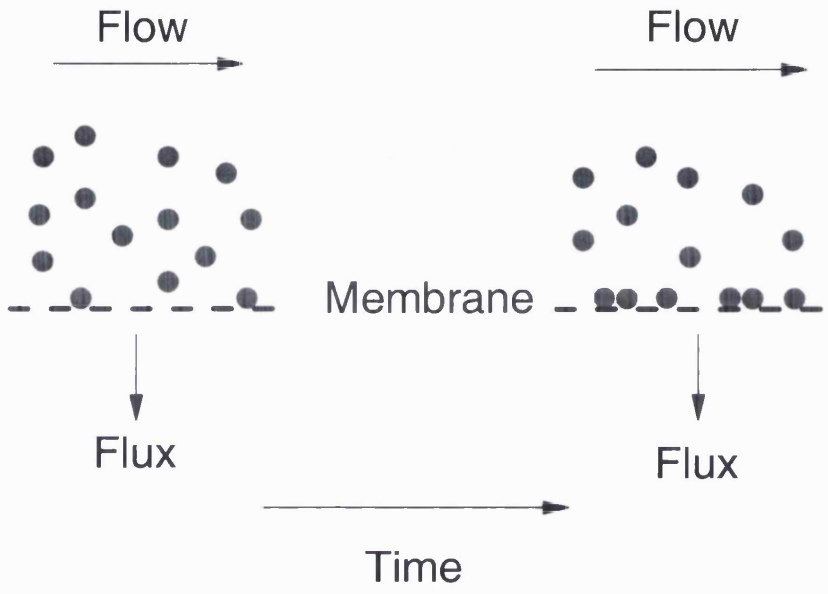

Figure 1.11. Diagrammatic representation of flow patterns in crossflow filtration.

1.2.3 Selection of Unit Operations for Primary Separation

In the choice of a primary separation process there are a number of factors that must be considered. The efficiency of the particle removal will determine if further clarification is required after the separation of the cells, the unit operation must be reproducible and should be economically viable at process scale. Operator time and services must also be examined as well as risks to personnel and equipment both through operation and contact with chemical and biological hazards. Table 1.2 shows some comparisons of the costs involved associated with crossflow filtration, centrifugation and vacuum filtration.

Centrifugal separation of cells from fermentation broth is not widely used as the primary purification step of antibiotic extraction (Carrington 1986). Although

centrifuges have a small footprint (Larsson 1974) they require a high initial capital cost and a high running cost due to power consumption and labour as shown in Table 1.2 (Zeman and Zydney 1996). Centrifuges also represent a considerable safety risk. Not only is the unit itself potentially dangerous, but uncontained centrifuges can release aerosols of cell particulates which can be harmful. With the increased use of recombinant organisms in the production of novel antibiotics the last point is of particular relevance. The shear forces experienced in the feed zone of the centrifuge due to the rapid acceleration from low to high angular velocity can have damaging effects on biological materials (Mannweiler 1990; Murrell 1998). Breakage increases the amounts of contaminants such as protein and DNA in the clarified stream and decreases the efficiency of the process.

Expense	Basis	Annual Cost ($.yr^{-1})		
		Crossflow Filtration	Centrifuga-tion	Vacuum Filtration
Depreciation	20% of capital	52,500	200,000	15,000
Membranes	\$175.m^{-2}.yr^{-1}	35,000	-	-
Diatomaceous earth	24kg per 1000L at \$1 per kg	-	-	336,000
Cleaning chemicals	\$25.m^{-2}.yr^{-1}	5,000	-	-
Power		4,200	8,000	1,500
Labour	0.2 persons per day (MF)	6,000	-	-
	0.8 persons per day (others)	-	24,000	24,000
Maintenance	2% of capital	8,800	20,000	1,500
Total		**111,500**	**252,000**	**378,000**

Table 1.2. Economic comparison of MF, vacuum filtration and centrifugation for the initial clarification of an antibiotic fermentation (from Zeman and Zydney 1996).

It has also been shown that, for large scale removal of mammalian cells, a clearer filtrate was obtained by crossflow microfiltration over disk stack centrifugation. The liquor from the microfiltration was sufficiently clear to put straight on to a

column, whereas the liquor after centrifugation required an additional filtration step (Berthold and Kemken 1994).

Precipitation requires the coagulation of particles which is achieved by electrostatic interactions between the precipitating agent and the target precipitant. This requires careful control over the operating conditions. Whilst precipitation precludes the use of organic solvents, the disadvantages of using a centrifugation step (high initial capital investment and high running costs), are still apparent. The specificity of precipitation is also questionable. However although an antibiotic product produced in this way is crude, it may be acceptable for animal health products, if not for human therapeutic use (Bulmer 1994).

Although RDVF is currently the most common way of separating biomass from the harvested broth, the filter aid, which can be added by pre-conditioning of the membrane, or as part of the feed stream, does cause problems. As can be seen from Table 1.2, the filter aid is the most significant cost in this process (around 90%). Gravatt and Molnar (1986) also highlighted the need for an increased waste disposal ability of the plant in question. The cost of the filter aid itself is added to the loss incurred through the unsuitability of the waste material for animal fodder (Zeman and Zydney 1996). The initial capital cost for the equipment is also very high, it has a large footprint and cannot be easily contained. (Carrington 1986). Despite of this it was still considered in the literature uneconomical to replace existing equipment (Meindersma *et al.* 1997), with the production of recombinant strains of *S. erythraea* producing novel antibiotics (Section 1.1.3) new processes will be developed and implemented, which may argue for the replacement of RVDF.

The use of organic solvents presents a problem both with disposal and safety (Carrington 1986), which are both likely to significantly increase costs at an industrial scale. The use of chemical agents to control the pH at this stage also may also affect processes downstream. This method has demonstrated higher yields than rotary vacuum filtration (Brunner 1985). However, formation of emulsions can reduce mass transfer within the extractor and therefore the efficiency of the process. Contamination of the harvested cells with organic solvents creates further disposal issues and revenue is lost from the inability to sell the biomass as animal feed.

The capital cost of an industrial scale microfiltration unit is low and the footprint is small. One of the major advantages of MF is that the system is totally contained which is of particular importance when processing genetically modified organisms (GMOs). It also presents few safety problems compared to other techniques, low pressures are used and only cleaning chemicals represent a risk. The advantage of using MF due to a reduced number of process steps has also been considered (Section 1.2.1). In comparison with the other methods: filter aid is not required which keeps the maintenance costs down and no chemical agents need to be added to the broth so that there is no complication at the more subtle purification steps. It has been shown that crossflow microfiltration (MF) was more efficient than RDVF in terms of product yield, filtrate quality and costs (Gravatt and Molnar 1986; Tutunjian 1986; Meindersma *et al.* 1997). Although the membranes themselves are expensive it can be seen from Table 1.2 that the overall running costs of a microfiltration system are far lower than those for centrifugation and vacuum filtration. Safety is also improved over solvent extraction since no organic solvents are involved. The clarity of the permeate means that additional steps are not

required, whereas in the use of precipitation, centrifugation and dead-end filtration further steps may be required. Overall, for cell separation in erythromycin recovery, microfiltration gives improved environmental and safety features, reduced labour and maintenance costs (Antoniou *et al.* 1990).

1.2.4 Product Purification

Purification of the erythromycin downstream of primary biomass removal will depend on the quality of the clarified liquor. Solvent extraction is a typical method of concentrating the erythromycin produced, but if the liquor contains too high a concentration of particulates (which is a possibility with the use of centrifugal or precipitation methods), columns can become quickly blocked (Berthold and Kempken 1994). Therefore pre-treatment of the clarified broth may be needed, this reduces the efficiency of the process by increasing the number of steps, as described in Section 1.2.1.

The presence of different compounds in the liquor may also adversely affect chromatographic media by blocking the binding sites that are required for separation. This can lead to longer processing time, more regular cleaning (and therefore downtime), larger volumes of chromatographic matrix or a combination of the above. Addition of chemicals to the feed stream such as higher anti-foam requirements or precipitation agents may make the purification more difficult and more expensive per unit product produced. Although human therapeutics are a high price product, profits must still be maximised.

1.3 Microfiltration Theory

1.3.1 Microfiltration Theory and Application

The terminology of crossflow filtration is not well defined, for the purposes of this thesis report crossflow filtration (CFF) and tangential flow filtration (TFF) are two different names for the same process. This process is then separated into several sub-classes based on the size of the species being separated; microfiltration (MF), ultrafiltration (UF), reverse osmosis (RO), nanofiltration (NF) and electrodialysis (ED).

Microfiltration (MF) is a balance of two parameters, shear and pressure. The transmembrane pressure (TMP), which forces material across the membrane and the shear at the membrane surface, which causes a back transport of material thus reducing fouling and gel layer formation (Cheryan 1998). Shear at the membrane surface can be created either by moving the broth past the membrane, by recirculation pumping, or by moving the membrane past the broth, rotating or vibrating the membranes (Lee and Buckland 1995). Theoretically, the higher the shear at the membrane the higher the permeate flux that will be achieved. There are however, upper limits, shear can damage cells and cause aggregations of proteins which lead to impurities and loss of product (Zeman and Zydney 1996). Increased power input can also increase the pressure on the system to such an extent as to make the shear rate immaterial, this will be discussed below.

The other factor acting at the membrane is the transmembrane pressure (TMP). The TMP is the pressure difference between the broth side, (feed stream and retentate) and the purified side, (permeate). Since there is a pressure drop across

the inlet and outlet of the system the mean pressure of the feed stream is taken, i.e. the mean of the inlet pressure (P_1) and the retentate or outlet pressure (P_2). From this is subtracted the pressure on the permeate side of the membrane (P_3) to measure the pressure drop across it i.e.:

$$TMP = \frac{(P_1 - P_2)}{2} - P_3 \qquad [1.4]$$

This TMP is a measure of the pressure acting on the materials in the broth, in the direction of the membrane surface. Again, theoretically the higher the TMP the stronger the force acting on the broth and the higher the permeate flux (see Equation [1.8]). However a limit is reached, for a given shear rate, there is a point at which the TMP is forcing material to the membrane surface faster than the back-transport away from the membrane is removing it. This is called concentration polarisation and the region where increasing TMP no longer increases permeate flux marks the experimental limit at that shear rate. This is called the *critical transmembrane pressure* (cTMP) and defines the pressure at which flux is no longer proportional to TMP. Any increase in TMP at this crossflow gives no, or reduced benefit in permeate flux.

1.3.2 Permeate Flux and the Effect of Crossflow

Optimisation of process parameters of MF can lead to increases in permeate flux (Porter 1972). Russotti *et al.* (1995) demonstrated this using a fermentation of *Strep. griseofucus* broth with 8 % soybean oil (v/v - initial concentration) and 0.27 % P-2000 (v/v) antifoam. With a small scale (0.12 m^2) membrane, flux was improved from between 10 and 30 $L.m^{-2}.h^{-1}$ to between 60 and 80 $L.m^{-2}.h^{-1}$ (at

70kPa TMP and a crossflow of 4.0 $m.s^{-1}$). This was scaled up to 200-400 L, giving a flux of 47.6 $L.m^{-2}.h^{-1}$. Different ways of improving flux have been observed by using a dynamic membrane. Permeate flux limited in MF by cake formation can be increased ten-fold by using a vibrating membrane system (Lee and Buckland 1995; Lee *et al.* 1996). Alex and Haughney (1998) used both vibrating and rotating membrane rigs to increase flux. In these methods the crossflow only imparts a driving force to recirculate the feed through the system and the shear is provided by the movement of the membrane itself.

Fouling is not the only cause of flux rate decline, it has been demonstrated that membranes are changed permanently after use. Hernandez-Pinzon and Bautista (1992) observed a sharper drop in flux when using new membranes at a starting TMP of 83 kPa (56 $L.m^{-2}.h^{-1}$ to 16 $L.m^{-2}h^{-1}$) than membranes used more than three times (22 $L.m^{-2}.h^{-1}$ to 16 $L.m^{-2}.h^{-1}$), suggesting that microfiltration membranes are permanently changed. Thus cleaning is not one hundred percent effective.

1.3.3 Microfiltration Modelling

It has been proposed (Porter 1972; Brose *et al.* 1996; Okec 1998) that flux can be predicted by:

$$J = k \ln\left(\frac{C_w}{C_b}\right) \qquad [1.5]$$

Where J is the flux of the permeate ($kg.m^{-2}.s^{-1}$), k is the mass transfer coefficient ($kg.m^{-2}.s^{-1}$), C_w is the wall concentration of cells (% wt/v) which is assumed to be 70 % (Okec 1998) and C_b is the bulk concentration in the feed stream of cells

(%wt/wt). The value of C_w is estimated based on the volume of packed spheres at the membrane surface (Porter 1972). Due to the investigation procedure it was impossible to determine the experimental value of C_w without affecting the results.

The mass transfer coefficient (k) can be calculated using experimental values. In a laminar flow, flat sheet membrane system the equation is given by Porter (1972) as:

$$k = K_P\left(\frac{Q}{bwL}\right)^{0.5}\frac{D^{0.66}}{\nu^{0.17}} \qquad [1.6]$$

where K_p is the proportionality constant, Q is the volumetric flow rate ($m^3.s^{-1}$), D is the diffusion coefficient ($m^2.s^{-1}$), b is the channel height (m), w is the channel width (m), L is the channel length (m) and v is the kinematic viscosity of the broth ($m^2.s^{-1}$). The diffusion coefficient is in turn given by the Stokes-Einstein relationship for diffusivity:

$$D = \frac{k_b T}{6\pi\mu r_p} \qquad [1.7]$$

where k_b is the Boltzman constant, T is the temperature (K), μ is the viscosity (Pa.s) and r_p is the radius of the diffusing particle (m). In this study a value of 3.5×10^{-10} $m.s^{-1}$ was used.

By assuming that the cells at the membrane surface resemble a layer of closely packed spheres having 65 - 75 % solids by volume (Porter 1972) the experimental values of steady state permeate flux to calculate K_p can be used to predict the

steady state permeate flux. It has been suggested (Okec 1998) that operating conditions using high volumetric crossflow rate and TMP be used to estimate K_p in order to reduce error caused by not operating the system in the polarised region.

1.3.4 Permeate Flux and the Effect of Fouling and Boundary Layers

The formation of fouling cake and boundary layers as has been explained previously, are causes of flux decline. Fouling is caused by solute/solid – membrane interactions that result in a physical adsorption of the solute/solid to the membrane. This can occur at the surface or within the pores (surface or entrapment respectively), the resulting cake impedes the flow of material through it, which can be worsened by the compression of the cake (Kawakatsu *et al.* 1993). The velocity boundary layer builds up because of friction between the static membrane and the fluid stream which reduces the crossflow velocity at the membrane surface. This in turn reduces the shear and therefore the back-transport of material away from the membrane surface as discussed in Section 1.3.1.

Figure 1.12 is a representation of the concentration boundary or gel layer. This gel layer is caused by the transport of solutes to the membrane surface faster than they can be removed by the crossflow and faster than they can pass freely through the membrane. This concentration polarisation can inhibit the passage of solutes across the membrane due to concentration or repulsion by the accumulation of like-charged proteins. The total hydrodynamic resistance of the membrane can be used to predict flux using the equation:

$$J = \frac{TMP}{\mu R_t} \qquad [1.8]$$

where TMP is the transmembrane pressure (Pa) and R_t is the total hydrodynamic resistance (m^{-1}).

R_t can be defined as the sum of the membrane resistance (R_m), the cake resistance (R_c) and the resistance due to blocking of the pores (R_b), which are related by the following equation (Kawakatsu *et al.* 1993):

$$R_t = R_m + R_c + R_b \qquad [1.9]$$

The membrane resistance can be measured using the clean water flux. When using pure water equation [1.8] becomes:

$$J = \frac{TMP}{\mu R_m} \qquad [1.10]$$

The resistance of the membrane can then be calculated by plotting flux against transmembrane pressure, the gradient of the graph being $1/R_m\mu$. It is more difficult to measure the cake resistance and the resistance due to blocking of the pores.

In crossflow filtration it is the shear caused by the tangential flow that minimises these boundary layer effects. Flux decay due to fouling and concentration polarisation can be minimised by increasing crossflow (Reismeier *et al.* 1989; Gyure 1992). Shear can also be increased through the use of cartridge designs which include the use of turbulence promoting spacer screens within the feed channel (da Costa *et al.* 1991), this causes the formation of vortices which enhance shear at the membrane surface. This can lead to deleterious effects, since vortex

formation and high crossflow rates can lead to air entrainment and it has been shown that air-liquid interfaces are the most common cause of protein denaturation in tangential flow filtration systems (Narendranathan and Dunnill 1982). Interactions between protein and the membrane is greater when calf serum albumin (CSA) is denatured (Chandavarkar and Cooney 1989) and a build up of protein at the membrane surface reduces flux.

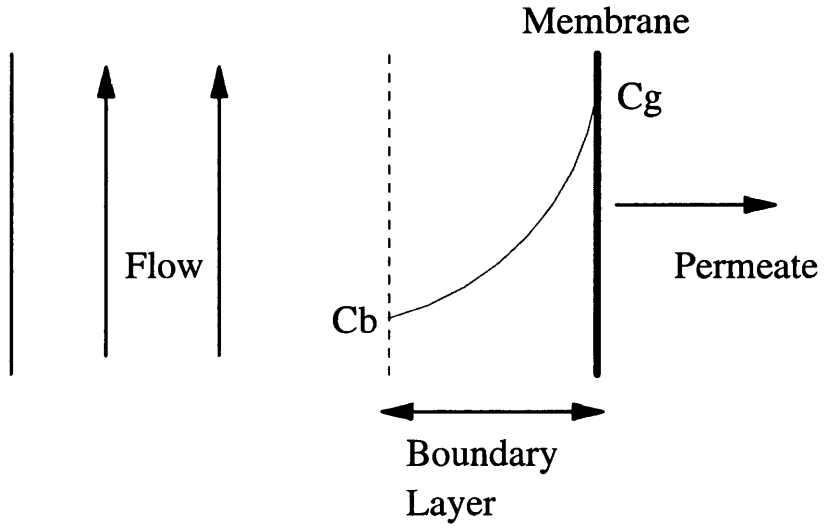

Figure 1.12. A diagram showing the boundary layer effect. A gel-like layer builds up at the membrane. The concentration of cells increases as the membrane is approached, from C_b - the bulk concentration in the feed stream to C_g the gel concentration at the wall (Porter 1972).

The modelling of fouling has been researched for some time, as has already been discussed, though the mechanisms of fouling are not well understood. Although protein is filtered by the cake formed on the membrane in MF, it is not filtered according to molecular weight. Different factors such as charge, hydrophobicity and formation of aggregates must be involved (Hernandez-Pinzon *et al.* 1997). Also, in a 'clean' system, blocking of the membrane is not caused by a uniform mono-molecular layer in cattle serum albumen (CSA) solution. It tends to build up around the pore entrances (Chandavarkar and Cooney 1989). Fouling by proteins can also be reduced by changing the materials of construction of the membrane.

Using a hydrophilic structure reduces the amount of protein binding by changing the surface chemistry in such a way as to reduce the protein-membrane interaction or to operate away from the iso-electric point on the protein which reduces the chance of precipitation and therefore adsorption.

1.3.5 Particle and Antibiotic Transmission

As has been previously stated, (Section 1.2.3), the transmission of particles through the membrane can have a detrimental effect on processes further downstream. Berthold and Kemken (1994) discussed the need for further clarification of supernatant after centrifugation before putting the liquor down a column, whereas microfiltration of fermentation broth required no pre-treatment.

It is clear that by increasing the efficiency of each unit operation, less product will be lost during the processing and therefore profit will increase. The transmission across the membrane is thus of great importance when considering the suitability of microfiltration to the biotechnology industry. A mean transmission percentage of 97% has previously been achieved by Antoniou *et al.* (1990) in simulated broth experiments. By optimising parameters for microfiltration according to harvest time, flux and transmission, the most effective conditions will be determined.

1.4 Process Interactions

Figure 1.12 shows some of the factors involved in the processing of an antibiotic, from the fermentation, through MF to a further downstream step such liquid-liquid extraction. It demonstrates that the whole process must be considered and in the case of the fermentation, the time of harvest also (discussed in Chapter 4).

1.4.1 Medium Composition

Media used for the industrial cultivation of micro-organisms can be highly variable and complex. By the time the broth has been harvested the complexity has also been increased by the growth of the organism, the extracellular products produced and the contents of lysed cells. The residual lipids of oil-based medium in the harvested broth can cause a considerable fouling effect on the membrane as discussed in Section 1.1.1.4.

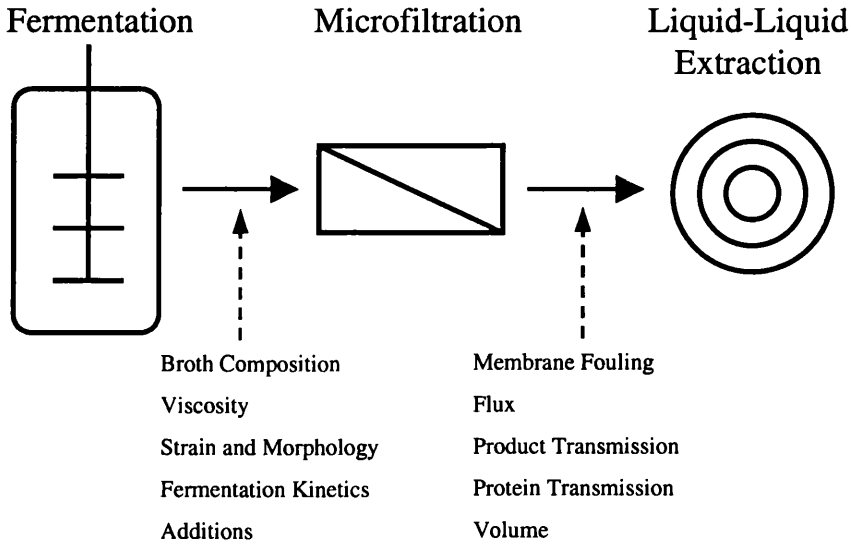

Figure 1.13. Some of the factors affecting processes upstream and downstream of MF.

1.4.2 Morphology and Rheology

The rheology of the broth is dependant on time within the reactor because of changes in mycelial concentration and morphological characteristics of the biomass in the media (Karsheva *et al.* 1997), as shown in Figure 1.6. The viscosity increases as the biomass concentration increases and the hyphae become more branched (Sarra *et al.* 1996). This affects MF due to the link between the time of the fermentation, the viscosity of the broth, and the crossflow velocity. This is

because as the crossflow is increased as does the shear rate (γ) and therefore the apparent viscosity decreases, as described in Section 2.3.3.3. To determine viscosity the shear rate in the system must be determined for a non-Newtonian fluid. The shear (γ) at the membrane surface can be described as (Porter 1972):

$$\gamma = \frac{6U}{b} \qquad [1.11]$$

where U is the crossflow velocity of the fluid ($m.s^{-1}$), b is the channel height (m) for the Minitan II, $b = 3.56 \times 10^{-4}$m.

The concentrations of DNA, tetrahydro-vitamin K (a cell membrane component) and free amino acids in the liquor increase dramatically late in the fermentation of *Nocardia lactamdurans*, which demonstrate that there is cell lysis in the later stages of the fermentation of micro-organisms (Chartrain *et al.* 1991). Details of intracellular component release under controlled breakage has been studied in *S. erythraea* (Heydarian 1998a). These components that are released after cell lysis can increase viscosity and therefore decrease flux. However, there is no average increase in apparent viscosity observed because of the associated decrease in biomass concentration. The cell lysis does increase the loading of impurities on primary separation and the processes downstream of it. In this way the time of harvest is therefore important, since left too long, cell lysis can lead to unfavourable process conditions.

1.4.2.1 Hyphal Morphology and Microfiltration

The type and size of particles and their effects on microfiltration have been studied, (Shimizu *et al.* 1997), as have the effects of the compressibility of the fouling layer

formed on the membrane surface, (Kawakatsu *et al.* 1993; Hamachi and Mietton-Peuchot, 1999). Kuberkar and Davis (1999) found that adding yeast in small amounts (<5 $g.L^{-1}$) improved the filtration of a protein solution by acting as a secondary filter, preventing the formation of protein aggregates. It has been shown for single celled bacteria that flux is related to the species being filtered, (Nakanishi *et al.* 1987). The specific resistance of the cake (see Equation [1.8] and [1.9]) depended on the species of the bacteria and similar sized and shaped species had similar flux rates. It was found that the more eliptical the bacterium, the less compressed the cake could become and the higher the permeate flow rates observed. If morphology affects the microfiltration performance and fermentation conditions affect morphology, then it may be possible to predict how a change in the fermenter will affect the microfiltration. As discussed in Section 1.1.4.3, the size of the hyphae can be related to the power input into the fermenter and it has been suggested that the hyphal size can be used to predict the steady state permeate flux (Davies *et al.* 2000).

1.4.3 Additives

Antifoams have been shown to adversely affect membrane fouling (Liew *et al.* 1997). Antifoams have high surface activity and are non-stabilising and therefore stop the build up of bubbles at air-liquid interfaces. However, this means that it is more likely to interact with the membrane surface (Flair 1985). This is complicated by the tendency in industry to use a tailored formulation comprising the primary antifoam mixed with a carrier, secondary antifoam, emulsifier and stabilising agent (Flair 1985). As a result any change in the formulation of the antifoam, or indeed any additive, will affect the filtration process.

The pH can have an effect on the flux of a broth as can salt concentration (Li *et al.* 1997). Since pH control takes place during a fermentation, the ideal growth conditions may be different from those for microfiltration. Further addition of buffer may be required for diafiltration, to maximise product recovery. The choice of buffer will depend on the chemical properties of the product in preparation for liquid-liquid extraction.

1.5 Scale Down

1.5.1 Incentives for Scale Down

Pharmaceuticals have only a limited life-span over which a company can reclaim the costs of the discovery, development and marketing of the product. Given that a patent only lasts for twenty years and time to market can be in excess of ten years, it is clear that the economic penalties are significant if the development of the production process is too long. The manufacture of supplies and/or the commencement of commercial production are the rate limiting activities for drug development (Vickroy *et al.* 1996). It must be considered that not only the costs of developing successful products must be recouped, but also the costs of products that do not reach the market place. In an industry where contracting or in-house production up to early clinical trials can cost hundreds of thousands of dollars a year, expenditure are important. Faster development can have tremendous paybacks, for example: 15 % interest on $200M development costs work out to be $80k per day. If it is estimated that a product has an annual revenue of $200M dollars, then for every day that it does not reach the consumer, $550k per day of revenue is lost.

The use of reduced scale models can increase the speed and efficiency of process development in a number of ways. The operational conditions for product preparation could be identified quickly and inexpensively (Mannweiler and Hoare 1992). Predicting the effects of changes to an existing process at small scale removes the expense of testing at large scale, and the need to run larger pilot scale tests for trouble shooting and further optimisation and the identification of process limits would be reduced (vanReis *et al.* 1997). Validation requirements would be reduced to a certain extent, however this is best performed in the manufacturing facility to be licensed (Gardner *et al.* 1996).

1.5.2 Scale Down of Fermentation

Scaling down fermentations has a number of repercussions on downstream operations. These include the composition of the harvested broth due to differing rates of substrate utilisation (Mirjalili *et al.* 1999). Altered morphologies of the biomass, since conditions can affect the nature of the growth of the organism (Bushell *et al.* 1997). Additives to the broth such as pH control and antifoam which will be distinct from larger scale operations because of different mixing techniques, aeration and growth considerations.

Bosnjak *et al.* (1985) noted that scale down of fermentation can be a reliable predictor of what can happen at larger scales by the application of mathematical models (see also Ozbek 1997). This does not predict what will happen further downstream as a result of these changes. If unit operations are studied independently then an improvement in one may result in an overall loss of productivity. For example, Martin and Bushell (1996) have discussed the effect of stirrer speeds in *S. erythraea* fermentations on the hyphal length of the broth. This

difference in morphology due to shear is likely to affect downstream processes such as centrifugation and filtration because of the physical nature of the separation. Mechanical shear effects will also change the rheology of the broth (Warren *et al.* 1995) which will in turn have direct effects on crossflow filtration systems, since the rate of permeate flux is inversely proportional to the viscosity. It has also been shown that for mycelial cultures, the rheology and morphology can be only partially dependant on each other (Lilly *et al.* 1992), indicating an even more complex relationship.

It has been shown that oxygen limitation induces secondary metabolite formation, with particular reference to *S. erythraea* (Clark *et al.* 1995). Since the concentration of product in the retentate will effect transmission of the product across the membrane (Porter 1972), the aeration conditions at industrial and bench scale could be critical. The problems associated with oxygen transfer and mixing during scale-down have been discussed in the literature (Oosterhuis 1983; Oosterhuis *et al.* 1985; Sweere *et al.* 1988).

Variations in additives, such as limited or no pH control at small scales is discussed by Dahlgren *et al.* (1991). Although this is discussed with relevance to biomass, there can be a deleterious effect on crossflow filtration, since altered pH at bench and larger scales can cause protein precipitation at the membrane surface. Addition of antifoam will also vary at differing scales, since reactor volume increases as a function of m^3 and the surface area of the vessel (at the liquid-gas interface) as a function of m^2. The amount of antifoam required is a function of surface area of the vessel and not the volume, therefore volume of antifoam does not increase proportionally with reactor size. Foaming is affected by the area of the liquid-gas

interface and therefore, at small scale a larger amount of foaming would be expected and so more antifoam per unit volume of fermentation is required. The effects of which have been discussed previously in Section 1.5.3. The inclusion of a mechanical foam breaker to reduce this problem is both expensive and impractical at smaller scales.

1.5.3 Scale Down of Microfiltration

Since truly scaleable crossflow filtration is a relatively new process to be adopted by the biotechnology industry, it is important to show reliable techniques in order to model or simulate the operation of larger equipment *i.e.* at the pilot or production scale (Mannweiler and Hoare 1992). Scaling of microfiltration equipment is difficult for a number of reasons. Due to the high biomass concentration in the feed stream, which can lead to severe membrane fouling and therefore a reduction in flux rate, there is usually a need for a diafiltration washing step which adds an additional factor to the calculation on scale-up (Okec 1998). Membrane loading at larger scales can also affect reproducibility (Lee and Buckland 1995; Russotti *et al.* 1995a). Russotti *et al.* (1995b) reported that there was a problem of flux decreasing with increased membrane fouling. Since this is affected by several factors, including, shear rate, transmembrane pressure, and medium composition - which are all scale dependant, they would need to be investigated to discover the effects on larger equipment.

As a result of the complex nature of the relationship between the different processing volumes, computer simulations based on experimental results are used in order to cope with the large number of variables (Okec 1998; Kuriyel 1993). Other methods to provide a structured approach to scaling experiments include

decreasing the number of factors investigated. vanReis *et al.* (1997a) cites constant membrane channel length as a more effective method of linear scale-up. The membrane is suggested as the only constant for both small and large scale (de-los-Reyes 1990). Brose *et al.* (1996), have shown that different devices at various scales will behave in distinct ways. These differences could be described mathematically and so could be taken into account for a prediction between scales.

In the literature excellent results have been obtained for the reproducibility of microfiltration permeate flux and product transmission for different processing volumes (vanReis *et al.* 1997; Brose, *et al.* 1996). These studies have, however used simulated broth for the feed stream. It is important that real broth is used in order to understand how a large scale broth will effect membrane performance since rheology, morphology and concentrations of solutes, suspended solids and residual oils will be different to an idealistic interpretation of what the harvested broth may be like.

1.6 Aims of Thesis

It is the aim of this thesis to better define the separation of *S. erythraea* cells from fermentation broth by crossflow microfiltration. It is not the goal of the research to optimise a single unit operation, but to understand how making changes to the fermenter media components and, or operating conditions impacts on the primary separation of the cells from the liquor via crossflow microfiltration. The driver for this research stems from the ability to create novel polyketides by the genetic modification of *S. erythraea.* These polyketides will require the development of manufacturing processes tailored to their biological and chemical characteristics. The interactions between fermentation and primary recovery take place in a

number of ways and are not independent of each other. Firstly the effects of changing medium composition and operating conditions on the profile and productivity of the fermentation will be investigated. These changes are then examined with respect to the impact to the MF step and how changing the operation of the MF will improve efficiency. This is in order to understand what the effects of changing the medium composition will be on subsequent processes.

In order to understand the processes that govern permeate flux decline the interactions between the membrane and the biomass will be examined. Image analysis is used to quantify the morphology of the organism to assess its affect on the microfiltration. It is also to be evaluated as a tool for at-line biomass determination in fermentation broth where conventional methods are not possible. Finally using the data collected, a model is to be developed for the prediction of permeate flux based on measured parameters which describe the organism, the fermentation and MF operation. This is then scaled from lab, to pilot plant equipment.

A 'tool-box' of methods and models for the investigation of process-process interactions will then be available for the rapid assessment of changes to individual unit operations and the effects of these changes on the wider aspects of the whole process.

2. Materials and Methods

2.1. Materials and Micro-organism

The strain used in these experiments was *S. erythraea* CA340 which was kindly supplied by Abbott Laboratories (Chicago, USA). Spore stocks were stored in a 20 % (v/v) glycerol solution at –70°C. Chemicals were purchased from Sigma-Aldrich Company (Dorset, UK) unless otherwise stated and were of analytical grade. Reverse osmosis (RO) water was used throughout for medium preparation.

2.2. Fermentation Media, Equipment and Operation

2.2.1. Fermentation Media

Two different media were used for the fermentation and microfiltration studies, one was a soluble complex medium (SCM) and the other an oil-based medium (OBM) which also contained suspended solids in the form of un-dissolved flour.

Soluble Complex Medium (SCM)	Concentration ($g.L^{-1}$)	Oil-Based Medium (OBM)	Concentration ($g.L^{-1}$)
D-Glucose	30	Soya bean flour	30
Yeast extract*	6	Rape seed oil^{+}	23
Bacto-peptone*	4	Dextrin	10
Glycine	2	KH_2PO_4	1.2
$MgSO_4.7H_2O$	0.5		
KH_2PO_4	0.68		
Poly-Propylene Glycol (PPG) 2025	2.5	Poly-Propylene Glycol (PPG) 2025	2.5

Table 2.1. The compositions of the two media used in this study. * denotes chemicals supplied by Oxoid (Poole, U.K.), $^{+}$ denotes chemicals supplied by Abbott Laboratories.

Both have previously been used in fermentation studies within this laboratory (Sarra *et al.* 1996; Heydarian 1998a; Mirjalili *et al.* 1999). Their compositions are listed in Table 2.1.

2.2.2. Fermentation Equipment and Operation

Two fermentation vessels were used during this work. Both were stirred tank reactors with three equally spaced, six bladed Rushton turbine impellers and were of comparable geometries, however some differences should be noted. The 20 L fermenter was top driven and used a bar sparger, the impeller shaft was supported by a bush in the bottom plate and the vessel was made from glass with stainless steel top and bottom plates. Heating was controlled by an electric element and cooling by passing process water through coils within the vessel. The 42 L vessel was bottom driven and used a ring sparger. The top of the impeller shaft stopped at approximately the working volume (gassed) and the vessel was of all stainless steel construction. Heating was also maintained by an electric element, but cooling was controlled by the flow of process water through the jacket. The complete dimensions of both vessels are given in Table 2.2.

For all fermentations dissolved oxygen tension (DOT) was measured using probes made by Ingold Messtechnik AG (Urdorf, Switzerland) which were sterilised *in situ*. The probe was calibrated for zero and 100 % readings using an Ingold DOT simulator. Probe response was tested outside the vessel by passing nitrogen gas (BOC, Surrey, U.K.) over the membrane and re-adjusting for 100% inside the vessel by sparging air at the desired flow rate through the sterile medium. The pH was measured using a Mettler Toledo probe (Mettler Toledo GmbH, Urdork,

Switzerland) also sterilised *in situ* and calibrated outside the vessel using standards at 4.01 and 7.00 (BDH chemicals, Merck Ltd., Lutterworth, U.K.).

Dimensions		Vessel (ID Number)	
		LH 42 02	LH 20 01
Total volume (L)		42	20
Working volume (L)		28	14
Vessel height (mm)		743	510
Vessel diameter (mm)		270	230
Shaft height (mm)		567	490
Shaft diameter (mm)		20.0	12.7
No. of impellers		3	3
Impeller diam. (mm)		88	68.7
Tip dimensions	Length (mm)	20	16
	Width (mm)	18	14.4
	Height (mm)	1.5	2
Sparger height (mm)		535	508
Sparger	Diameter (mm)	18	9.5
	Hole diam. (mm)	N/A	22
	No. of holes	N/A	6
Baffle dimensions	Height (mm)	586	355
	Width (mm)	25	22
	Thickness (mm)	5	1.8
Impeller positions	1 (mm)	90	75
(from base)	2 (mm)	265	155
	3 (mm)	399	245

Table 2.2. The dimensions of the fermentation vessels used in this study.

2.2.2.1. Inoculum Preparation

Spore stocks were initially prepared from *S. erythraea*, the medium used contained 2 $g.L^{-1}$ D-glucose, 1 $g.L^{-1}$ sucrose, 5 $g.L^{-1}$ soy peptone (Oxoid, Poole U.K.), 2.5 $g.L^{-1}$ yeast extract (Oxoid, Poole U.K.), 1.0 $g.L^{-1}$ calcium carbonate, 20 $g.L^{-1}$ agar (Technical No 1 – Oxoid, Poole U.K,). The pH was adjusted to 7.0 using 0.1 M NaOH before autoclaving. The Petri dishes were incubated for three weeks at 28°C, spores were then removed and placed in 20 % (v/v) glycerol containing 0.1 % (v/v) Tween 80 and stored at –70°C.

For the inoculation of the fermenters, 1 mL of spore stock was first thawed and added to 50 mL of nutrient broth in a 500 mL baffled, conical flask which was then placed in an orbital shaker (model G25 New Brunswick Scientific Co. Inc. N.J. U.S.A.) at 28°C for 48 h. This culture was then transferred to 450 mL of the relevant medium (SCM or OBM) in a 2 L baffled conical flask and placed in an orbital shaker at 28°C for 30 h (SCM) or 48 h (OBM). The inoculum volume used was 10 % of the final working volume of the relevant fermenter.

2.2.2.2. 20 L Fermentations

These fermentations were carried out in a LH 2000 series fermenter (Inceltech Ltd., Pangbourne, U.K.) having a total volume of 20 L and a working volume of 14 L. The vessel had a height to diameter ratio of 2.2:1, the impeller consisted of three 6-bladed Rushton turbines. Four equally spaced baffles were present. The fermenter was sparged with air at a variable aeration rate (0.33 to 1.0 vvm) and maximum impeller speeds between 750 and 1250 rpm were used depending on the dissolved oxygen tension (DOT) which was manually kept above 20 % without exceeding the upper impeller speed of 1250 rpm.

The fermenter was controlled and data logged using Bioview (Adaptive Biosystems Ltd., Luton, U.K.). On-line exit gas composition was measured using a mass spectrometer (model: MM8-80S VG Gas Analysis Ltd., Cheshire, U.K.). The maximum volume of broth removed from the fermentation for the subsequent microfiltration studies (and analysis) was 3 L in order to keep the level of broth above that of the top impeller. Each fermentation was carried out in triplicate.

2.2.2.3. 42 L Fermentations

The LH 42 L fermenter (Inceltech Ltd., Pangbourne, U.K.) was used to carry out fermentations on SCM broths for tip speed and morphology investigations, (Sections 3.3 and 5.2 respectively) and for subsequent microfiltration studies (Sections 4.4). Vessel height to diameter ratio was 2.7:1, agitation is via three equally spaced, six-bladed Rushton turbine impellers and the tank contains four baffles. Control of parameters was carried out by individual control units (Turnbull Control Systems Ltd., Worthing U.K.). and logging was carried out using Propack (Acquisition Systems Ltd., Sandhurst, U.K.). The airflow rate was kept at 0.5 vvm and on-line gas analysis was carried out using a mass spectrometer (Model: VG Prima, VG Gas Analysis Ltd, Cheshire, U.K.). The DOT was not controlled since it did not fall below the minimum value of 20 % for any of these fermentations.

2.2.3. Off-line Analytical Techniques (Fermentation)

2.2.3.1. Residual Glucose Concentration

The glucose assay used was based on the reducing sugar method with dinitrosalicylic acid (DNS) as described by Miller (1959). Broth samples were diluted by factors of 10 or 20 with RO water, 0.4 mL of diluted samples were then dispensed into test tubes to which 0.5 mL of DNS reagent was added. Samples were incubated in boiling water for 5 min. The tubes were then placed on ice and 4 mL of water added, after which the absorbance was read at 540 nm. Glucose concentrations were calculated from a standard curve, as shown in Appendix I. All measurements were performed in triplicate, with the mean of all recorded measurements having a standard error of 2.8 %.

2.2.3.2. *Residual Oil Concentration*

Residual oil levels were determined by hexane extraction based on the method of Junker *et al.* (1998). A 5 mL volume of sample was vigorously mixed with 15 mL of hexane for 3 min and then centrifuged at 4000 rpm for 30 min to separate the phases. A 1 mL sample of the hexane phase was then dispensed into a pre-weighed aluminium container and dried at 85°C in an HG53 Halogen Moisture Analyser (Mettler-Toledo GmbH, Urdorf, Switzerland) to constant weight. All samples were measured in duplicate and the mean and standard deviation calculated, average standard error in the assay was 4.2 %.

2.2.3.3. *Biomass Concentration*

For SCM broth samples, biomass concentrations were determined by filtering 5 mL of broth through a 0.2 μm, 25 mm diameter filter (Whatman Industries Ltd., Surrey, U.K). The biomass sample was then dried to constant weight using a HG53 Halogen Moisture Analyser (Mettler-Toledo, Urdorf, Switzerland). All samples were measured in triplicate and a mean and standard deviation calculated, the standard error was 4.2 %. The biomass concentration of the OBM broth could not be determined directly due to the presence of large quantities of undissolved soya flour.

2.2.3.4. *Broth Viscosity*

For OBM fermentations viscosity values were used as a substitute for direct biomass measurement as the undissolved solids content of the OBM meant that direct biomass determination was impossible. It has been shown previously that biomass concentration is directly proportional to broth viscosity (Karsheva *et al.* 1997).

Viscosity of the OBM broth was measured as a comparative value at a single shear rate (71 s^{-1}) using a Brookfield cone and plate rheometer (model: DV-II+, U.K.). Viscosity measurements were carried out in triplicate and the mean error of the assay was found to be 2.4 %.

2.2.3.5. Image Analysis

Image analysis of SCM and OBM broth samples were carried out using the method described by Packer and Thomas (1990). Image were processed using a Magiscan 2A image analyser (Joyce Loebl Ltd., Gateshead, U.K.) which was connected to a Polyvar microscope (Reichert-Jung, Vienna, Austria). This was fitted with an automated stage which measured 25 separate areas on each slide in a 5 x 5 grid pattern. A video camera (Bosch, UK) was used for image capture. The variables measured were main hyphal length (ML), branch length (BL), total hyphal length (HL), number of tips (NT), major axis (OL), minor axis (OB), mycelial area (MA), clump area (CA), projected area (OD), total area (OA) and circularity (OC) as described by Heydarian (1998a). The number of objects measured varied between 30 to 988 individual objects per sample.

Measurement	Mean Error (±)	Measurement	Mean Error (±)
ML	6.7 %	MA	9.1 %
BL	10.8 %	CA	21.9 %
HL	8.7 %	OD	17.8 %
NT	3.9 %	OA	20.7 %
OL	6.6 %	OC	6.1 %
OB	10.1 %		

Table 2.3. Mean errors for morphological measurements.

2.2.3.6. Erythromycin Concentration by HPLC

Erythromycin A concentration was determined by HPLC using a method described by Heydarian *et al.* (1998b). Fermentation broth samples were centrifuged at 4000 rpm for 20 min (Beckman CS-6R centrifuge, Beckman, Bucks. U.K.) and the supernatant was collected for analysis. For OBM samples further centrifugation at 12000 rpm and filtration through a 0.2 μm membrane were required to obtain a clear sample. Erythromycin was then concentrated (x 10) using C18 bond elute cartridges (Phenomenex, Cheshire U.K.). HPLC analysis was then performed on a Beckman model 126 HPLC system equipped with a Beckman model 166 UV detector operated at 215 nm. The column used was a Polymer Laboratories PLR P-S (8 μm). Acetonitrile in 10 mM potassium dihydrogen phosphate (pH 7) (45:55 v/v) pumped at 1.0 $mL.min^{-1}$ was used as the mobile phase. The column temperature was controlled at 70°C with a block column heater and the sample injection volume was 20 μl. Due to the cost of the C18 columns, the assay was carried out once on each sample. The mean percentage standard deviation of this assay was found to be 3.4 %

2.3. Microfiltration Rigs and Operation

2.3.1. Minitan II Rig and Operation

The Minitan II rig (Millipore, U.K.) was used for the majority of the microfiltration studies and was operated in concentration mode with a single pump configuration as shown in Figure 2.1. This system was chosen due to the small volume of broth that could be processed (<500 mL), thus enabling a number of microfiltration studies to be carried out during the time course of each fermentation. The pump used was a peristaltic Watson-Marlow Du505 (Watson-Marlow, Poole, U.K.). The volumetric

crossflow rate was kept constant close to the maximum value possible, at 800 $mL.min^{-1}$ which gave a crossflow velocity of 0.60 $m.s^{-1}$ at the membrane surface. The membrane used was a 0.2 μm hydrophilic Durapore membrane, a single membrane plate was used with a membrane area of 6 x 10^{-3} m^2. A hydrophilic membrane was chosen to minimise fouling by proteins (Zhang *et al.* 1998) and anti-foaming agents (Liew *et al.* 1997). The connecting tubing used was silicon (Altec, Hamp. U.K.) with internal diameter of 6.2 mm and wall thickness of 1.6 mm. The total path length was 1.5 m giving a tubing hold-up volume of 45 mL.

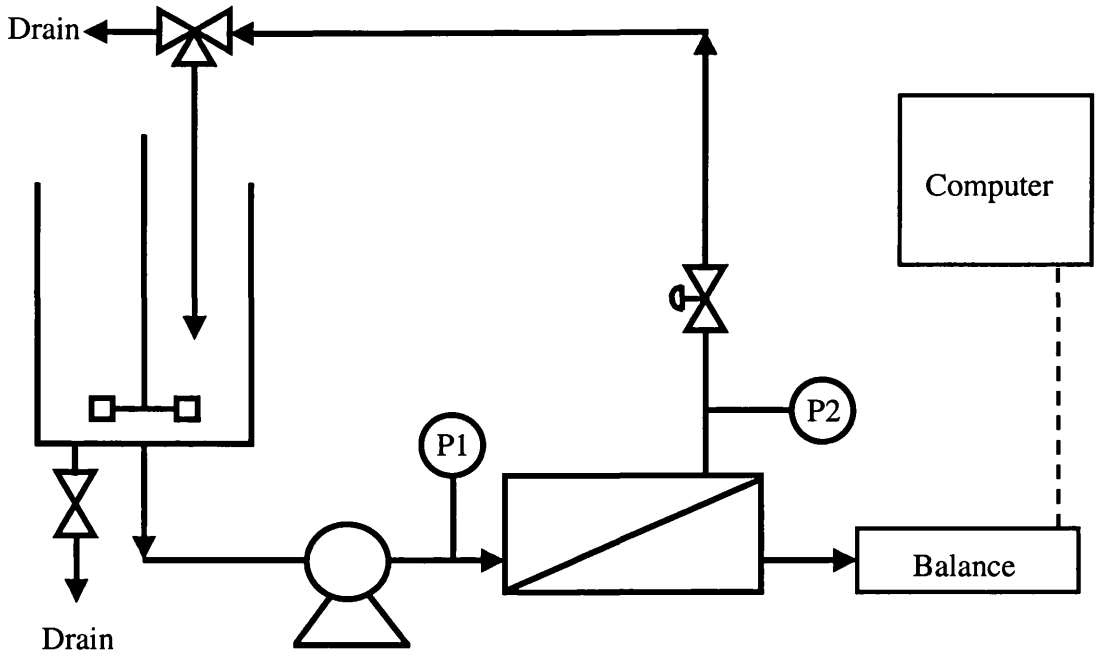

Figure 2.1. Diagrammatic representation of the Minitan II Acrylic rig. P1 and P2 are the inlet and outlet pressure gauges respectively.

The fermentation broth feed was kept homogenous in the reservoir by using an SS2 stirrer (Stuart Scientific, U.K.) with a 7 cm diameter 6-bladed Rushton turbine impeller rotated at 100 rpm. The permeate flux and the volumetric crossflow rate were measured using an electronic balance (model BB2400 Metler-Toledo Ltd., Leicester, U.K.). The balance was connected to a Macintosh IIcx (Apple Computer

Inc., CA., U.S.A.) through a Lab-NB digital to analogue converter card (National Instruments, U.K.). Data from the balance were recorded using Labview the virtual instrumentation software, (National Instruments, U.K.).

Following each experiment, the membrane was washed in reverse osmosis (RO) water to remove solids from the membrane surface. The rig was then flushed with 5 % (v/v) hypochlorite at 50°C for 1 h and 5 % (v/v) Redphos Special SN557 (Kleancare Hygiene, Cheshire, U.K.), a phosphoric acid based cleaner (Laporte ESD Ltd., Cheshire U.K.) at 50°C for 1 h. The membrane was then rinsed with RO water and the clean water flux established; if this was below 0.03 $L.m^{-2}.h^{-1}.Pa^{-1}$ (80 % of the original clean water flux) then the cleaning steps were repeated. Experiments took place at 21°C in a temperature controlled room and no increase in temperature during the pumping of broth could be detected.

2.3.1.1. Effect of Transmembrane Pressure

For each experiment individual permeate flux measurements were taken (over a twenty second time interval) for a period of 30 min; steady state flux values were obtained from the final three readings and a mean and standard deviation calculated. This was repeated over a range of transmembrane pressures, starting with the lowest. Critical transmembrane pressure (cTMP) was taken as the point at which the maximum permeate flux was reached.

2.3.1.2. *Effect of Crossflow Velocity*

For crossflow velocity determination the pump was run at different rotational frequencies (80 - 180 Hz) and this was converted to volumetric crossflow rates and velocities using the balance to determine the rate of change mass of the broth (density was assumed to be that of water). The conversion from pump frequency to volumetric and linear crossflows is displayed in Table 2.4. Transmembrane pressure was kept constant and below the critical transmembrane pressure during the experiments.

Pump Frequency (Hz)	Volumetric Crossflow ($mL.min^{-1}$)	Volumetric Crossflow ($m^3.s^{-1}$)	Linear Crossflow ($m.s^{-1}$)	Reynold's Number (no units)
80	490	8.17E-06	0.4	354
100	610	1.02E-05	0.5	443
120	730	1.22E-05	0.6	531
140	850	1.42E-05	0.7	620
160	970	1.62E-05	0.8	708
180	1100	1.83E-05	0.9	797

Table 2.4. Volumetric crossflow rates and calculated linear velocities. Linear crossflow was calculated by dividing the volumetric crossflow ($m^3.s^{-1}$) by the cross-sectional area of the feed channel (2.02×10^{-5} m^2). Reynold's number was calsulated as described in Section 2.3.3.4.

2.3.2. Pellicon Rigs and Operation

Millipore (MA., U.S.A.) have previously developed a scaleable filtration system in collaboration with Genentech (CA., U.S.A.) based on the theory that constant path length was the best way to scale effectively (van Reis *et al.*, 1997a). The cartridges containing the membranes come in three sizes; 0.1 m^2, 0.5 m^2 and 2.5 m^2. The larger membrane area between 0.1 to 0.5 m^2 was achieved by using a wider membrane channel, whereas the 2.5 m^2 cartridge was the same width as the 0.5 m^2 cartridge but,

uses more channels through which the feed stream passes. The problems related to variable pressure drop across the cartridge, for different path lengths and the associated variations in flux and transmission were therefore avoided.

The cartridges come in different formats depending on the type of turbulence promoting screens that were employed. For the broth used here, the open channel V-Screen cartridge was used because of the low pressure drop. As shown in Section 3.2.3 the broth can get very viscous and the presence of mycelial clumps could block tighter channel designs. As in the Minitan II experiments a hydrophillic Durapore membrane was used with a pore size of 0.2 μm.

2.3.2.1. Pellicon Mini Rig

The Pellicon Mini cartridge holder is designed to take up to four Pellicon-2 0.1 m^2 membrane cartridges. For these experiments however only one cartridge was used so that the maximum difference in scale could be achieved. The holder was connected to the Millipore Proflux M12 self-contained microfiltration rig, which is represented diagrammatically in Figure 2.2. The system consisted of a peristaltic pump, three pressure transducers and a baffled reservoir. Cleaning was carried out as for the Minitan II rig (as described in Section 2.3.1) however the Pellicon Mini was flushed with 9 L of water prior to and after cleaning. The membrane was considered clean once the clean water flux test reached 80 % of the original value.

Flux was measured using a balance (model BB2400 Metler-Toledo Ltd., Leicester, U.K.) and stopwatch over 1 min intervals for 4 replicates after steady state permeate flux had been reached. Although the reservoir on the Proflux M12 was fitted with a baffle to aid mixing induced by the retentate flow, this was found to be inadequate

for such viscous broths. An impeller was thus added to the rig (as described in Section 2.3.1) to ensure thorough mixing of the feed stream. The process was run in concentration mode, and although the crossflow was not measured, the transcartridge pressure drop (TCP), an analogue of crossflow, was kept constant between the two rigs.

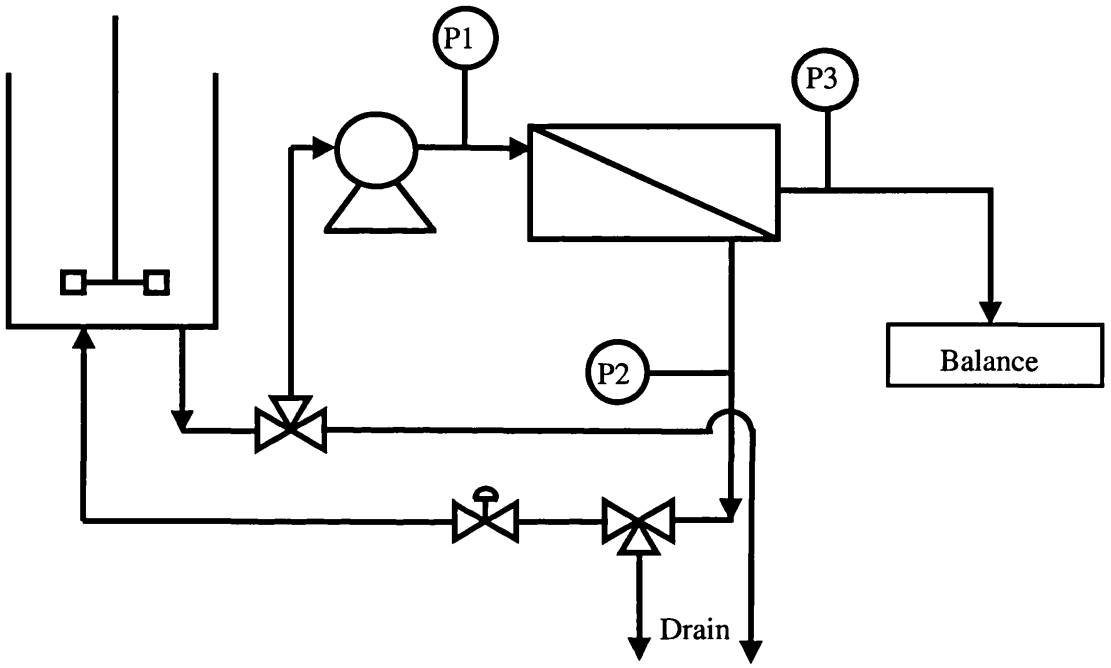

Figure 2.2. Diagrammatic representation of the Proflux M12 rig in one pump format connected to the Pellicon Mini cassette holder. P1, P2 and P3 are the inlet, outlet and permeate pressure transducers respectively.

2.3.2.2. Pellicon Rig

As discussed previously the Pellicon holder can accept cartridges of area 0.5 m^2 and upwards. The rig used to run the larger types of Pellicon cartridges is shown in Figure 2.3. The feed stream was re-circulated using a 0.75 h.p. 50 Hz Lafert motor (Venezia, Italy) and a Procon vane pump head controlled by an SKF Variable speed AC motor drive (SKF Automation Systems Ltd., U.K.). This gave a maximum flow

rate of approximately 15 L.min^{-1}. Flow was measured using a Altometer SC 80 AS magnetic flowmeter and converter (Sliederecht, The Netherlands). Flux was measured using the same equipment as used for the Minitan II experiments (Section 2.3.1). The experiments were carried out under exactly the same conditions as those conducted using the Pellicon Mini (Section 2.3.2.1). Maintaining the inlet, outlet and permeate pressure values identical to those used on the larger pumping rig leads to direct linear scale-up by scaling membrane area by process volume. Volumetric flow rates ranged from 0.48 to 3.84 L.min^{-1}, producing between 5,400 and 43,000 s^{-1} shear rate at the membrane wall. The process was run in concentration mode and temperature was controlled at 21°C.

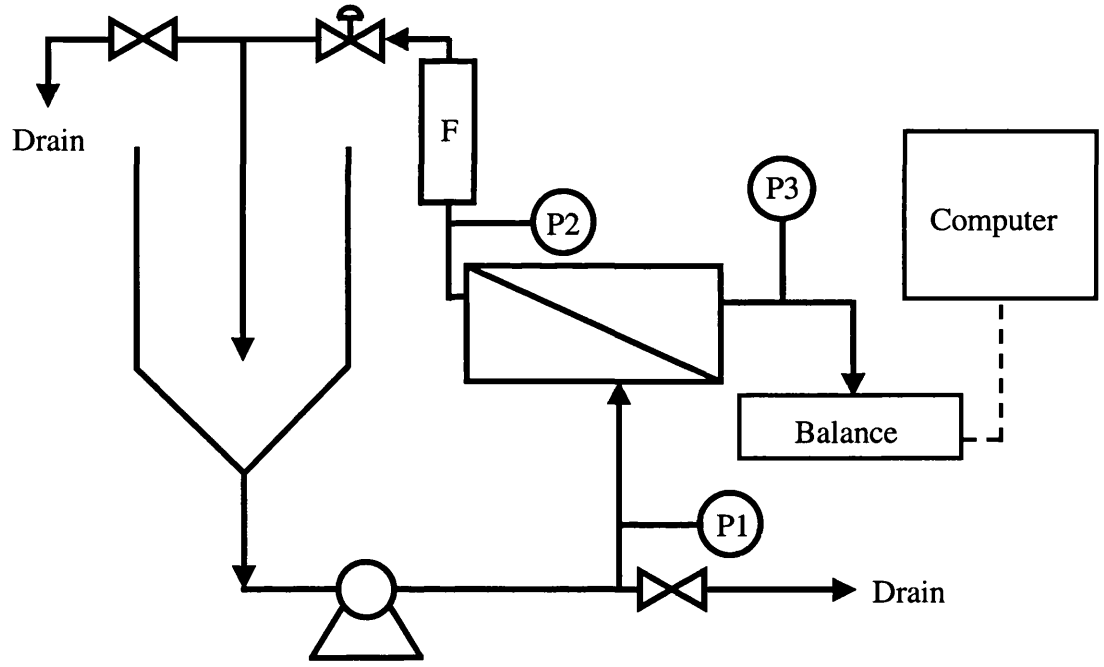

Figure 2.3. Diagrammatic representation of the Pellicon holder (0.5 m^2 and upwards), P1, P2 and P3 are the inlet, outlet and permeate pressure gauges respectively and F is the flowmeter.

Cleaning was carried out by connecting the membrane holder to a model 605 Di Watson-Marlow peristaltic pump (Poole, U.K.). This was because the rig was made

of stainless steel and the cleaning solution (sodium hypochlorite) damaged the piping. Silicon tubing was used in the peristaltic pump and the membrane was cleaned by flushing with 40-50L of water (not returning the retentate to the reservoir) until the retentate was clear and then re-circulating warm (<50°C) sodium hypochlorite for 1 h. This was flushed out (40-50 L of water) and the membrane was rinsed with warm Redphos (<50°C) at 5 % v/v for 1 hour. Temperature was maintained using an MC 810 digital controller and a 500 W heater bar – BD 6933 Red Rod (Electrothermal Engineering Ltd., Essex U.K.). The membrane was then flushed with 40-50 L of RO water, if the clean water flux returned to 80 % that of the original clean water flux then cleaning was deemed successful, otherwise the process was repeated.

2.3.3. Off-line Analytical Techniques (Microfiltration)

2.3.3.1. Protein Transmission

Total soluble protein was measured using Bio-Rad reagent (Bio-Rad Laboratories, Herts., U.K.), a commercial product based on the colour change of Coomassie Blue dye. 50 µL of sample was mixed in a 4 mL curvette with 2.5 mL of Bio-Rad reagent (1:5 dilution) for 5 minutes and the absorbance measured at 595 nm. This was blanked against 2.5 mL of reagent with 50 µL of sterile medium. Protein concentrations were calculated from a standard curve determined using bovine serum albumin (BSA) as the standard protein. An example calibration curve is presented in Appendix I. For the determination of protein transmission values the protein concentration in the permeate was compared to that in a sample of the feed broth which had been spun down at 13,000 rpm in a microfuge (Beckman Bucks. U.K.) to

remove biomass. Each soluble protein measurement was carried out in triplicate and the mean and standard deviation were calculated. The standard error in the assay was found to be 3.3 %.

2.3.3.2. Erythromycin Transmission

Determination of the total erythromycin concentration, i.e. all forms of the antibiotic and not just erythromycin A, in broth and permeate samples was performed using a colourmetric method (Gallagher and Danielson, 1995). This was based on the reaction of a ferric ion (Fe^{3+}) with the lactone ring of the macrolide antibiotics. This method was adapted by drying clarified broth samples under vacuum at room temperature for 2 h (Speed Vac SC 110, Savant, N.Y., U.S.A.) to avoid the interference of water on the assay. After drying, the samples were dehydrated by resuspending the pellet in glacial ethanoic acid to the original volume and heating at 45°C for 45 min in a Grant SS-40 water bath (Grant Instruments Ltd., Cambridge, U.K.). An equal volume of the assay mix (320 mg iron III chloride in 8 mL water plus 8 mL concentrated sulphuric acid and made up to 400 mL with glacial ethanoic acid) was added and then heated at 50°C for 15 min. The samples were then spun down at 13,000 rpm for 5 min to remove solids and the absorbance was measured at 592 nm. The erythromycin concentration in broth samples was determined from a pre-prepared standard curve using known concentrations of erythromycin. An example is shown in Appendix I. Samples were measured in triplicate from which the mean and standard deviation were calculated, the standard error in the assay was found to be 1.5 %.

2.3.3.3. *Broth Rheology and Apparent Viscosity*

Broth rheology was measured using a Contraves Rheomat 115 rheometer (Contraves Industrial Products Ltd., Middlesex U.K.) operated at 20°C (Haake DC1 Circulator and K15 Bath; Haake, Sussex, U.K.). The rheology of the SCM fermentation broth was measured using a concentric cylinder over a range of shear rates between 24.3 s^{-1} and 1256 s^{-1}. For the more viscous OBM broth, a cup and bob attachment was used since solids in the broth can cause inaccurate readings due to friction between the particulates and the walls of the cylinders. These measurements were carried out over a range of shear rates between 6.65 s^{-1} and 117 s^{-1}.

Both culture media were found to exhibit non-Newtonian behaviour and both were found to adhere to the pseudoplastic Power Law or 'shear-thinning' model of viscosity (Atkinson, and Mavituna, 1991):

$$\tau = K\gamma^n \qquad [2.1]$$

where τ is the shear stress exerted on the system (Pa), γ is the shear rate (s^{-1}) and K and n are the consistency and flow behaviour indices respectively (both dimensionless) that describe the behaviour of the fluid. From the values of K and n, the apparent viscosity, μ_a (Pa.s) at a given shear rate can be calculated:

$$\mu_a = K\gamma^{n-1} \qquad [2.2]$$

The apparent viscosity at the membrane surface is determined by first calculating the shear rate at the membrane surface as described by Porter, (1972):

$$\gamma = \frac{6U}{b} \qquad [2.3]$$

Where U is the crossflow velocity ($m.s^{-1}$) and b is the channel height (m). The calculated value of γ is then used with the appropriate values of K and n for each broth sample in Equation 2.2.

2.3.3.4. Reynolds Number

The Reynold's number was calculated to identify laminar or turbulent conditions within the filtration module. The equation used was from Porter (1972):

$$\mathrm{Re} = \frac{U(2b)}{\nu} \qquad [2.4]$$

Where Re is the Reynold's number (no units), U is the mean fluid velocity ($m.s^{-1}$), ν is the kinematic viscosity ($m^2.s^{-1}$) and b is the channel height (3.54×10^{-4} m). From this calculation, the highest Reynold's number is when U is a maximum and ν is a minimum. This happens when U = 0.9 $m.s^{-1}$ (see Table 2.4) and $\nu = 8.05 \times 10^{-7}$ $m^2.s^{-1}$. The maximum Reynold's is therefore 792 (no units), which is in the region of laminar flow.

3 The Effect of Medium Composition and Agitation Rate on S. erythraea Fermentations

3.1 Introduction

In this Chapter the use of different media formulations and varying agitation conditions on the kinetics of growth and erythromycin synthesis by *S. erythraea* are investigated. The composition and physical properties of the fermentation broth over time are also described in order to characterise the feed streams used in subsequent microfiltration studies (Chapter 4). As previously explained in the Section 1.1.4 the media used for fermentation operations can have profound effects on product titres, fermentation duration and broth rheology. These in turn can be expected to significantly influence the performance of a subsequent microfiltration operation and the conditions required to optimise permeate flux and product transmission. Part of the work presented in this chapter has also been published as Davies, J.L., Baganz, F., Ison, A.P. and Lye, G.J. **2000**. Studies on the interaction of fermentation and microfiltration operations: erythromycin recovery from *Saccharopolyspora erythraea* fermentation broths. *Biotech. And Bioeng.* **69** 429 – 439.

3.2 Effect of Medium Composition

3.2.1 Medium Selection

Two different formulations of media were selected for use in this thesis based on previous work in this laboratory (Sarra *et al.* 1996; Heydarian, 1998a; Mirjalili *et al.*; 1999). The first represented a complex medium that was totally soluble in water and provided a complete source of nutrients required by the organism. This

is termed the soluble complex medium (SCM) throughout this thesis. The composition was given previously in Table 2.1. The primary carbon and energy source was glucose with nitrogen and trace elements being supplied via the yeast extract, bactopeptone and mineral additions. Potassium di-hydrogen phosphate provided some buffering capacity and a source of phosphate ions.

The second medium was more representative of the type used in industry for the production of antibiotics. This utilises rape seed oil as the main carbon and energy source and soya bean flour as a complex source of nitrogen and trace elements. The composition of this oil based medium (OBM) is also shown in Table 2.1. The rape seed oil is immiscible with water and the soya flour is only partially dissolved in the aqueous phase leading to the formation of a 3 phase system. Dextrin is also present as an initial carbohydrate source to boost growth of the inoculum before the organism switches to oil metabolism (Mirjalili *et al.* 1999). Potassium di-hydrogen phosphate is again used as a supply of phosphate and as a buffer.

The OBM is much cheaper than the SCM since the main components are readily available in bulk and require minimal processing. When dealing with fermentations of up to 300 m^3 scale, media costs become important as described in Section 1.1.4. The slower growth of *S. erythraea* on OBM can also lead to increased product titres, hence the widespread use of this type of media throughout the industry. Reducing growth rates by strain selection has been used to increase the product titres of erythromycin and other antibiotics (Riviere 1977).

3.2.2 20 L Fermentations

For the purpose of comparing different types of media *S. erythraea* fermentations were carried out in the LH 20 L fermenter as described in Section 2.2.2.2. Three fermentations using each type of medium (SCM and OBM) were carried out in the same vessel to supply broth for fermentation characterisation and subsequent microfiltration experiments (Section 4.2). Each fermentation was operated until the process was past the stage of maximum erythromycin titre. Table 3.1 shows the nomenclature used to describe each of the fermentations from which data are presented. The difference in growth rates, evolved gas analysis, product titres and broth rheology will be discussed later in this Chapter.

Fermentation	Conditions and Uses of Broth	Comments
SCM20L1	20L SCM. Medium comparison Sections 4.1 & 4.2	-
SCM20L2	20L SCM. Medium comparison Sections 4.1 & 4.2	-
SCM20L3	20L SCM. Medium comparison Sections 4.1 & 4.2	-
OBM20L1	20L OBM. Medium comparison Sections 4.1 & 4.2	-
OBM20L2	20L OBM. Medium comparison Sections 4.1 & 4.2	-
OBM20L3	20L OBM. Medium comparison Sections 4.1 & 4.2	-
OBM20L4	20L OBM. Crossflow experiments Section 4.3	No logging
OBM20L5	20L OBM. Crossflow experiments Section 4.3	No logging
OBM20L6	20 L OBM for EFD study Appendix II	-
SCM42L1	SCM, 531 rpm. Morphology experiments Section 5	No logging
SCM42L2	SCM, 710 rpm. Morphology experiments Section 5	No logging
SCM42L3	SCM, 353 rpm. Morphology experiments Section 5	Long lag
SCM42L4	SCM, 353 rpm. Morphology experiments Section 5	-
SCM42L5	SCM, 531 rpm. Crossflow experiments Section 4.3	-
SCM42L6	SCM, 531 rpm. Crossflow experiments Section 4.3	-
SCM42L7	SCM, 531 rpm. Scale-down experiments Section 6	-
SCM42L8	SCM, 531 rpm. Scale-down experiments Section 6	-
SCM42L9	SCM, 531 rpm. Scale-down experiments Section 6	-

Table 3.1. Details of all *Saccharopolyspora erythraea* CA340 fermentations carried out, showing the type of medium used and usage of the broth.

3.2.2.1 Growth of S. erythraea on SCM

Figure 3.1 demonstrates the profile of a typical SCM fermentation (SCM20L3). Biomass increases during the log phase of the fermentation, reaching a maximum concentration of 12 $g.L^{-1}$ at around 40 h. The glucose carbon source showed a corresponding decrease in concentration over this period. The DOT reached a minimum of approximately 20 % at 20 h, at which point the airflow was increased from 5 $L.min^{-1}$ to 7 $L.min^{-1}$ and then to 10 $L.min^{-1}$ so to ensure that sufficient oxygen was available to the organism. The OUR and CER both peaked at 35 hours (~28 $mmol.L^{-1}.h^{-1}$) and the respiratory quotient remained at around 1.0 throughout the duration of the fermentation.

Erythromycin A synthesis exhibited a peak approximately 20 h later at a concentration of 230 $mg.L^{-1}$. This observation is supported by numerous studies that have shown secondary metabolite formation is related to nutrient limitation and a reduction, or cessation of growth (Wallace *et al.* 1992; Lohr *et al.* 1989; Shapiro and Vining, 1983). During the death phase the airflow was stepped down to avoid excessive foaming as oxygen demand decreased. OUR and CER decreased rapidly after maximum biomass concentration was achieved, whereas the cell mass decreased only slowly showing a physiological change in the organism during the production of erythromycin. Finally the RQ decreased at 70 h, which could be due to the utilisation of carbon sources other than carbohydrates after this time.

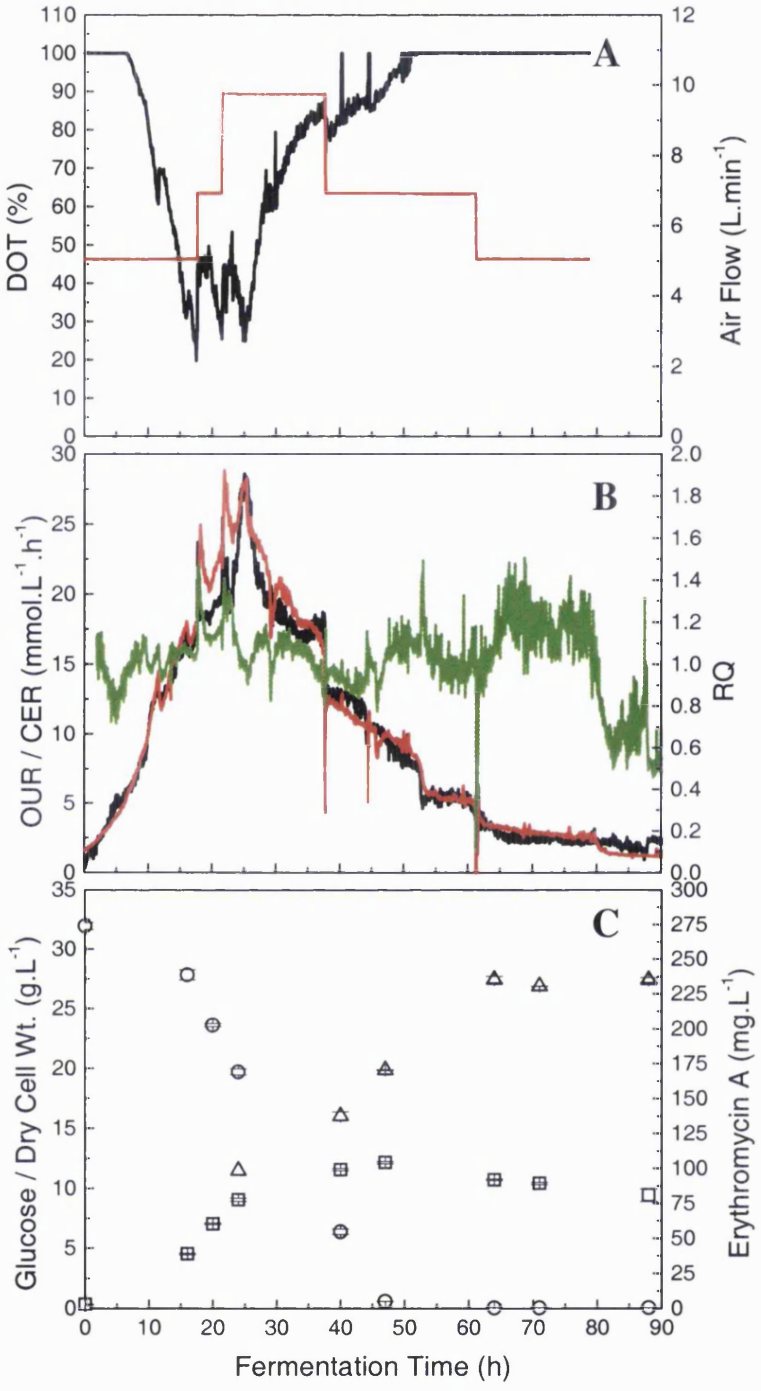

Figure 3.1. Typical fermentation profile for a 20 L SCM fermentation (SCM20L3). Graph A: DOT; —, air flow rate; —. Graph B: OUR; —, CER; —, RQ; —. Graph C: biomass; □, glucose; ○, erythromycin A; △. Fermentations carried out as described in Section 2.2.1.2, off-line analysis as described in Section 2.2.2. Error bars show the standard deviation of three replicate measurements.

3.2.2.2 Growth of S. erythraea on OBM

Figure 3.2 shows the profile of a typical oil based medium fermentation (OBM20L1). Growth leads to increases in oxygen demand, as can be seen by the decreases in DOT, and oil concentrations. The airflow and the impeller speed were both increased to raise the low DOT, however, maximum values were reached, beyond which the gassed volume of the stirred liquid was too great and foaming was too high. The DOT reached zero after 60 h. The RQ remained at approximately 1.0 whilst the organism utilised the dextrin but then dropped to 0.7 as the carbohydrate is depleted and the organism started to grow on the rape seed oil. The OUR reached a peak of 23 $m.mol.L^{-1}.h^{-1}$ after 90 hours.

The decrease in OUR and CER corresponds to a period of zero DOT in the fermenter as operating conditions could no longer support the oxygen demanded by the organism, highlighting the problems of mixing in such viscous broths. The DOT rapidly reaches 35 % before beginning to decrease until 10 – 15 %, where it rapidly decreases to 0 % for 10 h. This is followed by another increase. These cycles are matched by a period of reduced OUR and CER also suggesting that growth is affected. This suggests a rapid metabolic change in the organism after a sustained period of low oxygen availability, which changes again once the dissolved oxygen becomes relatively abundant again. Maintaining oxygen above these levels (35 – 40 %) may be necessary for growth, but not necessarily erythromycin production (Wallace *et al.* 1992). Controlling DOT during this experiment would not have altered the lack of available oxygen in the fermenter since stirrer speed and aeration rate were limited by organism shear and foaming respectively.

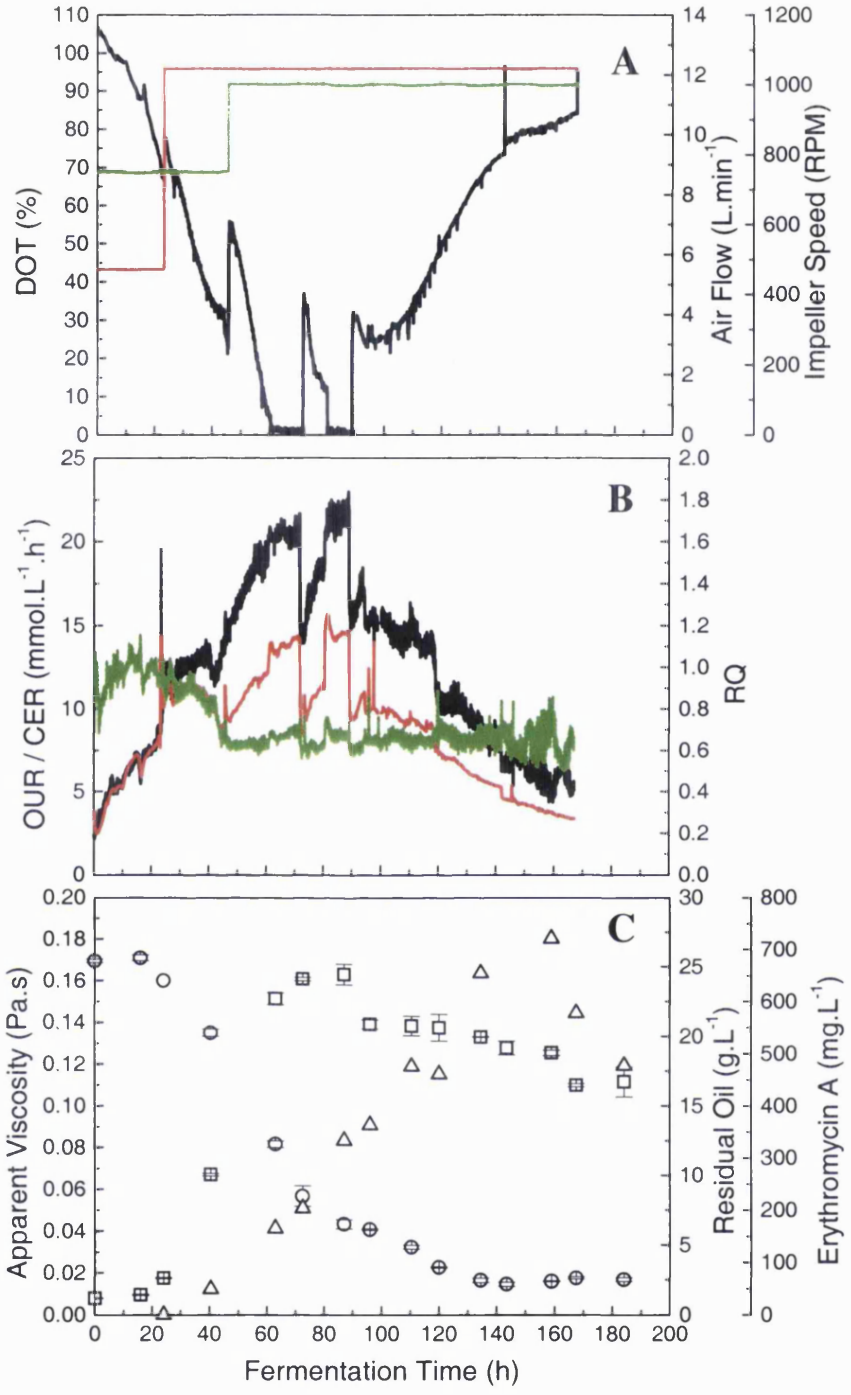

Figure 3.2. Typical fermentation profile for a 20 L OBM fermentation (OBM20L1). Graph A: DOT; —, Air flow rate; —, Impeller speed (RPM); —. Graph B: OUR; —, CER; —, RQ; —. Graph C: Viscosity; □, Oil; ○, Erythromycin A; △. Fermentations carried out as described in Section 2.2.1.2, off-line analysis as described in Section 2.2.2. Error bars show the standard deviation of three replicate measurements.

Graph C in Figure 3.2 gives the off-line data for the fermentation. Since biomass cannot be measured directly because of the insoluble media component, the time course of the growth can be monitored by measuring the apparent viscosity of the broth. Since it has been demonstrated that broth viscosity is proportional to the biomass concentration (Karsheva *et al.* 1997), which peaked at 80 to 90 h. The main carbon source, rape seed oil decreased as it was metabolised. As has been noted previously, not all of the oil was used (Mirjalili *et al.* 1999, Large *et al.* 1998), which is thought to be due to mass transfer limitations at the lipid-aqueous interface. Erythromycin A reached a maximum concentration at approximately 160 h of around 721 $mg.L^{-1}$.

3.2.3 Time Dependant Rheology of SCM and OBM Broths

One of the main factors governing the microfiltration of fermentation broths is its rheology. For this reason a detailed investigation of the rheology of the two medium types was undertaken. Figure 3.3 shows raw viscosity data and derived apparent viscosity values for a typical SCM broth. Experiments were carried out using the concentric cylinder viscometer, as described in Section 2.3.3.3. Figure 3.3A shows the relationship between shear stress and shear rate for broth harvested at different times throughout the fermentation. From this plot, the flow behaviour index (n) and the consistency index (K), were determined from the gradient and the inverse log of the ordinate intercept respectively. Figure 3.3B shows how the derived values of K, n and the apparent viscosity (μ_a), calculated at a shear rate of 10,000 s^{-1}, vary with fermentation time. This shear rate represents a typical value calculated at the membrane surface using Equation [2.3]. It is clear from these graphs that both types of fermentation exhibit shear thinning rheological properties, as the shear rate increases, the apparent viscosity is reduced.

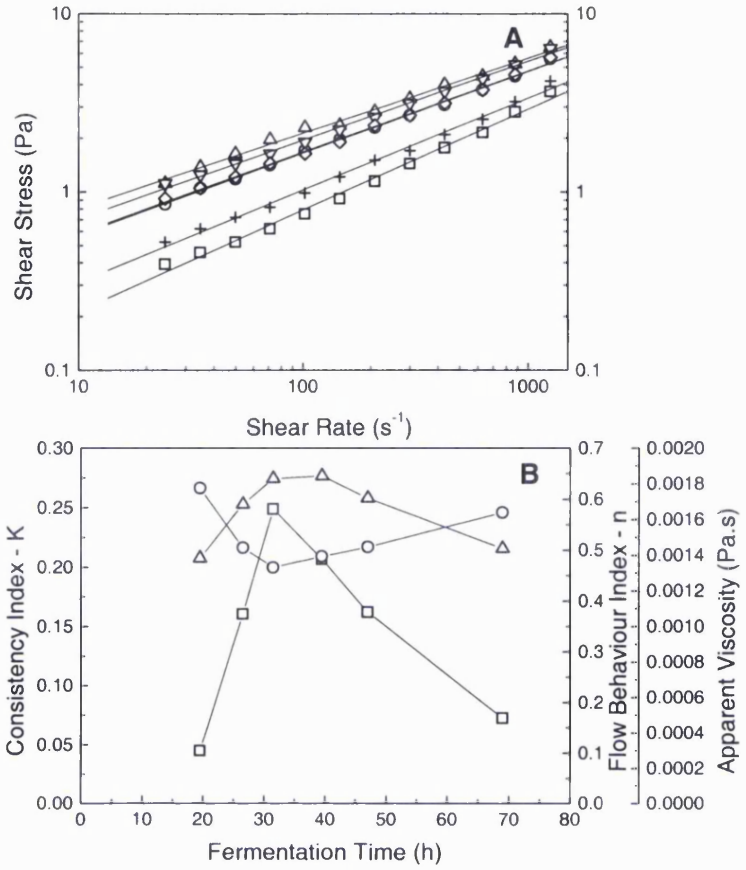

Figure 3.3. Rheology of a typical SCM broth (SCM20L2). Graph A displays the relationship between shear rate and shear stress for broth harvested at 19.5 (□), 26.5 (○), 31.5 (△), 39.5 (▽), 47 (◇) and 69 (+) hours. Graph B shows how K (□), n (○) and μ_a (△) vary with fermentation time. Rheology was measured as described in Section 2.3.3.3 and K and n were determined.

The same parameters were also determined for the OBM broths. In this case, results were obtained using a cup and bob attachment as described in Section 2.3.3.3. Figure 3.4 A shows the shear stress and shear rate plots for broths harvested at various fermentation times. Figure 3.4 B show K, n and μ_a of a markedly different form to that of Graph 3.3 B. SCM broths show time dependant variation in both K and n and exhibit a peak in apparent broth viscosity at approximately 30 h, which is then stable for 10 h before declining slightly. In

OBM cultures, n remains relatively constant and K increases with time. Apparent viscosity values increase and then plateau between 80 and 115 h before increasing again.

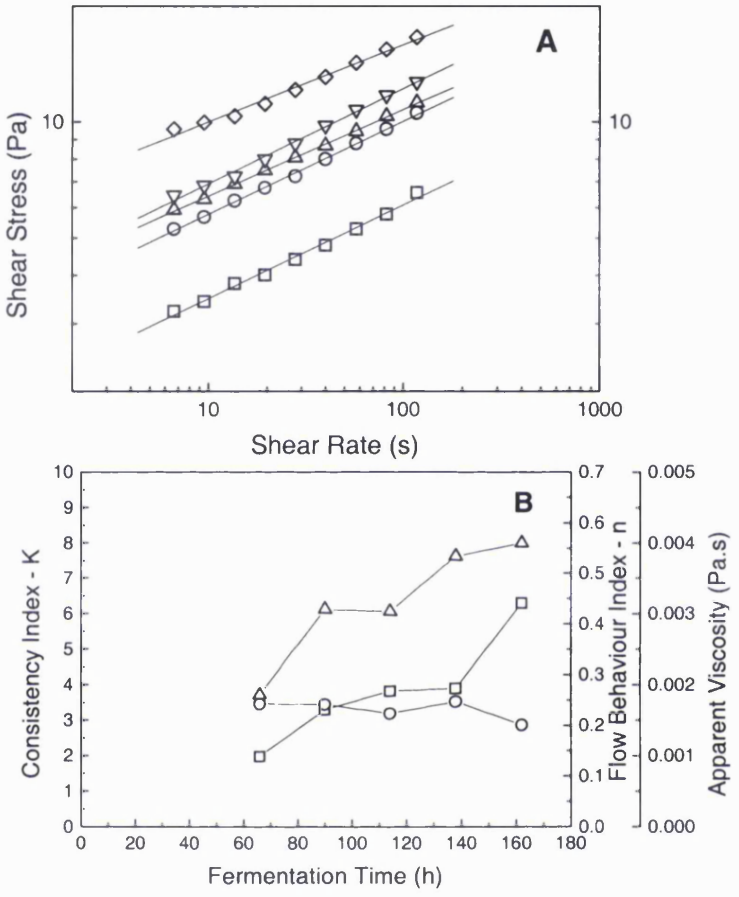

Figure 3.4. Rheology of a typical OBM broth (OBM20L3). Graph A shows the relationship between shear rate and shear stress for broth harvested at 66 (□), 90 (○), 114 (△), 138 (▽) and 162 (◇) hours. Graph B is the variation of K (□), n (○) and μ_a (△) with fermentation time. Viscosity was measured as described in Section 2.2.2.4. K and n were determined as described in Section 2.3.3.3.

In the case of the SCM, the variation in viscosity with time has been shown to be related to biomass concentration during the growth phase (Buckland *et al.* 1985; Sarra *et al.* 1996). For OBM cultures, the higher viscosity in the later stages of the fermentation is thought to be due to insoluble media components and the contents

of lysed cells such as nucleic acids being released into the media (Chartrain *et al.* 1991). The viscosity will be a critical factor affecting the flow of permeate through the microfiltration membranes as discussed in Section 1.3.1. Permeate flux is known to decrease with increasing broth viscosity and the change in apparent viscosity may therefore influence the choice of harvest time. This is discussed further in Section 4.4.

Note that Figures 3.3B and 3.4B show the apparent feed viscosities of the two fermentation broths at a typical shear rate experienced at the membrane surface (10,000 s^{-1}), as opposed to the values shown in Figures 3.1C and 3.2C which are measured at 71 s^{-1}, the shear rate of the Brookfield viscometer (Section 2.2.3.4).
It is clear from Figures 3.1 C and 3.3 B that the apparent viscosity of the SCM broth at the membrane surface will decrease as a function of fermentation time, after the maximum erythromycin concentration is reached while that for the OBM broth shows a marked increase. The higher feed viscosities and solids loading of the OBM broths is likely to have adverse effects on the microfiltration performance.

3.2.4 Medium Composition Summary

The initial aim of the study was to compare the growth and antibiotic production rates on the two different types of media used. Figures 3.1 and 3.2 show that there are a number of notable effects related to the medium composition. For the SCM fermentations, the biomass concentration reached a maximum approximately 40 h after inoculation, while the erythromycin A concentration peaked after approximately 70 h at 235 $mg.L^{-1}$. In contrast the duration of the OBM runs were found to be significantly longer, since the rate of oil utilisation (the main carbon

source) was slower than the rate of glucose utilisation. As mentioned previously, the presence of insoluble components in the OBM means that the biomass concentration can not be measured directly and so broth viscosity is taken as an indicator of biomass concentration during the growth phase (Sarra *et al.* 1996; Karsheva *et al.*, 1997). The viscosity of the OBM fermentation reaches a maximum at around 70 h, with the erythromycin concentration peaking at 160 h at 721 mgL^{-1}. This is approximately three times higher than was found for the SCM medium. Table 3.2 summarises the comparison between the two different media. Permeate viscosities were measured and found to be the same for both media. Both exhibited Newtonian characteristics with viscosities approximately the same as water. The higher antibiotic titres reached however, will increase the mass flux of erythromycin through the membrane. Growth rate was calculated by determining the rate of change of biomass through non linear regression of a biomass against time plot.

Fermentation	Time of max biomass conc. / μ_a (h)	Time of max eryth. A conc. (h)	Max eryth. A conc. (mgL^{-1})	Max growth rate (h^{-1})	Residual oil conc. ($g.L^{-1}$)
SCM20L1	44-48	64.5	150	0.125	-
SCM20L2	40-44	64	340	0.100	-
SCM20L3	40-47	64	235	0.087	-
OBM20L1	73-87	159	721	0.080	2.42
OBM20L2	112-120	184.5	ND	0.046	3.34
OBM20L3	ND	185	513	ND	1.77

ND : not determined

Table 3.2. Comparison of SCM and OBM characteristics. Displaying the time of maximum biomass (SCM) or apparent viscosity - μ_a (OBM), the maximum erythromycin A concentration and the time at which it occurs. The maximum growth rates in terms of biomass increase for SCM and apparent viscosity increase for OBM and the residual oil concentration at the time of maximum erythromycin concentration in $g.L^{-1}$.

The media composition also changed throughout the period of the fermentation as media constituents were utilised and biomass growth took place. Residual glucose

and oil concentrations are also shown in Figures 3.1C and 3.2C. The carbon source in the SCM is glucose, a small water-soluble molecule which will have little effect on the subsequent microfiltration of the broth. In contrast, oil is a known foulant of microfiltration membranes (Conrad and Lee, 1998). Since there may be residual oil left at the desired harvest time of the fermentation, (approximately 2.5 gL^{-1} at the maximum erythromycin concentration), it will have a negative effect on the permeate flux and may also influence antibiotic transmission. The OBM also contains another insoluble component, soya flour. Approximately 25% (w/v) dissolves in the medium (figure quoted by supplier) leaving a considerable amount left in suspension. Although the amount of undissolved flour remaining at the end of the fermentation is not known, because of the inability to separate it from the biomass, visual observation (increased packed cell volume) and final total solids concentration of the broth indicated that there was a significant amount left in suspension.

The on-line exit gas profiles for both SCM and OBM fermentations are shown in Figures 3.1B and 3.2B; CER, OUR, RQ and DOT are displayed. From the RQ values it is clear that for the SCM the RQ is approximately 1.0, which is expected for growth on carbohydrates. For the OBM the organism initially displays an RQ of 1.0 as it uses the dextrin as the carbon source. When this is depleted the rape seed oil is used and the RQ drops to around 0.7. The slower growth on oil is apparent since for the SCM fermentation the OUR and CER rise quickly and reach a peak at 35 h, corresponding to the maximum biomass concentration measured (see Figure 3.1B and C). The OBM broth OUR and CER reach a peaks at 90 h and they increase relatively slowly towards the maximum with respect to SCM values.

The viscosities of the two types of fermentation broth are also quite different. Although in both cases the broths adhere to a pseudoplastic rheology, the apparent viscosity of the OBM is approximately 2 – 3 times higher compared to the SCM values at the shear rates experienced at the membrane surface. The higher viscosity of the OBM is probably responsible for the lower DOT values recorded, compared to the SCM fermentations, due to a reduction in the oxygen combined mass transfer coefficient k_La, (the rate of oxygen diffusion through the liquid films surrounding the gas bubbles is proportional to $1/\mu$). The poor mixing at high μ_a can be improved with an increase in impeller speed. However there is a maximum that can be achieved before the shear rate near the impeller will cause breakage of the mycelia (Heydarian, 1998a; Bushell *et al.* 1997). Maximum impeller speed can also be limited by the amount of foaming, vortexing of the broth and also the physical and economic limitations.

3.3 Effect of Agitation Rate

In order to investigate the effect of agitation rate on fermentation characteristics and the subsequent microfiltration of the broth, two impeller tip speeds were compared. These experiments were performed as earlier investigations had shown a link between morphology and steady state permeate flux at the critical transmembrane pressure during microfiltration (Davies *et al.* 2000). Previous work has also shown there to be a relationship between power input to the vessel via the impeller and hyphal morphology (Heydarian 1998a). The fermentations were carried out using the SCM as described in Section 2.2.2.3.

Figure 3.5 shows a comparison between two SCM fermentations carried out at different tip speeds: 1.63 $m.s^{-1}$ and 2.45 $m.s^{-1}$ representing impeller speeds of 500

and 750 rpm of the 7 L vessel used by Heydarian (1998a; 1998b). Fermentations SCM42L3 and SCM42L4 were carried out a tip speed of 1.63 ms^{-1} and SCM42L6 and SCM42L7 at a tip speed of 2.45 ms^{-1}. Only OUR traces (as opposed to both OUR, CER and RQ) are shown for the purposes of clarity. The CER and RQ profiles were similar in all cases to those previously described in Section 3.2.

Replicate fermentations for each tip speed showed comparable DOT traces (Figure 3.5A). At a tip speed of 1.63 $m.s^{-1}$ the minimum DOT was approximately 40 % and was reached between 27 and 33 h for SCM42L4. At a tip speed of 2.45 $m.s^{-1}$, the minimum DOT was between 55 % and 60 % at 29 to 32 h and 30 to 35 hours for SCM42L5 and SCM42L6 respectively. Previous studies (Heydarian *et al.* 1996) have shown that low values of DOT do not adversely affect the concentrations of erythromycin produced. Graph 3.5B shows the corresponding biomass values for the fermentations and reach 8.5 to 9.5 $g.L^{-1}$. Figure 3.5C plots the OUR against time which at their peak range from 14 to 16 $mmol.L^{-1}.h^{-1}$ with no clear variation between different tip speeds and are comparable to those seen in Section 3.2.

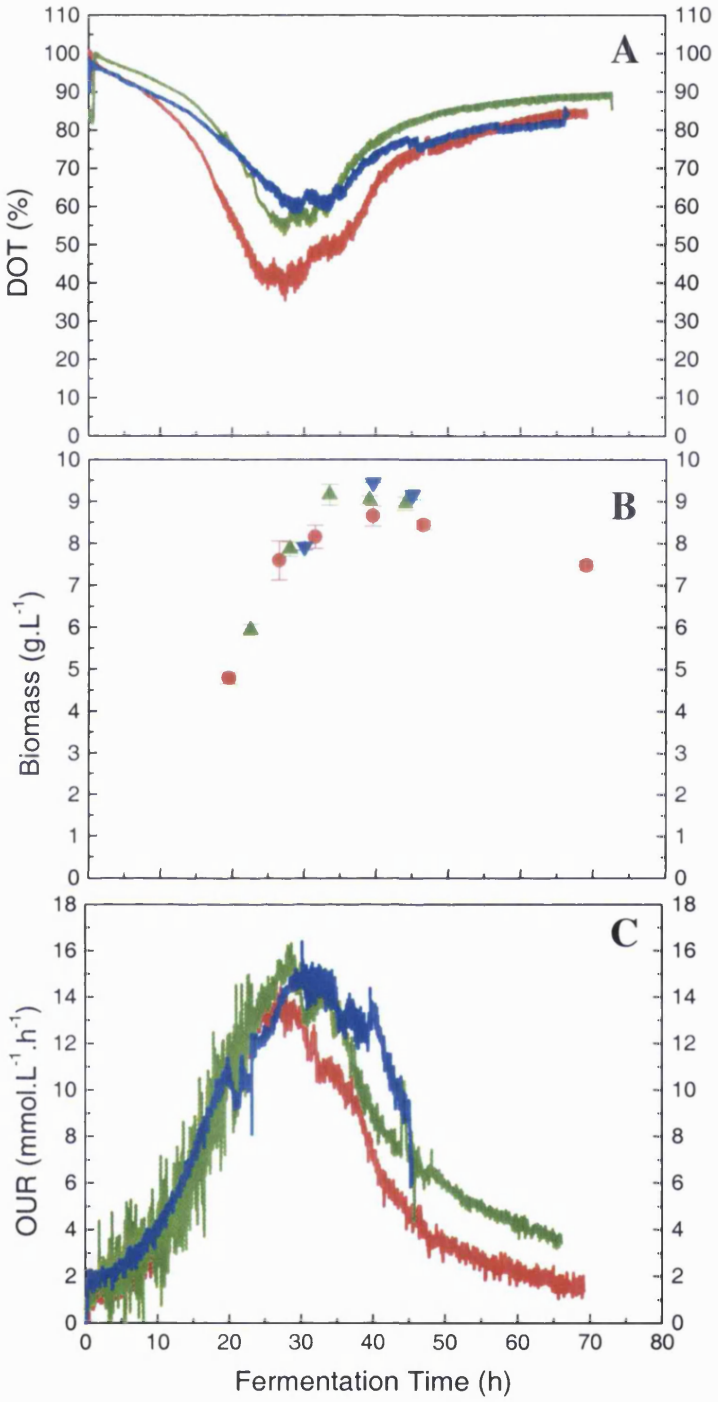

Figure 3.5. Effect of agitation rate on SCM fermentations. Graph A shows DOT; Graph B records the biomass and Graph C shows the OUR , all against fermentation time (h), for all graphs SCM42L4 — (1.63 $m.s^{-1}$), SCM42L5 — and SCM42L6 — (2.45 $m.s^{-1}$). Fermentations carried out as described in Section 2.2.1.3, off-line analysis as described in Section 2.2.2. Error bars show the standard deviation over three replicate measurements.

3.3.1 Relationship Between Off-gas Data, Biomass Concentration and OBM Broth Viscosity

The ability to measure a fundamental process variable on-line rather than off-line is advantageous in limiting the sample requirements, which are time consuming and increase the risk of contamination. Disadvantages are method dependant, for example using probes such as capacitance monitors (Sarra *et al.* 1996) can risk contamination and space is limited on the small fermenters used for development work. The high cost of retro-fitting and validating new equipment also hinders change. By using the existing off-line gas data from a mass spectrometer or gas analyser, only software is required to produce the required data.

There was an observed correlation between the OUR and CER data and the biomass concentration as shown in Figure 3.6. The increase in OUR and CER during growth correlates with the biomass concentrations for all the fermentations. Due to the small sample size, the graph was plotted with data from both OUR and CER data sets combined since the respiratory quotient was approximately 1.0 in all cases. This is supported by the statistical analysis of both OUR and CER showing that there was no difference between the two populations. The gradient of the line in Figure 3.6 was found to be 1.67 with a correlation coefficient (R^2) of 0.81, indicating that the confidence was high that the variation of OUR and CER was due to the change in biomass concentration.

This correlation was then compared in OBM to the apparent viscosity (μ_a) during the exponential growth phase, which as previously discussed in Section 2.2.3.4 is proportional to the biomass.

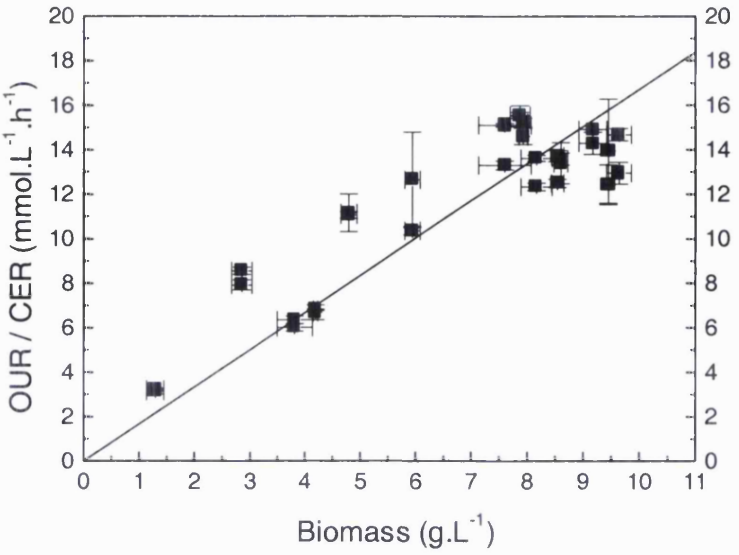

Figure 3.6. Comparison of biomass concentration during the growth phase with OUR and CER data from all 42 L fermentations except SCM42L5.

Figure 3.7 shows a plot of the OUR of fermentations OBM20L1 and OBM20L3 against the viscosity during the exponential growth phase of the fermentation.

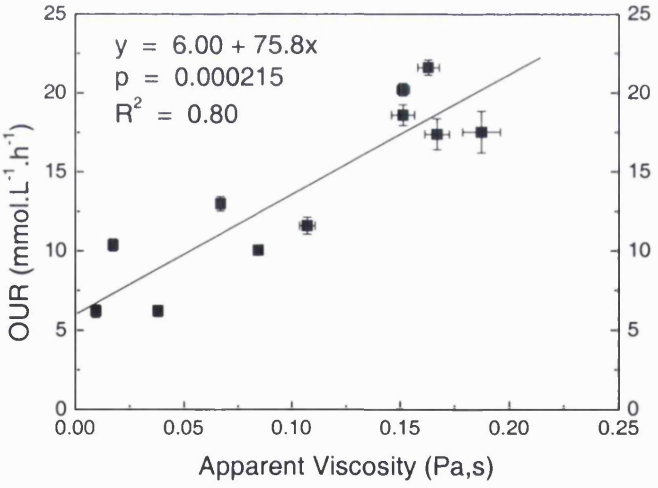

Figure 3.7. Apparent viscosity and OUR during growth phase of fermentations OBM20L1 and OBM20L3.

There is a good correlation between the OUR and μ_a suggesting that there is a proportional relationship between the oxygen uptake rate during growth and biomass production observed in the OBM fermentation. If the correlation between OUR and biomass for the SCM fermentations is also true in this case, then the expected maximum biomass values can be calculated for the OBM fermentations where mass spectrometry data is available. These predictions are to be compared later in Chapter 5 with those made using image analysis techniques.

3.3.2 Agitation Rate Summary

In Table 3.3 a comparison table from the 20 L fermentations is displayed. The maximum biomass figures and growth rates have been estimated for the OBM runs using data derived by the previously described relationships between OUR and biomass.

The identical traces for DOT, biomass and OUR/CER with fermentation time suggest that varying the impeller speed had little or no effect on growth other than to maintain oxygen availability in the broth at different levels. It has been shown that oxygen limitation can affect growth, both in terms of biomass and rheology (Wallace *et al.* 1992). It has been noted previously in Section 3.1.1 how low DOT can change metabolism unless maintained above certain levels. It can also have an effect on secondary metabolite formation since increasing shear in the reactor may increase breakage leading to a shift in the size distribution towards smaller hyphae (Heydarian 1998a) and therefore fewer mycelia capable of erythromycin production (Bushell *et al.* 1997).

Fermentations	Max. eryth. A conc. ($mg.L^{-1}$)	Max. growth rate ($g.h^{-1}$)	Max biomass conc. ($g.L^{-1}$)
SCM20L1	150	0.125	10.9
SCM20L2	340	0.100	12.8
SCM20L3	235	0.087	12.13
OBM20L1	721	0.028	12.3
OBM20L2	ND	0.028	10.6
OBM20L3	513	ND	ND

ND : Not determined

Table 3.3. Comparison of 20 Litre fermentations using values of biomass derived from OUR values in the case of OBM and measured values for SCM. Biomass concentrations are measured for SCM using the method described in Section 2.2.3.3 and calculated using the method described in this chapter. Erythromycin A concentration was determined using the method described in Section 2.2.3.6.

3.4 Fermentation Summary

In this Chapter it has been demonstrated that altering the fermentation medium composition can have a profound effect on fermentation process performance. Using two fundamentally different media, (SCM and OBM) differences with respect to the fermentation duration and antibiotic concentrations achieved have been quantified as have the kinetics of biomass synthesis and antibiotic formation.

4 The Interaction Between Fermentation and Microfiltration Operations

4.1 Introduction and Aims

The variation in broth composition and rheology seen within and between *S. erythraea* fermentations has been highlighted in the previous chapter. Here, the effects of this variation on the primary recovery of the antibiotic by crossflow microfiltration (MF) is investigated. Differences in the feed stream composition and the design and operation of the MF step will influence both biomass removal and recovery of the antibiotic.

Initially, comparisons are drawn between the use of the soluble complex medium (SCM) and oil based medium (OBM) fermentation broths, to examine how the choice of medium changes the approach to the downstream processing. The influence on microfiltration performance of the harvest time changes in composition and rheology of each broth are then investigated. This will potentially allow identification of optimum harvest times and any trade offs between permeate flux and product transmission.

Part of the work presented in this chapter has also been published as Davies, J.L., Baganz, F., Ison, A.P. and Lye, G.J. **2000**. Studies on the interaction of fermentation and microfiltration operations: erythromycin recovery from *Saccharopolyspora erythraea* fermentation broths. *Biotechnol. Bioeng.* **69** 429 – 439.

4.2 Transmembrane Pressure

As described in Section 1.4.2, the transmembrane pressure provides the driving force responsible for the movement of material, both solid and liquid, towards the membrane surface. This leads to a localised increase in the concentration of colloidal materials and dissolved solutes at the surface of the membrane. This can lead to a reduction in permeate flux and product transmission due to the formation of a gel layer and fouling of the membrane surface. A balance must therefore be achieved to maintain acceptably high flux and transmission values while not increasing transmembrane pressure (TMP) too far which could have a deleterious effect on permeate flux and product transmission (Cheryan 1998).

4.2.1 Flux Decay and Critical Transmembrane Pressure for OBM and SCM Broths

In order to assess the fouling of the membrane and the optimum operating conditions for each microfiltration experiment, the changes in permeate flux over microfiltration time were logged. Figures 4.1 A and B show the variation in steady state permeate flux over a range of different transmembrane pressures, for SCM and OBM broths at one time point during the course of each fermentation. This illustrates the different flux decline profiles of the cultures grown on two types of media and demonstrates how the values for steady state permeate flux at the critical transmembrane pressure were determined.

From Figure 4.1 it can be seen that OBM broth causes the membrane to foul more rapidly and leads to steady state permeate flux values approximately 50 % lower than those seen with SCM broth. Figure 4.1 also illustrates how the value for steady state flux is determined for these experiments in concentration mode. For

all the microfiltration experiments the permeate flux was measured over a period of thirty minutes, after which time the flux became constant in all cases and achieved steady state. Crossflow and TMP were kept constant throughout the experiment, adjustment of the TMP was made using the retentate back-pressure valve. Any further decrease in flux would be due to an increase in the solids concentration of the feed stream. Since the volume of the feed was high in these experiments in relation to the volume of permeate collected, concentration effects of the feed stream on permeate flux over these relatively short periods of time is negligible.

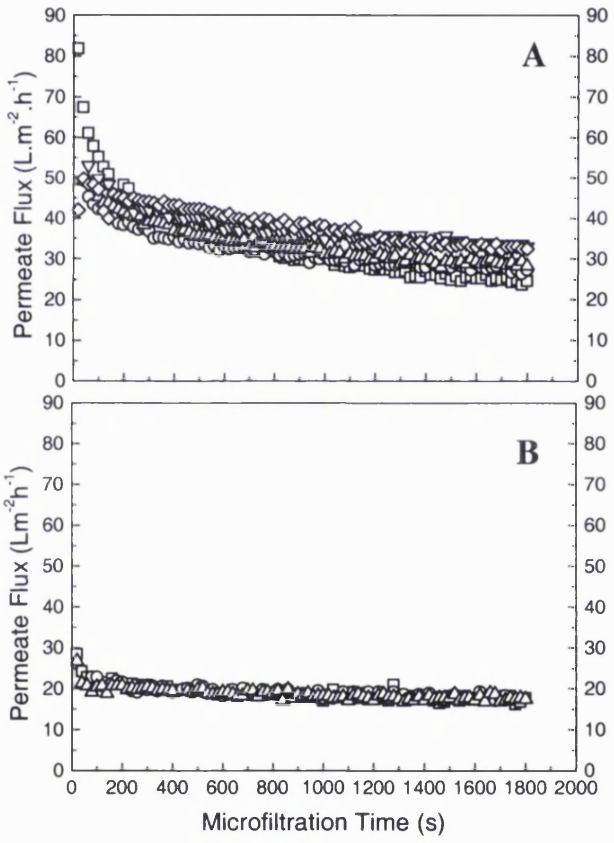

Figure 4.1. Variation of permeate flux during microfiltration of SCM and OBM fermentation broths; Graph A for an SCM broth □ - 12.5 kPa, ○ - 22.5 kPa, △- 39.0 kPa, ▽ - 56.5 kPa and ◇ - 76.0 kPa. Graph B for an OBM broth □- 22.5 kPa, ○ - 49.0 kPa and △ - 75.0 kPa. Broths were harvested from SCM20L1 at 40 h and OBM20L1 at 90 h. Microfiltration was performed using the Minitan rig as described in Section 2.3.1.1.

A plot of the reciprocal of permeate flux against microfiltration time is known to demonstrate the way in which the membrane fouls (Tracy and Davis, 1994). These authors showed that in a model broth of yeast cells and BSA, internal blocking of the pores was characterised by a concave slope (the gradient of the slope increases with increasing time). Surface blocking of the membrane, on the other hand, would be characterised by a convex slope. For both types of culture used in this work, the slopes of the reciprocal of permeate flux against fermentation time were convex throughout the microfiltration time. This suggested that the fouling was caused mostly by surface occlusion of the pores. The flux decay can be modelled in relation to the steady state permeate flux (ssJ) and the flux at any given time (J_s) with relation to microfiltration time (t) and constants f (an extrapolated value of the initial rate of permeate flux in $L.m^{-2}.h^{-1}$) and g (which describes the rate of flux decline in reciprical hours), (rearranged from Cheryan, 1998):

$$J_s - ssJ = fe^{-gt} \qquad [4.1]$$

Figure 4.2 is a plot of J_s-ssJ against the natural log of microfiltration time for fermentation SCM20L3 at 40 h and OBM20L1 at 90 h, the results plotted are one sample time point during each fermentation. The steady state flux was determined from the experimental values as described in Section 2.3.1.1. The gradient of the line gives the constant g; a relative rate of permeate flux decrease over time relative to the steady state permeate flux. This difference between the two is attributed to the very rapid increase in fouling over the first 50 seconds of the MF operation in OBM broths. The effect of fermentation time on flux decay in both media is investigated in Section 4.3.1.

In Figure 4.3 the last three measurements from each of the transmembrane pressures displayed in Figure 4.1A and B are given. The means and standard deviations are then calculated and can be seen plotted in Figure 4.3, giving a plot of mean flux against transmembrane pressure. Here, examples of the microfiltration of both broths are shown.

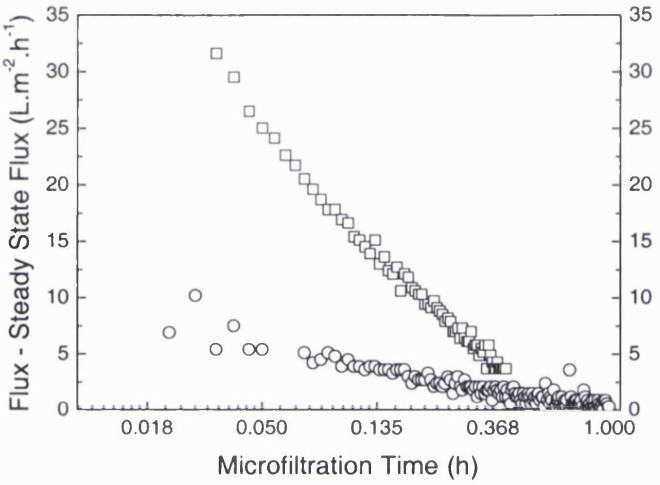

Figure 4.2. Permeate flux (J_s) minus the steady state permeate flux (ssJ) against MF time plotted as the natural log. Data is from fermentations SCM20L3 at times: 44 h - □, and OBM20L1 at 90 h - ○. MF was carried out using the Minitan rig as described in Section 2.3.1.1.

From a plot of the steady state permeate flux against the transmembrane pressure (TMP) imposed on the system, such as that shown in Figure 4.3, the critical transmembrane pressure (cTMP) can be determined. As discussed in the Section 1.4.2, the critical transmembrane pressure can be defined as the point at which the relationship between the flux and TMP changes from dependant to independent of each other. In the region preceding the cTMP, the flux is pressure dependent i.e. as the pressure difference across the membrane is increased so does the permeate flux. Above the cTMP, flux is independent of the transmembrane pressure and increasing TMP will no longer lead to an increase in the permeate flux. At this

point the membrane has become polarised (Section 1.4.4). In this study the cTMP is to be the reading at which the flux is at a maximum.

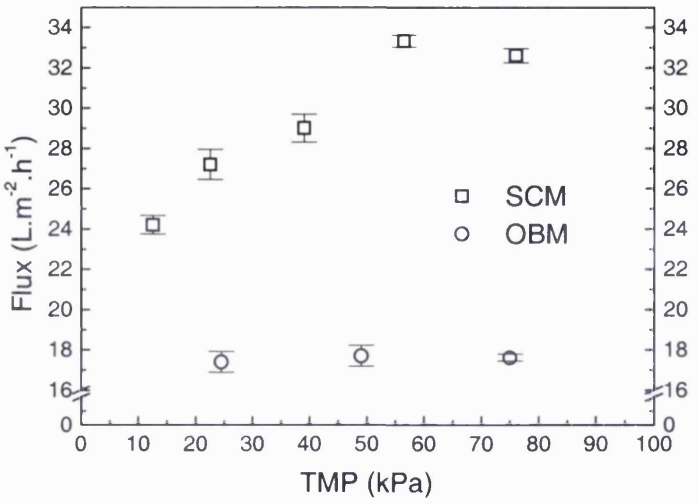

Figure 4.3. Mean steady state permeate flux against TMP for SCM (□) and OBM (○) broths calculated from the final three readings at each TMP from Figure 4.1 from SCM20L1 at 40 hours and OBM20L1 at 90 hours. Microfiltration was carried out using the Minitan rig as described in Section 2.3.1.1.

4.2.2 The Effect of TMP on the Microfiltration of SCM Broths

The methodology described in the previous section was used to investigate the variation of steady state permeate flux and the transmission of protein and erythromycin across the membrane as a function of TMP. Protein transmission can lead to fouling of equipment downstream of the primary recovery operation and product transmission is of prime importance in relation to overall process economics.

4.2.2.1 Steady State Permeate Flux

Figure 4.4A shows the variation of steady state permeate flux measurement as a function of TMP values below the critical transmembrane pressure (cTMP). Data is determined for broths harvested at each time point of fermentations 20LSCM1, 2 and 3. As can be seen from Figure 4.4A, if flux is compared for all time points of all fermentations there is a great deal of variation. This is related to the variability in conditions (biomass concentration, broth rheology) at each time point for each fermentation. It was observed that within each data set, the steady state permeate flux did increase in relation to the TMP.

This variability can be overcome if the same data is plotted but by using a relative change in steady state permeate flux rate for a given change in TMP. Figure 4.4B is a graph of relative change in flux against the difference in transmembrane pressure, described by:

$$100\left[\left(\frac{J_{new}}{J_{initial}}\right)-1\right]=0.512(P_{new}-P_{initial}) \qquad [4.2]$$

where the subscript 'initial' denotes the measurement of flux at the first sample point during the fermentation time ($J_{initial}$) at the initial TMP ($P_{initial}$) TMP and the new denotes flux (J_{new}) and pressure at a higher value of TMP (P_{new}). This shows how pressure influences permeate flow rates in the pressure dependent region for all fermentations. This relationship is examined further in Chapter 6.

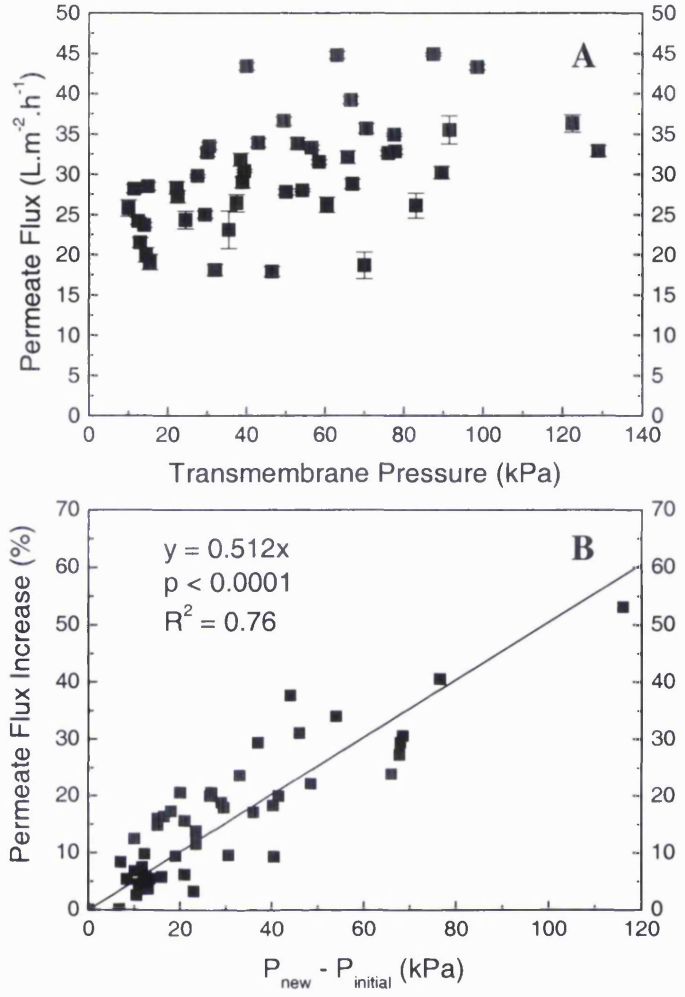

Figure 4.4. The relationship between TMP and steady state permeate flux. Graph A shows the permeate flux against TMP for all time points of fermentations SCM20L1, 2 and 3 using the Minitan rig as described in Section 2.3.1.1. Graph B shows the relative permeate flux change per unit increase in TMP as described by Equation [4.2].

4.2.2.2 Erythromycin Transmission

Transmission of erythromycin during the microfiltration of SCM broths, was not found to change by varying TMP. Figure 4.5 plots the erythromycin transmission at different TMPs for fermentations 20LSCM 1, 2 and 3. The reason for this trend being different to that found for proteins, due to the much smaller size and low concentration of the erythromycin. The small molecular weight minimises

adsorption and retardation by the membrane, the cake and the low concentration of erythromycin, by reducing the effects of solute rejection and precipitation.

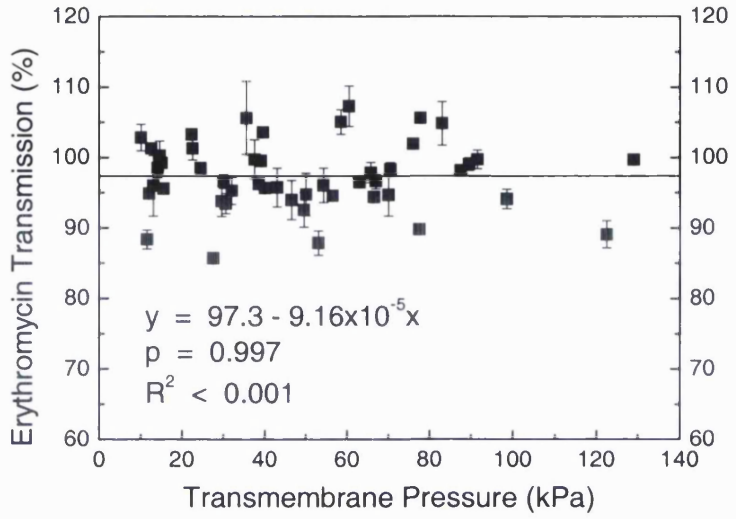

Figure 4.5. Erythromycin transmission against transmembrane pressure for fermentations SCM20L1, 2 and 3 measured as described in Section 2.3.3.1, from experiments carried out using the Minitan rig as described in Section 2.3.1.2.

4.2.2.3 Protein Transmission

Figure 4.6 shows a plot of protein transmission against TMP for fermentations 20LSCM 1, 2 and 3. There was a clear trend of protein transmission decreasing with increased TMP. Increased TMP increases the solute concentration and suspended solids concentration at the membrane surface (gel polarisation and cake formation respectively). This can impede the passage of proteins across the membrane in a number of ways. High concentrations of solutes at the membrane surface can cause protein to precipitate out of solution (Cheryan 1998). The gel layer can also cause solute rejection due to raised concentrations of material at the membrane which cause physical and chemical impedances to other solutes passing through this layer (Cheryan, 1998). Adsorption of proteins onto solid surfaces such

as the membrane, membrane support, housing and suspended solids in the broth will remove protein from solution thus lowering transmission.

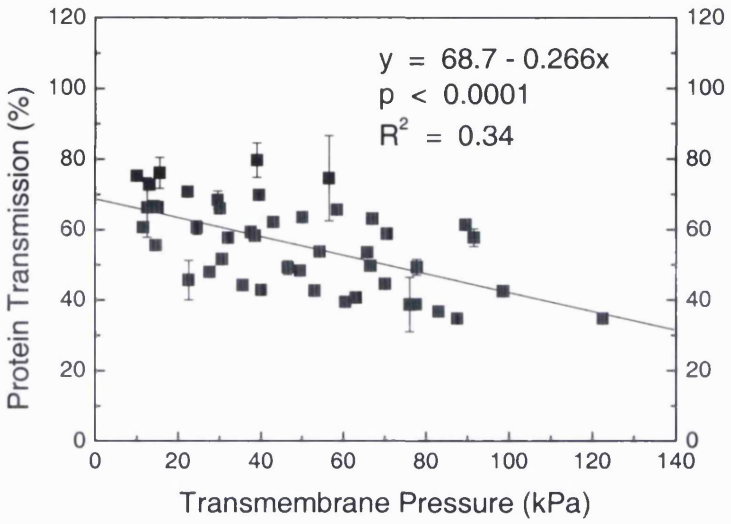

Figure 4.6. Protein transmission as a function of TMP for fermentations SCM20L1, 2 and 3 measured as described in Section 2.3.3.1, from experiments carried out using the Minitan rig as described in Section 2.3.1.1.

4.2.3 The Effect of TMP on the Microfiltration of OBM Broths

4.2.3.1 Steady State Permeate Flux

In contrast to the SCM data, Figure 4.7 shows that for the MF of OBM broths, there are no observed relationships between the steady state permeate flux and the TMP. However, the cTMP for OBM broths was reached at much lower TMPs than those observed for microfiltered SCM broths. In many cases the cTMP was surpassed without any backpressure being imposed on the system. This means that nearly all of the points plotted in Figure 4.7 are from the pressure independent region of the process. The permeate fluxes are also much lower than those seen for

SCM broths since the solid loadings and apparent viscosity of the OBM broths are higher.

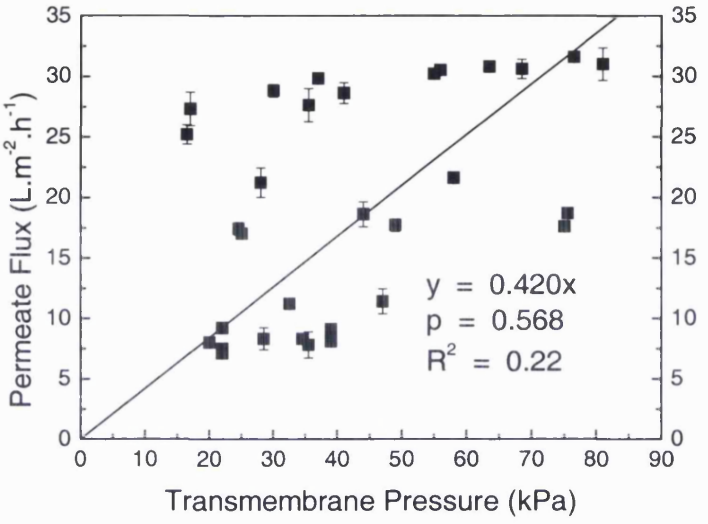

Figure 4.7. Steady state permeate flux against transmembrane pressure for fermentations OBM20L1, 2 and 3, using the Minitan rig as described in Section 2.3.1.1.

4.2.3.2 Erythromycin Transmission

Figure 4.8 shows that as for SCM runs, there is no evidence of a statistically significant relationship between erythromycin transmission and TMP in OBM fermentation broths.

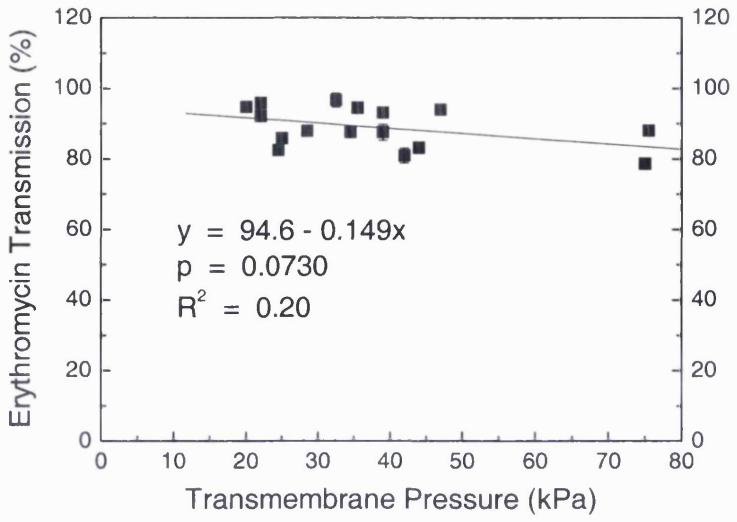

Figure 4.8. Erythromycin transmission against transmembrane pressure for fermentations SCM20L1, 2 and 3 measured as described in Section 2.3.3.1, from experiments carried out using the Minitan rig as described in Section 2.3.1.2.

4.2.3.3 Protein Transmission

Figure 4.9 shows that there was no statistically significant relationship between protein transmission and TMP, although the probability (0.0534) was close to the assumed confidence level of 0.05. Protein transmission was generally lower than that seen in SCM broths (Figure 4.6) by approximately 40 %. In this case the large amount of undissolved solids and colloidal oil present at the membrane surface provide numerous sites at which protein can become associated. The lack of relationship is probably due to the high rejection and retention of the gel layer that had already become established, which was indicated by the low values obtained for the cTMP.

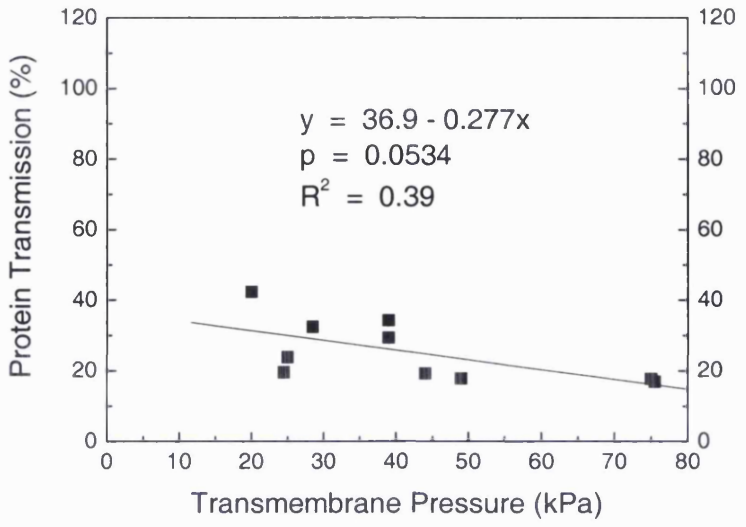

Figure 4.9. Protein transmission as a function of TMP for fermentations OBM20L1, 2 and 3 measured as described in Section 2.3.3.1, from experiments carried out using the Minitan rig as described in Section 2.3.1.1.

4.2.4 Discussion of Transmembrane Pressure Effects

There have been a number of notable effects of transmembrane pressure on the microfiltration of oil and soluble media. Schafer *et al.* (2000) reported that a significant flux decline is often observed even in process streams of low solute concentration. In both cases the decrease from values of clean water flux to those seen at the start of flux measurement were rapid. OBM broths experienced a faster flux decline than SCM broths in the first 50 to 100 seconds of microfiltration. Tiller and O'Melia (1993) stated that for colloids in the natural environment, their negative surface charge can stabilise the cake formed by the solids.

In filtration systems, the driving force for the flow of material across the membrane is the transmembrane pressure (TMP). For movement of materials across the membrane, this driving force must be higher than the osmotic pressure of the

stream being filtered. However, in most MF processes this osmotic pressure is negligable (Cheryan *et al.* 1990), since only very large molecules or solids need be retained. It is known that cake resistance is greater when the feed stream solids content is high (Brown and Kavanagh, 1987) and that cake resistance is higher at larger values of TMP due to increased cake depth and compression of the cake (Kawakatsu *et al.* 1993; Fradin and Field, 1999). The cTMPs are lower for OBM runs and are reached by the backpressure imposed by the flow rate alone. This is assumed to be due to the higher solids loading of the feed stream in comparison to SCM broths.

For the pressure dependant region of the microfiltration process, it has been long established that for a given set of feed stream conditions, the TMP is proportional to the flux (Zeman and Zydney, 1996). Within this pressure dependent region of the SCM broth runs, the percentage increase in flux for an increase in TMP can be used to predict flux at a given set of conditions from a previous measurement at any given pressure below the cTMP. Testing and the relevance of this work is explored in Chapter 6.

The transmission profiles of erythromycin were similar to those seen in previous studies (Antoniou *et al.* 1990). There is no significant relationship between erythromycin transmission and transmembrane pressure. Since erythromycin is a small molecule (see Section 1.1.2) it is unlikely to be retarded by the fouling layer. Since erythromycin's concentration in the feed stream is low (see Section 3.2.4) it is unlikely to be rejected from the polarisation layer. Although these fouling and gel polarisation processes can reduce the molecular weight cut off (MWCO) of a

membrane (Cheryan, 1998), it would require over a 2000 times reduction in MWCO to retain erythromycin.

Hernandez-Pinzon and Bautista (1992) described how, even in MF processes where the pore size is much greater than that of the protein, the transmission of the molecule is less than 100 percent. It has also been observed that protein transmission can be affected by deposition and pressure-driven compaction (Turker and Hubble, 1987). In this study it was observed that protein transmission was inversely proportional to TMP in SCM broth (Figure 4.6), whereas for OBM broths, no definite relationship was apparent although this may have been due to the small data set available. This inversely proportional relationship between TMP and percentage protein transmission in SCM broths may lead to the application of pressures above the cTMP as a method of sieving protein out of the permeate in order to reduce the concentrations of this contaminant on steps downstream of the microfiltration.

4.3 The Effect of Broth Age on Microfiltration Performance

Broth age was also investigated in terms of the steady state permeate flux rates and protein transmission and erythromycin transmission. This was carried out to ascertain the best point of harvest in terms of mass flux of product across the membrane and overall product recovery from SCM and OBM broths. The Minitan rig allowed small samples (0.5 – 1.0 L) to be taken from the fermenter to allow multiple time points in each fermentation to be investigated.

4.3.1 Flux Decay and Broth Age

Figure 4.10 shows the parameter g (Equation [4.1]), a measurement of the permeate flux decrease with respect to MF time. At high values of g, the drop in permeate flux relative to the steady state permeate flux per unit time of MF operation is large as described in Section 4.2.2.1. Over the course of *S. erythraea* fermentations grown on either SCM or OBM, g decreases.

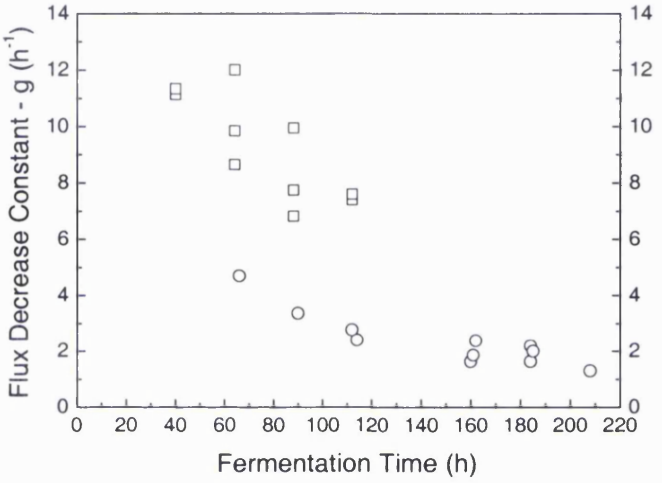

Figure 4.10. The constant g (h^{-1}) from Equation [4.1] – a measure of the magnitude of permeate flux decrease with respect to microfiltration time, against the age of the fermentation broth. Results from fermentations SCM20L1, 2 and 3 and OBM20L1, 2 and 3. MF carried out using the Minitan rig as described in Section 2.3.1.1.

This shows that the change in permeate flux per unit MF time was reduced as the fermentation progresses. MF permeate flux decay measurements were taken at the start of each optimisation run i.e. at low TMP. The effect that this would have on flux decay at the cTMP is difficult to predict. Arnot *et al.* (2000) reported that in the MF of oily emulsions, there is variation in flux decay that depends on the TMP, crossflow, mode of filter operation and fouling mechanism (surface or pore blocking). Since a proper evaluation of flux decay requires that the membrane be

clean and the cTMP is not known until an optimisation experiment had been run it was not possible to evaluate decay at the cTMP.

4.3.2 Steady State Permeate Flux

Figure 4.11 shows the variation of steady state permeate flux for both SCM and OBM broth samples removed and processed over the course of the respective fermentations (each performed in triplicate). The two broths showed marked differences in the observed steady state flux rates over the duration of the fermentation. It is apparent from Figure 4.11 that the steady state permeate flux over the time course of each fermentation is more stable and reproducible for the OBM broth than for the SCM. For the OBM broth, the permeate flux decreases asymptotically to the time axis for each fermentation, whereas for the SCM there is no obvious trend that can be drawn from the data. It is thought that this difference is due to the fouling of the membrane in each case.

In the OBM fermentations, the limiting factor affecting flux is thought to be the media components and in particular, the residual flour. Table 4.1 details the results of a series of experiments designed to further understand the different flux profiles for the two broths shown in Figure 4.11, the effects of different media components from the OBM, either individually or in combination, were examined in the absence of biomass. Rape seed oil, soya flour and the antifoam agent, PPG, were selected at representative concentrations likely to be found towards the end of the fermentation.

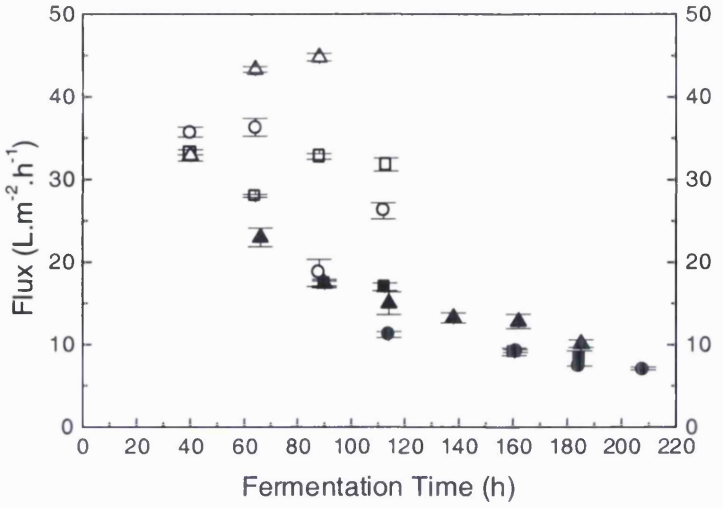

Figure 4.11. Mean steady state permeate flux against fermentation time for six fermentations; □ - SCM20L1, ○ - SCM20L2, △ - SCM20L3, and ■ - OBM20L1, ● - OBM20L2, ▲ - OBM20L3. MF runs were carried out using the Minitan as described in Section 2.3.1.1. Values displayed are mean steady state permeate flux at the cTMP

The results clearly show that the steady state permeate flux in a simulated system appears to be dominated by the residual undissolved soya flour. The measured flux levels were approximately constant for all runs containing either flour on its own (~29 $L.m^{-2}.h^{-1}$) or in combination with any of the other two media components (~30 $L.m^{-2}.h^{-1}$). The cause of this limitation in permeate flux in the presence of soya flour is thought to be due to formation of a solid cake at the membrane surface. The measured permeate fluxes are, however, still higher than the whole broth samples (see Figure 4.3), indicating a more complex interaction between the soluble, insoluble medium components and the biomass in the whole OBM broth samples compared to the model systems used in Table 4.1. In the SCM fermentations, however, the fouling layer consisted primarily of the biomass and the contents of lysed cells. This effect for the SCM broth is studied further using image analysis and is discussed in Chapter 5.

PPG 0.2 % (v/v)	RSO 0.3 % (v/v)	Soya flour 1.0 % (w/v)	Permeate flux ($Lm^{-2}h^{-1}$)
X			953 ± 6
	X		251 ± 9
		X	28.3 ± 0.8
X	X		119 ± 2
X		X	30.8 ± 1.5
	X	X	31.2 ± 1.0
X	X	X	31.6 ± 0.7

Table 4.1. Measured steady state permeate flux using various combinations of insoluble media components in water using the Minitan rig as described in Section 2.3.1.1 at 80 kPa TMP. X indicates components present in a continuous water phase, these are PPG – polypropylene glycol (the antifoam), RSO – rape seed oil and soya bean flour.

4.3.3 Erythromycin Transmission

In addition to a high permeate flux being desirable, a high percentage of antibiotic transmission across the membrane (and fouling layer) is an important factor in determining overall product recovery. Figure 4.12 shows the percentage transmission of erythromycin across the membrane during the time course of the fermentation for both the SCM and OBM derived feed streams. The values displayed are those measured at the critical transmembrane pressure although it was previously shown in Sections 4.1.2.2 and 4.1.3.2 that TMP had no significant effect on erythromycin transmission. Although there is variation within each data set, a significant difference between the means of the transmission data for each type of broth was found. The calculated means are 97.3 ± 1.6 % (w/w) transmission and 89.1 ± 1.4 % (w/w) transmission for SCM and OBM broths respectively ($p = 0.01116$, two population independent t-test). Erythromycin A (and its homologues) is a small molecule (c. 730 Da) and therefore should not be retarded by the membrane itself. Erythromycin however, may become associated with the suspended solids in the medium (or filter cake) and may also dissolve in

the residual oil of the OBM broth. Experiments to assess the levels of erythromycin adsorption onto the *S. erythraea* biomass and the solubility of the target molecule in the oil-phase, have shown that the amount of erythromycin lost from the continuous aqueous phase to these physical processes is insignificant.

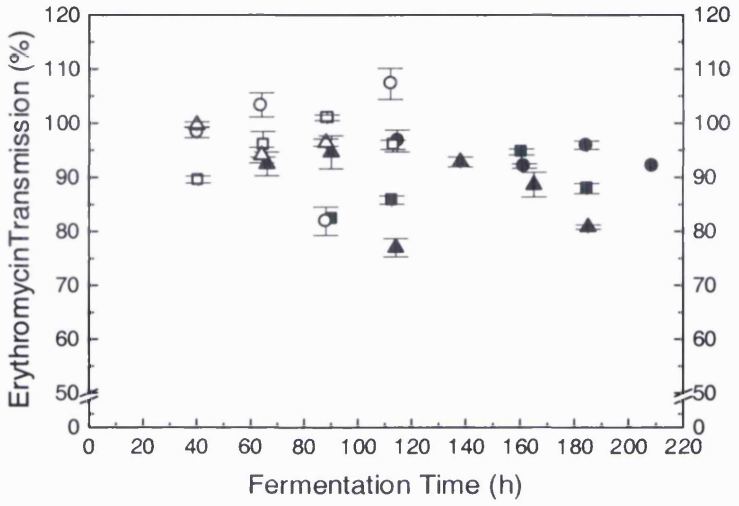

Figure 4.12. Transmission of erythromycin against fermentation time for the six fermentations; □ - SCM20L1, ○ - SCM20L2, △ - SCM20L3, and ■ - OBM20L1, ● - OBM20L2, ▲ - OBM20L3. Erythromycin transmission was measured as described in Section 2.3.3.2, from experiments carried out using the Minitan rig as described in Section 2.3.1.1.

The equilibrium partition coefficient for erythromycin, K_{eryth} in a rape seed oil – water two phase system was found to be 0.02, and this did not vary significantly over a pH range of 4 to 10, (the pK_a of erythromycin A is ≈ 8.6). The low loss of erythromycin to biomass adsorption and solubility processes is reflected by the fact that there is no significant variation in the transmission percentage across the membrane with fermentation time, over which the broth components are varying in concentration.

4.3.4 Protein Transmission

Figure 4.13 shows the differences between protein transmission derived from OBM and SCM broths during microfiltration as a function of culture age. The transmission tends to decrease in SCM broths as they age, whereas, the reverse is true in OBM broths. The transmission of protein is also lower for OBM broths as found previously in Section 4.1.3.3. Both of these effects are considered to be due to the presence of media components in the OBM that impede transmission through association with protein.

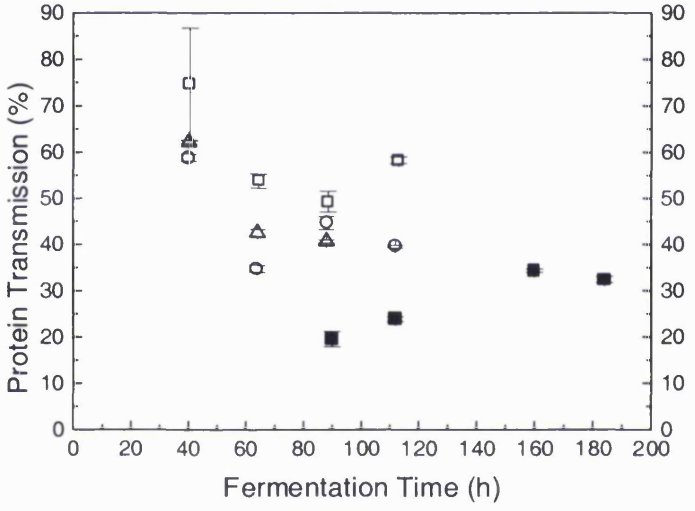

Figure 4.13. Soluble protein transmission against fermentation time for three SCM runs; □ - SCM20L1, ○ - SCM20L2, △ - SCM20L3, and one OBM run; ■ - OBM20L1. Protein transmission was measured as described in Section 2.3.3.1 and MF was carried out using the Minitan rig as described in Section 2.3.1.1.

For the SCM broths, increasing biomass and protein concentration over time decrease the protein transmission through cake formation and gel layer polarisation respectively. For OBM broths, rape seed oil and soya bean flour are decreasing in concentration throughout the fermentation and these components are thought to

hinder the passage of protein across the membrane by hydrophobic interactions and adsorption.

4.3.5 Discussion of Broth Age Effects

Permeate flux decreases relative to steady state permeate flux over MF time are reduced in both SCM and OBM broths the older the broths are. In SCM broths where no effect was observed between steady state permeate flux and fermentation time i.e. ssJ was just as likely to be high at the end of the fermentation as it was to be low relative to the ssJ at the earliest time point. This suggests that the average permeate flux over the concentration step may be higher in the later stages of the fermentation than at the beginning. In OBM broths where ssJ decreases over fermentation time combined with the small decreases seen in permeate flux drop over the main part of the MF step, the emphasis that should be placed on flux decay and it's importance to the speed of the concentration step are limited.

For OBM, the majority of the fouling occurs at the very start (up to 50 seconds) of the concentration cycle and therefore the average permeate flux is affected little. Therefore, when considering overall process performance, SCM broths should be harvested as late as possible whereas OBM broths should be harvested as soon as the product concentration is at a maximum. For organic/electrolyte suspensions the flux decline depends on the deposition of solids at the membrane surface (Schafer *et al.* 2000) and given that deposition of solids is increased at higher solid concentration (Porter, 1972) the OBM was expected to undergo more rapid fouling. The inversely proportional relationship between flux and apparent viscosity is well documented, as is that for flux and biomass concentration. Steady state flux decreased with fermentation time and increased μ_a in OBM, but a relationship was

less clear for SCM. In OBM where apparent viscosity can be up to 8 times higher than that seen in SCM at the calculated shear rates observed at the membrane surface, the viscosity was the dominant factor affecting ssJ. For SCM broths, both biomass concentration and apparent viscosity decreased after approximately 40 h and the levels of total suspended solids were reduced compared to OBM, due to the absence of undissolved media components. It has also been observed that uniformed sized solids resulted in less flux reduction than gelatinous non-uniform particle (Antoniou *et al.* 1990) such as a water-flour mixture.

Erythromycin transmission showed no variation in relation to the broth age for either medium compositions, although the transmission was higher for SCM broths than OBM broths, 96.4 ± 1.6 % and 89.6 ± 1.4 % respectively. From experimentation it was known that the erythromycin was not dissolving in the residual organic phase (Section 4.1.3). The difference in erythromycin was presumed to be an interaction between the solid phase and the erythromycin in the OBM, this is supported by observations that large gel layers at the membrane surface can decrease percentage erythromycin transmission to 70 % (Antoniou *et al.* 1990).

Statistical analysis of the mass flux data calculated from the steady state permeate flux, transmission percentage and concentration of erythromycin, showed that there was no significant difference between the mean mass flux data derived from the MF of SCM and OBM broths, SCM_{mean} = 1.47 x 10^{-6} $kgm^{-2}s^{-1}$, OBM_{mean} = 1.38 x 10^{-6} $kgm^{-2}s^{-1}$. The low permeate flux and slightly reduced erythromycin transmission observed in the microfiltration of the OBM broth was thus

counteracted by the higher erythromycin titres obtained during the fermentation. The choice between use of a soluble or oil-based medium would thus be based on economic criteria and the acceptable level of diafiltration.

In Section 4.1.4 the protein transmission across the membrane can be limited by rejection at the membrane surface due to fouling and in the polarisation layer. It has also been reported that protein losses can occur through adsorption onto solid surfaces including medium components in the rig and broth (Turker and Hubble, 1987). The differences are therefore assumed to be due to increased solids loading and polarisation at the membrane.

4.4 The Effects of Volumetric Crossflow on Microfiltration

The flow of the process stream across the membrane surface allows high permeate flux and transmission values compared to those achievable by conventional dead-end filtration. The shear caused by the crossflow of liquid reduces cake and gel layer formation as has been discussed in Section 1.4. In this section the effects of crossflow rate on microfiltration performance during the processing of *S. erythraea* grown in SCM and OBM is discussed.

4.4.1 SCM Fermentations

Microfiltration operating conditions for the processing of SCM broths were selected based on the minimum TMP at the slowest volumetric crossflow rate that was to be used. Since increasing the rate of crossflow may increase the observed cTMP (Porter, 1972), a value had to be established that would be in the pressure dependent region of the flux-pressure relationship at the smallest values of

crossflow, yet could be achieved at high crossflow. High transcartridge pressure drop (TCP) defined by:

$$TCP = P_1 - P_2 \qquad [4.3]$$

is observed at high rates of crossflow, and a value of P_2 greater than zero must be maintained to ensure the entire area of the membrane is utilised. As can be observed in Figure 4.14, at 69 kPa TMP the crossflow has no impact on the steady state permeate flux. The transport of material to the membrane by the pressure is greater than or equal to the back-transport of solids and solutes away from it at any of the crossflow velocities used. At the lower TMP of 41 kPa there was an observed increase in flux with an increase in volumetric crossflow. The test at 41 kPa was repeated at 43 hours, the time of maximum biomass (±3 hours). The crossflow was again shown to be proportional to the steady state permeate flux and it was therefore decided to use this pressure for the rest of the crossflow experiments.

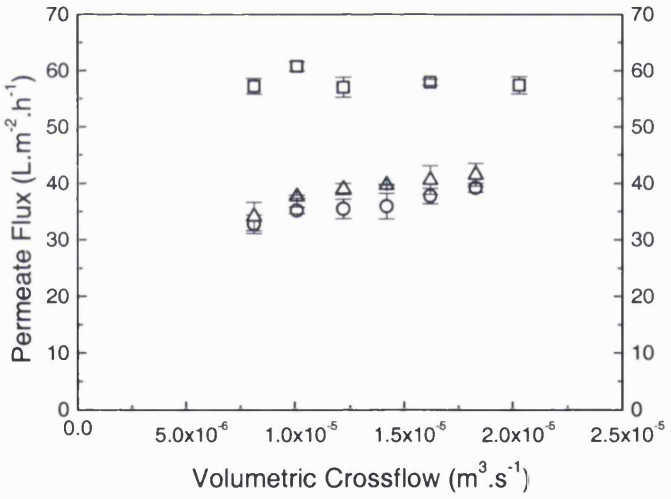

Figure 4.14. Changes in the relationship between steady state permeate flux and crossflow at different transmembrane pressures; □ - 30 h at 69 kPa; ○ - 37 h at 41 kPa; △ - 43 h at 41 kPa from fermentation SCM42L05. Microfiltration carried out using Minitan rig as described in Section 2.3.1.2. Reynold's numbers were calculated as described in Section 2.3.3.4 and shown in Table 2.4, they show the system is operating in laminar conditions.

4.4.1.1 Membrane Fouling

As with the TMP studies described in Section 4.2.1, the permeate flow rates were calculated from triplicate measurements once steady state had been attained. Figure 4.15 A, shows the flux decay against microfiltration time, the highest crossflow was run first to stop irreversible fouling occurring.

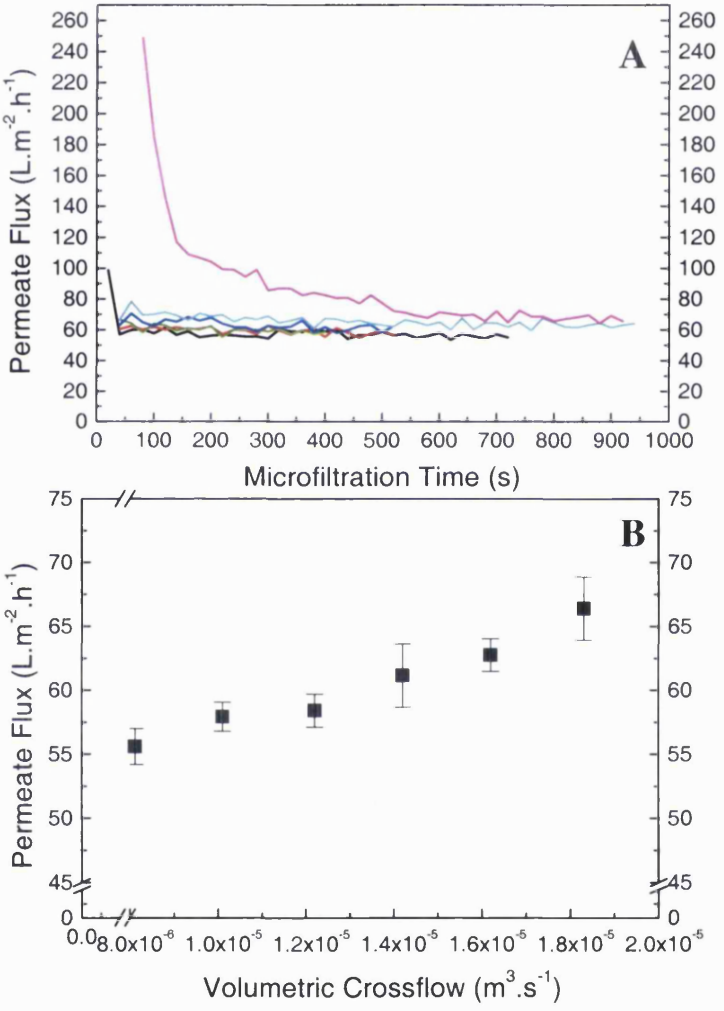

Figure 4.15. Flux decay against microfiltration time (A) and steady state flux against volumetric crossflow rates (B); — 8.11 x 10^{-6} $m^3.s^{-1}$; — 10.14 x 10^{-6} $m^3.s^{-1}$; — 12.17 x 10^{-6} $m^3.s^{-1}$; — 14.19 x 10^{-6} $m^3.s^{-1}$; — 16.22 x 10^{-6} $m^3.s^{-1}$ and — 18.25 x 10^{-6} $m^3.s^{-1}$. Results were taken from fermentation SCM42L6 and microfiltration carried out as described in Section 2.3.1.2.

Blinding of the membrane occurs quickly and the total hydrodymamic resistance of the membrane is not significantly increased by back-flushing the permeate through the membrane at the end of each crossflow velocity run. Figure 4.15 B, shows how steady state permeate flux changes with increasing volumetric crossflow. As crossflow is increased, so does the rate of flow of the permeate as predicted by the higher shear rate at the membrane surface reducing fouling and the formation of a gel polarisation layer at the surface of the membrane.

4.4.1.2 Steady State Permeate Flux

Although increasing crossflow also increases the cTMP (Porter 1972), thus allowing higher steady state flux, the major effect at constant TMP is an increase in flux due to a lower apparent viscosity (μ_a) at high crossflow. Figure 4.16 is a plot of steady state permeate flux against A: volumetric crossflow and B: apparent viscosity at 41 kPa TMP at time points during fermentation SCM42L6.

Since the broth is a pseudoplastic non-newtonian liquid as described in Section 3.1.3 and as shear varies with volumetric crossflow defined by Equation [1.15], therefore apparent viscosity is inversely proportional to crossflow and therefore proportional to the steady state permeate flux.

The apparent viscosity calculated from the different shear rates caused by changing the volumetric crossflow and the consistency index (K) and flow behaviour index (n) calculated as described in Section 2.3.3.3.

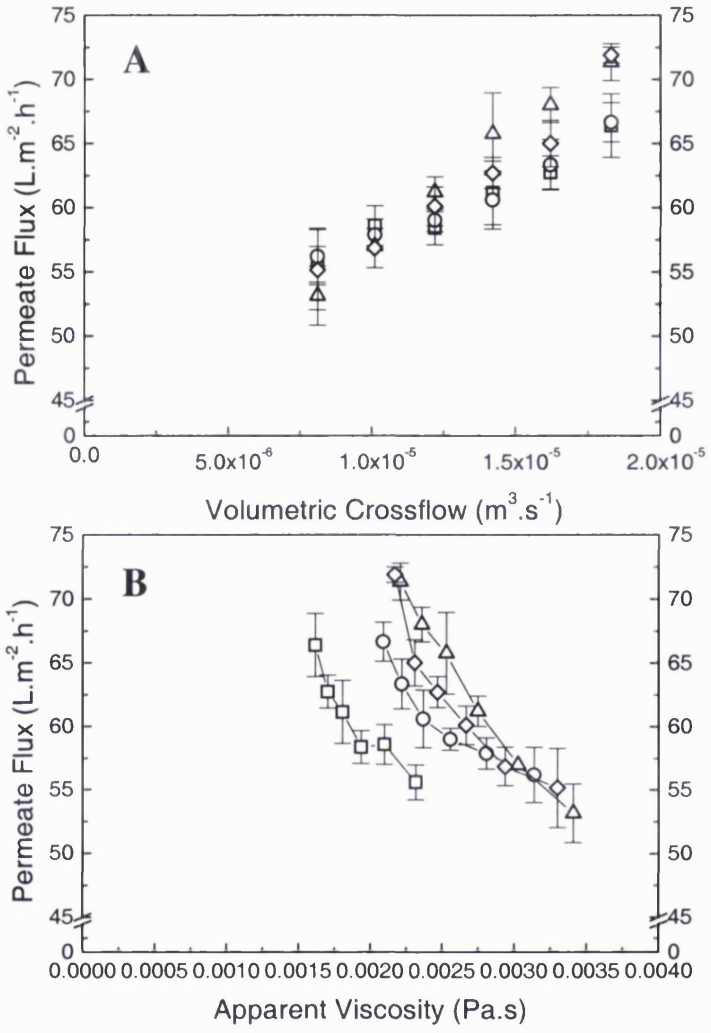

Figure 4.16. The effect of volumetric crossflow and apparent viscosity on steady state permeate flux. Graph A: permeate flux against volumetric crossflow Graph B: apparent viscosity at 11,000 s^{-1} against steady state permeate flux, both for fermentation SCM42L6 at times: □ - 22.5 h; ○ - 28 h; △ - 33.5 h and ◊ - 39 h. MF was carried out as described in Section 2.3.1.2 and in all cases the TMP was 41 kPa. Calculation of apparent viscosity was carried out as described in Section 2.3.3.3.

As for TMP studies in Section 4.1.3.1 a relative increase in permeate flux was compared to a relative decrease in the apparent viscosity, as described by Equation [4.3]:

$$100\left(\frac{J_{new}}{J_{initial}}\right) = -A\left[100\left(\frac{\mu_{anew}}{\mu_{ainitial}}\right)\right] \qquad [4.4]$$

Figure 4.17 shows experimental data from SCM42L5 and 6 plotted in the form of Equation [4.4]. As previously used in the TMP correlation (Section 4.1.2.1), the correlation is relative to a value of μ_a previously measured on that sample of broth. The high value of the correlation coefficient (R^2) suggests that the majority of the effect on steady state flux is caused by a reduction in viscosity, rather than the direct action of the crossflow itself reducing fouling and gel polarisation. This effect although seen at 0.4 bar, was not apparent at 0.7 bar (Figure 4.14). Under the higher TMP conditions, where the membrane is gel polarised, neither the viscosity or the crossflow had any noticeable effect on the steady state permeate flux.

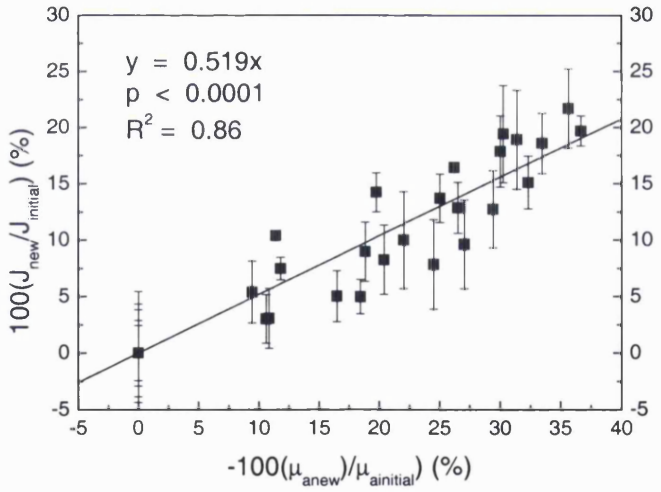

Figure 4.17. A graph of the change in viscosity of SCM fermentations affecting the percentage change in steady state permeate flux, data are combined from SCM42L5 and SCM42L6.

Further investigation is suggested in order to understand this effect, however it is presumed from the available data that the gel layer caused at high pressures cannot be removed by the increased shear at higher crossflows, and is not effected by the lower viscosities of the broth due to the thickness of the gel layer.

4.4.2 OBM Fermentations

Although a similar experiment was carried out using OBM broths fewer data points were available, the high apparent viscosity of the fermentations meant that there was a limited range of crossflows at constant TMP under pressure dependant conditions that could be achieved. This was because of the higher TCP associated with higher apparent viscosity and the low value of the cTMP in OBM broths. Two time points were investigated from fermentation OBM20L4.

4.4.2.1 Steady State Permeate Flux

The relationship between steady state permeate flux and apparent viscosity was investigated using three values of volumetric crossflow (8.11, 10.1 and 12.2 $x10^{-6}$ $m^3.s^{-1}$) at two time points of fermentation OBM20L4. The relationship defined by Equation [4.3] was used and gave a linear relationship (viscosity dependant constant (A) was 1.64, $p < 0.0001$ and $R^2 = 0.91$). Drawing definite conclusions from a small data set is questionable, however the data does support a link between apparent viscosity and relative permeate flux rates. As in the case of SCM fermentations, the variation in flux seen through changing the crossflow velocity in the pressure dependant region of operation, is due to the change in apparent viscosity.

4.4.3 Discussion of the Effects of Volumetric Crossflow

Below high values of TMP increased crossflow velocities lead to increased steady state permeate fluxes. Although most studies display an increased permeate flux with an increase in crossflow (Fradin and Field, 1999; Cumming *et* al. 1999; Zhang and Song 2000; Porter 1972) this relationship is not always the case. Nagata *et* al. (1989) found that increasing crossflow led to increased TCP and therefore increased TMP which resulted in the compaction of the fouling layer and a reduction in permeate flux in *Bacillus polymyxa* broths. Lu and Ju (1989) concluded that selective particle deposition at high crossflow velocity resulted in a larger cake resistance. This increase is due to the higher shear rate associated with increased crossflow leading to reduced apparent viscosity owing to the shear thinning properties of both OBM and SCM fermentations. In shear thinning viscous streams of magnesium hydroxide suspensions with a broad distribution of particle size it was found that streams with higher apparent viscosity showed greater increases of permeate flux with increases in Reynold's number (Fradin and Field, 1999). This paper also reported that there was no single linear relationship between shear stress and J_{ss} for all concentrations of particles, but the relationship is linear for each individual concentration, which supports the findings in this thesis.

4.5 Microfiltration Summary

In this chapter it has been shown how using the different media formulations as described in Chapter 3 has affected the microfiltration process and how varying the MF parameters affects the process performance of the primary separation of the two types of fermentation broth. The characterisation of the separation has led to

the realisation of the link between OBM broth apparent viscosity and the steady state permeate flux. No trend could be found for SCM broths.

Due to previously published data describing a link between bacterial shape and ssJ the next chapter investigates the morphology of *S. erythraea* using image analysis with respect to the fermentation and microfiltration to consider the effects of the morphology of the organism on MF performance. The final chapter then uses the information and correlations gathered in this chapter to model the MF process and investigate scale-down with a view to decrease development time and costs.

5 Hyphal Morphology and the Effect on Microfiltration Performance

5.1 Introduction and Aims

The importance of mycelial morphology during the fermentation on the production of erythromycin by *S. erythraea* has been recently noted in the literature (Martin and Bushell, 1996; Bushell *et al.*, 1997). It was found that only mycelia over 88 μm in diameter were capable of producing erythromycin, suggesting that antibiotic production occurred at a fixed distance from the growing hyphal tip. Previous studies have also highlighted the link between the agitation rate in the fermenter and the resultant morphology attained by mycelial bacteria (Heydarian *et al.* 1996; Heydarian 1998a; Justen *et al.* 1998; Amanullah *et al.* 1999).

These studies have found correlations between the energy dissipation over circulation time (EDC) function and the morphology of the organism. Heydarian (1998a) described a relationship between EDC and mean major axis of the mycelia (OL) in *S. erythraea* in 7 L and 450 L vessels. Justen *et* al. (1998) demonstrated that increased biomass concentrations and increased growth rates were related to higher stirrer speeds and shorter mycelial hyphae in *Penecillium chrysogenum* broths grown in fed batch cultures using given impeller type and geometry. This was concluded to be due to the larger number of growing tips created through the shear imposed on the organism. Amanullah *et al.* (1999) found that at higher agitator intensity the size distribution was skewed towards smaller mycelial sizes in continuous cultures of *Aspergillus oryzae.* In all these cases the mycelial size

increased rapidly followed by a sharp decrease and then a steady state size was achieved over fermentation time.

Microbial morphology has been shown to impact on the performance of filtration operations. Nakanishi *et al.* (1987) showed that the shape of various species of discrete bacteria affected the permeate flux in a dead end filtration system. Elliptical species such as *E. coli* formed more rigid, less compressible cakes, leading to lower specific cake resistance and therefore higher permeate flux. In crossflow filtration systems cake compressibility is also important since more rigid cakes lead to higher permeate flow rates (Kawakatsu *et al.*, 1993). The shape of cells is also affected by and has an effect on crossflow filtration, Tanaka *et al.* (1994) showed through microscopy how that rod shaped bacteria lined up in the direction of flow in the cake layer on the membrane surface.

In this chapter image analysis of *S. erythraea* grown using the SCM has been used to quantify the size and shape of the mycelia as a function of fermentation time. The subsequent effect of hyphal morphology on the flow of filtrate through the Minitan Durapore MF membrane was then investigated. The aim was to develop a predictive relationship for the performance of the primary separation step based on knowledge of fermenter operating conditions. A secondary aim is to confirm the quantitative relationship between morphology and biomass concentration described by previous studies (Packer *et al.* 1992; Paul and Thomas 1998), as this will allow direct measurement of the biomass concentration in more complex fermentation broths such as the oil based medium used in previous chapters.

5.2 Variation of S. erythraea Morphology During Fermentation

5.2.1 Variation With Fermentation Time

Figure 5.1 shows the variation of the mean main hyphal length (ML) of *S. erythraea* with fermentation time for fermentations SCM20L1, SCM20L3 and OBM20L2. In order to aid comparison between the different fermentations, the data is plotted with a time scale relative to the maximum biomass concentration attained in the case of SCM fermentations, or maximum apparent viscosity attained for the OBM fermentation (Section 2.2.3.4). ML describes the length of the longest hyphae present in a mycelium as illustrated schematically in Figure 5.2. The highlighted hyphae is the longest in the mycelium; it's overall length was measured using the software developed by Packer and Thomas (1990) as described in Section 2.2.3.5.

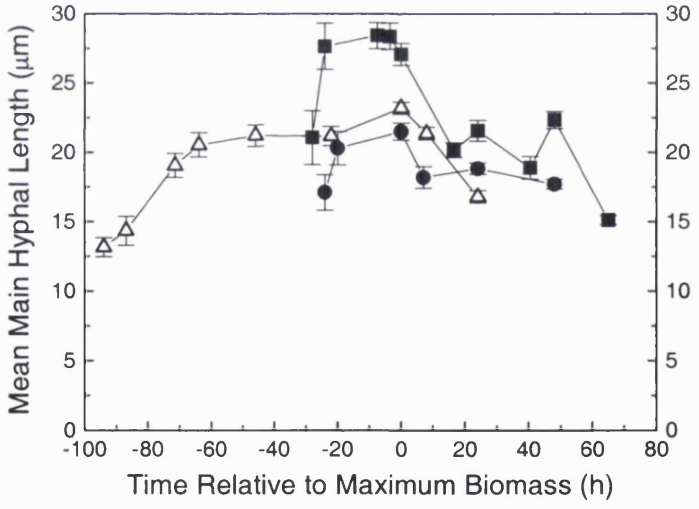

Figure 5.1. Variation of mean main hyphal length (ML) with fermentation time for SCM20L1 - ■, SCM20L3 - ● and OBM20L2 - △. The fermentations were carried out as described in Section 2.2.1.2 and the characterisation of the morphology as described in Section 2.2.2.5.

The two SCM fermentations display similar profiles although the magnitude of the measured mean main hyphal length is different, this may be due to the variable impeller speeds used during these fermentations which were not comparable with respect to both fermentation time and tip speed. The ML increased rapidly during the early exponential phase of growth (-30 h to –20 h) then shows little increase during late exponential and stationary phase until maximum biomass is reached. ML then decreases rapidly during late stationary phase after which ML continues to decrease slowly towards the end of the fermentation. This is in agreement with the findings of Heydarian (1998a).

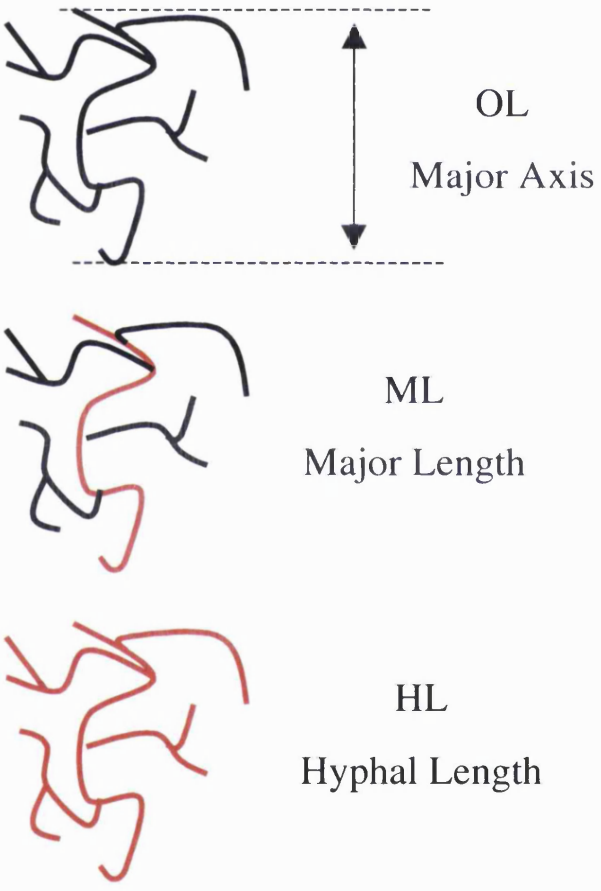

Figure 5.2. Diagrammatic representation of the measurement of the major axis (OL), mean main hyphal length (ML) and total hyphal length (HL) as described in Table 1.1, Section 1.1.3.3. The measured length of the hypha in the mycelium is represented by the red lines.

The profile shown for the OBM fermentation is comparable although the plateau is apparently extended due to the longer fermentation time (Figure 3.2). Early exponential growth phase (-90 h to –70 h) shows a rapid increase in the ML followed by a slow increase in late exponential growth and stationary phases (-70 h to 10 h) followed by a rapid decrease during early death phase. The ML can be lower than that seen in SCM, which is contrary to the relative concentrations of erythromycin A seen between the different fermentations (see Table 3.2). As discussed in Section 1.1.3.2 the length of hyphae is proportional to the erythromycin concentration, from the results of this study the relationship is probably more complex. Investigation into the distribution of the hyphal size should be considered in future studies to obtain a more detailed picture of the relationship between media selection, product concentration, biomass and the morphology of the organism.

5.2.2 Variation With Agitation Rate

Heydarian (1998) has previously reported a relationship between the power input to the fermenter, the mixing time (t_c) and the major axis (OL) of the mycelia. The OL is defined as the shortest line that can be drawn across the mycelium at it's widest point. This is illustrated schematically in Figure 5.2. Heydarian's findings suggested that the higher the impeller speed, the smaller the average size of the mycelia produced in the fermenter. This is as would be expected is consistent with studies of shear damage on various organisms in stirred tank reactors (Cherry and Papoutsakis, 1988; Thomas, 1990). Quantitatively the relationship derived by Heydarian is given by:

$$OL = S_F E\left[\frac{\rho\mu\varepsilon}{\sqrt{t_c}}\right]^{-0.15} \quad [5.1]$$

where OL is the major axis (μm), S_F is the critical total strain energy (J), E is the modulus of elasticity of the hypha ($N.m^{-2}$), ρ is the density of fluid (≈ 1,000 $kg.m^{-3}$), μ is the viscosity of the fluid (Pa.s), ε is the energy dissipation rate per unit mass ($W.kg^{-1}$) and t_c is the mixing time of the fermenter (s^{-1}). This was verified experimentally for small (7L) and pilot scale (450 L) reactors, however the constant to which the bracketed group was raised was found to be –0.12.

Figure 5.3 shows the OL plotted against the bracketed group from Equation [5.1] from data collected during fermentations SCM42L1, 2, 4 and 5, at tip speeds of 1.63, 2.45 and 3.28 $m.s^{-1}$.

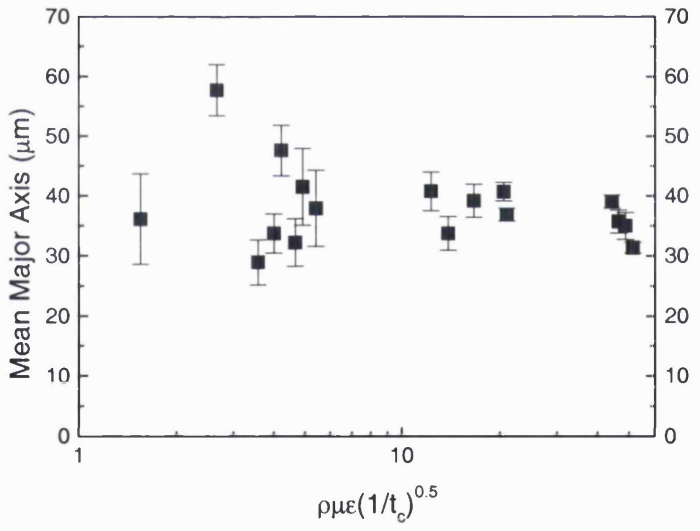

Figure 5.3. Relationship between the mean major axis and the bracketed group in Equation 5.1. The morphology was measured by image analysis as described in Section 2.2.3.5 and the energy dissipation and recirculation time were calculated as described in Appendix I and the apparent viscosity as described in Section 2.3.3.3. From fermentations SCM42L1, 2, 4 and 5.

Although a visible trend towards lower values of OL at higher values of $\rho\mu\varepsilon(1/t_c)^{0.5}$ was observed, this was proven not to be statistically significant. This is thought to be due to the sampling undertaken to provide material for subsequent microfiltration experiments as described in Section 5.3. As seen in Appendix I, the calculation of energy dissipation in the reactor (ε) is dependant on the value of the liquid height (H_T) in the vessel which decreased due to sampling and this led to increases in ε.

Figure 5.4 summarises the results of all the possible morphological measurements for the three fermentations carried out at different tip speeds. In general there is no obvious difference between the impeller speed and the morphology of *S. erythraea.* Apart from the outliers, most notably at the lowest tip speed (1.63 $m.s^{-1}$) and the point of maximum biomass concentration for ML, BL, HL and MA, the variations are within the standard deviations of the means of the measured values. The final experimental points in fermentation SCM42L4 appear unusually high in all characteristics whereas all the other fermentations show a declining trend. This is probably due to the liquid level in the fermenter which falls below that of the top impeller for the final sample. In each case of an observed outlier, the measurement of morphological features was repeated on a duplicate slide prepared at the same time as the initial slide. No significant difference was observed between the two slides.

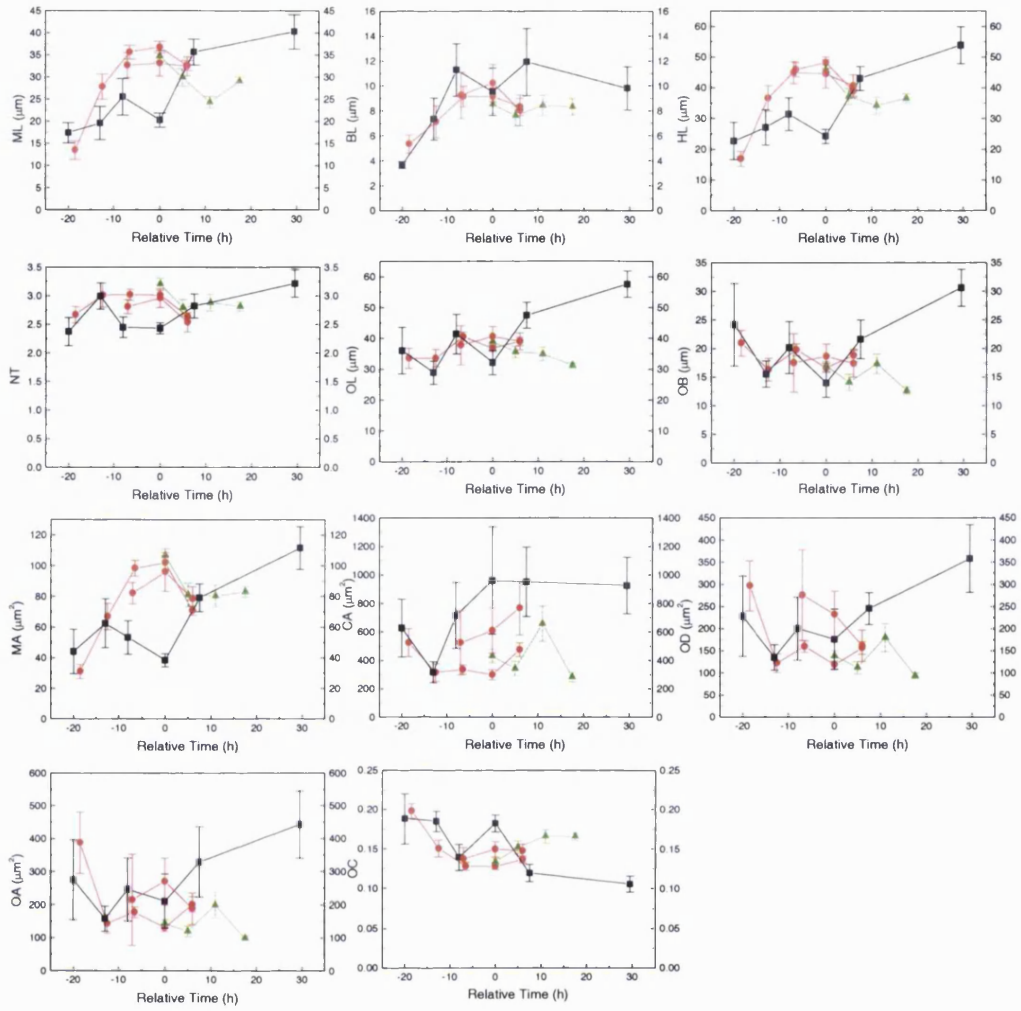

Figure 5.4. Summary of the different morphological measurements (as described in Section 2.2.2.5) for fermentations performed at different tip speeds. ■ - 1.63 $m.s^{-1}$ – SCM42L4, ● - 2.45 $m.s^{-1}$ – SCM42L1 and SCM42L5 and ▲ - 3.28 $m.s^{-1}$ – SCM42L2. Time is plotted relative to the time maximum biomass concentration.

5.2.3 Prediction of Biomass Concentration Using Image Analysis

Previous studies have shown the biomass concentration of a complex mycelial organism can be estimated from image analysis data, Packer *et al.* (1992) used a manual measurement of hyphal diameter using digital pictures and a light pen combined with automated measurement of hyphal lengths to give a value for cell volume in *P. chrysogenum* which was then combined with literature values of dry

cell weight per unit volume of cells to give a biomass concentration. Paul and Thomas (1998) in a review of the morphological characterisation of mycelial organisms using image analysis described various techniques for the determination of biomass concentrations including assessing areas of hyphal degradation to improve accuracy in fungi. In *Streptomycetes* the limitation becomes the optics of the microscope and the resolution of digital images of the image analysis system. Treskatis *et al.* 1997 used various morphological classes such as pellets, aggregates and mycelial flocks etc. in *Streptomyces tendae* to estimate biomass concentration and physiological state with a good degree of accuracy. In this study the total hyphal length (HL), of the mycelium as shown in Figure 5.2 has been multiplied by the number of mycelia measured (N) in a sample prepared as described in Section 2.2.2.5. This gives the total length of all hyphae measured over 25 areas on a slide for broth diluted 1000 times. This method assumes that all hyphae are of equal diameter at all stages of development of the mycelium.

Figure 5.5, shows the relationship between the total measured hyphal length (HL x N) against the measured biomass concentration for all the SCM fermentations in which image analysis was used. This indicates a reasonably good correlation between the two measured variables. The ordinate intercept is assumed to be an error inherent in the measurement of the morphology using the Magiscan 2A. This could be due to a number of different factors. These include slight variations in light intensity throughout the measurement of each slide leading to increased interference by media components and the background, or the incorrect conclusion that the hyphal width remains constant throughout the growth of the organism.

Pons *et al.* (1998) showed that hyphae became narrower with age in *Streptomyces ambofaciens*.

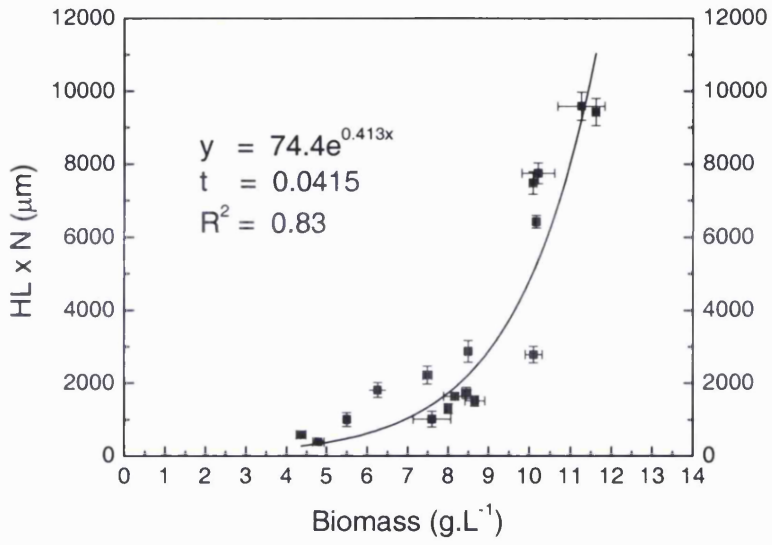

Figure 5.5. Graph of HL x N against biomass concentration for SCM fermentations. Measurements were made as described in Sections 2.2.2.2 and 2.2.2.5. Error bars for biomass concentration are the standard deviations calculated from triplicate measurements; error bars for HL x N were the calculated standard deviation of the mean from the Magiscan 2A software.

This relationship was used to compare the morphology of OBM20L2 with viscosity measurements, which as previously stated (see Section 2.2.2.4) is proportional to the biomass. Figure 5.6 shows a graph of $\log_{10}$ HLN against viscosity measured at a shear rate of 71 s^{-1} and gives a linear relationship, indicating that the model of HLN to predict biomass can be used for the measurement of biomass in OBM fermentations.

The relationship derived from the SCM fermentation data from Figure 5.7 is:

$$C_B = \left(\frac{\log HLN}{0.144} \right) - 2.43 \qquad [5.2]$$

where C_B is the biomass concentration ($g.L^{-1}$) and HLN is the total hyphal length multiplied by the number of mycelia measured (μm). Using this relationship, the biomass concentration of an oil based medium fermentation (OBM20L2) was calculated and compared to the calculation of biomass using OUR (see Section 3.3.1) using the equation:

$$C_B = \frac{OUR}{1.67} \qquad [5.3]$$

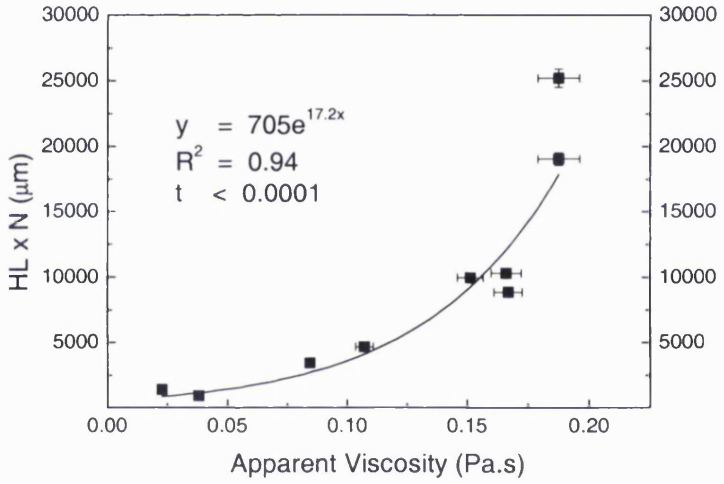

Figure 5.6. Graph of $\log_{10}$ HL x N against apparent viscosity in OBM20L2. Measurements were made as described in Sections 2.2.2.4 and 2.2.2.5, error bars for viscosity are the standard deviations calculated from triplicate measurements and error bars for HLN were the calculated standard deviation of the mean from the Magiscan 2A software.

where OUR is the oxygen uptake rate ($mmol.L^{-1}.h^{-1}$) and a and m are constants relating to the oxygen utilisation of the organism in terms of its biomass concentration. The two correlations for the prediction of biomass concentration from off-gas data and from image analysis data were compared to apparent viscosity (Pa.s) measured at a shear rate of 71 s^{-1}, since it is the latter which is the

established analogue to monitor cell growth. These data are plotted for comparison in Figure 5.7. It can be seen that the two methods can most accurately predict biomass concentration in OBM during different areas of the fermentation profile. Image analysis overestimates the biomass at low concentration, which as previously described, could be due to interference from media components and variable light fluctuations, or the assumption that hyphae diameter is constant. Paul and Thomas (1998) quoted the width of a typical Actinomycete hypha was between 0.5 and 1.5 μm, since growth is associated with the growing tip. The assumption made is that the hyphal diameter is constant and that there are no effects caused by the x1000 dilution of the broth during slide preparation (Section 2.2.3.5). The measurement of hyphal diameter is suggested if resolution allows. The inaccuracy could also be due to a limited sample size, as at low concentrations the hyphae are too disperse, in which case a lower dilution would be suggested.

The prediction of biomass concentration using the OUR trace follows the viscosity closely at low values of oxygen uptake rate. At approximately 70 hours the OUR prediction peaks before biomass has finished increasing, then shows a slow predicted decline until the point of maximum biomass at approximately 110 hours, after which predicted biomass drops quickly. This deviation from the viscosity is assumed to be a metabolic change in the organism, which reduces the oxygen demand but does not cause the cessation of growth. It is proposed that the OUR model predicts growth accurately from inoculation to late exponential, early stationary phase and the morphology model predicts accurately between mid to late exponential phase until the end of the fermentation.

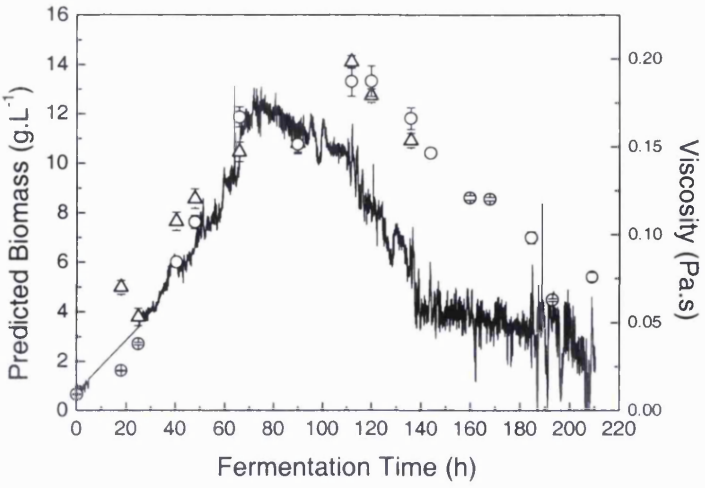

Figure 5.7. Predicted biomass concentration using OUR data - — and predicted by HL x N using the model from SCM fermentations - ○ against fermentation time in h. The apparent viscosity - △ is plotted as reference since it is the standard technique for determining growth. All data is derived from fermentation OBM20L2. Measurements were made as described in Sections 2.2.2.2 and 2.2.3.5, error bars were derived as described in Figure 5.6.

The initial results are very promising and show that with improved methodology the measurement of biomass concentration using morphological characteristics can be used accurately throughout the entire duration of OBM fermentations. Recent studies (Bittner *et al.* 1998) have shown that automated image analysis can be used to measure the biomass of single-celled organisms (*Sacc. cerevisiae*) on-line. The correlation to dry cell weight was accurate over the range tested (0.01 $g.L^{-1}$ to 12 $g.L^{-1}$). This method was also found to be robust enough to replace flow cytometry during the study. The development of at-line measurement for mycelial organisms using image analysis was found to be a useful tool in the monitoring of *Streptomyces tendae* fermentations (Treskatis *et al.* 1997). An automated aseptic sampling and dilution method was used, connected to a flow cell in a microscope with digital imaging capability, which was controlled by a personal computer. The

development of such a system for the measurement of biomass concentration in *S. erythraea* in both soluble and multiple phase processes would be of use in the monitoring of the fermentation.

5.3 Effect of S. erythraea Morphology on Microfiltration Performance

5.3.1 Morphological Effects on Microfiltration in 20 L SCM fermentations

Initial experiments to investigate how mycelial morphology affected steady state permeate flux during crossflow microfiltration were conducted using broths from fermentations SCM20L1 and 3. This work was carried out due to previously published data linking the morphology of different discrete bacterial species and permeate flux during dead-end filtration (see Section 5.1). It was considered that the cake structure formed during crossflow microfiltration might also be dependent upon mycelial morphology. This would probably explain the time-variant microfiltration performance of the SCM broths previously described in Section 4.3. For all of the image analysis parameters determined from the SCM broth samples (Figure 5.6), the most significant relationship was found between steady state permeate flux and the mean main hyphal length (ML), as shown in Figure 5.8. In this case the variation in ML is brought about due to changes in fermentation harvest time as described in Section 5.2.1.

The results show that for lower values of ML the permeate flux is increased. While this is a statistically significant relationship, the coefficient of correlation is low at just over 0.70. The correlation coefficient improves if the two fermentations are considered separately, suggesting that a proportion of the variation comes from inherent differences between the two fermentation broths. A number of hypotheses

can be drawn from these results. It suggests that longer hyphae form fouling layers of larger resistance than those formed by short hyphae. This could be due to packing efficiency and voidage of the cake, or the compressibility of the cake or a combination of these effects.

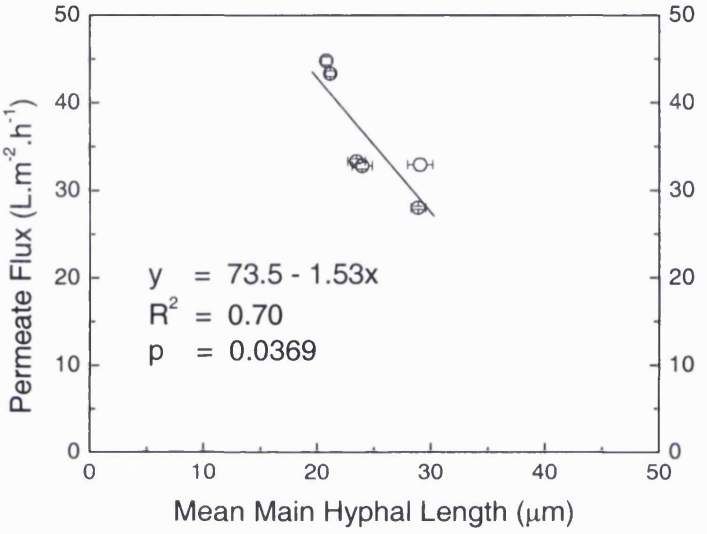

Figure 5.8. Mean main hyphal length against steady state permeate flux. Data from fermentations SCM20L2 and 3 were used (Section 2.2.2.2) and the subsequent microfiltration of the broth using the Minitan (Section 2.3.1.1).

In addition to the use of image analysis results to predict biomass concentrations (Section 5.2.3) it would also be useful if such data could be used to give a preliminary insight into the performance of the subsequent MF operation. For the purposes of predicting permeate flux from ML a correlation developed from the two fermentations has been used. Figure 5.9 represents the permeate flux predicted from image analysis results of the ML data using the following relationship derived from the data shown in Figure 5.8:

$$ssJ = 73.5 - (1.53 \times ML) \qquad [5.4]$$

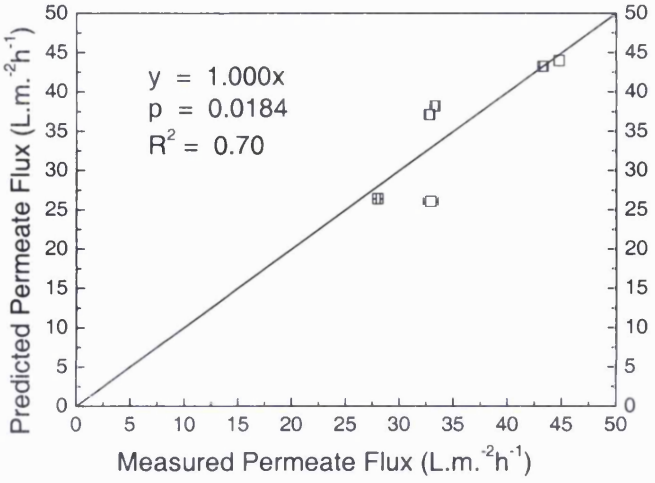

Figure 5.9. Predicted permeate flux against measured permeate flux. Predicted from ML using the relationship given in Equation [5.4] from fermentations SCM20L2 and 3 (Section 2.2.2.2) using the Minitan rig as described in Section 2.3.1.1.

Figure 5.9 demonstrates a linear relationship exists between values of steady state permeate flux at the cTMP predicted by the measured ML morphological characteristic and the measured steady state permeate flux at cTMP. The regression line shows a statistically significant relationship ($p = 0.0184$), which accurately predicts the flux (gradient = 1.00) with a correlation coefficient of 0.70.

5.3.2 Morphological Effects on Microfiltration in 42 L SCM fermentations

The results of the initial study were not supported by a subsequent, more detailed investigation of the relationship between ML and permeate. Figure 5.10 is the result of applying the relationship defined by Equation [5.4] to the ML data for fermentations SCM42L1-SCM42L5. The values of permeate flux predicted from ML are statistically different to the experimentally determined values. Taking the results of the fermentations individually did not change the result, nor did deriving a formula from 42L fermentations. It is therefore concluded that it is not possible

to predict the performance of the primary separation by tangential flow microfiltration from the morphology of the organism.

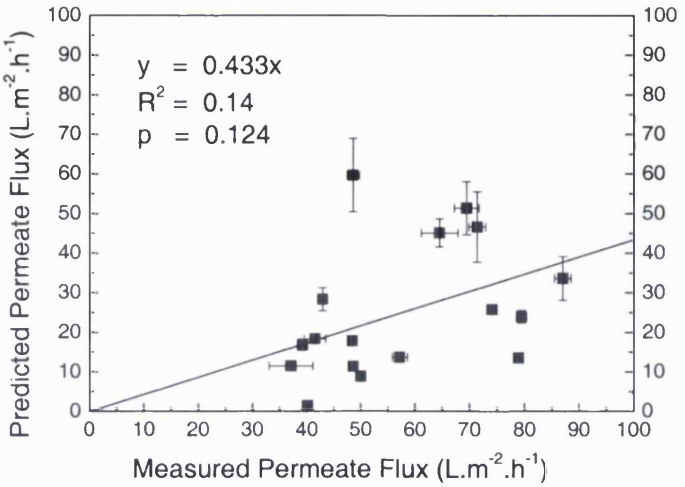

Figure 5.10. Predicted steady state permeate flux against measured steady state permeate flux using the relationship shown in Figure 5.10 and described by Equation [5.4]. The values of ML at different time points in the fermentations SCM42L1, 2, 4 and 5 (Section 2.2.2.3) were compared to permeate flux at cTMP using the Minitan rig (Section 2.3.1.2).

5.4 Morphology Summary

The work presented in this chapter has exploited the power of image analysis tools to quantify the size and shape of *S. erythraea* mycelia as a function of fermentation time and fermenter operating conditions. No correlation between OL or other morphological parameters could be proven. This was assumed to be due to the large volume changes caused by relatively large samples of broth being removed for subsequent microfiltration experiments. This was thought to affect fermenter mixing characteristics and calculation of the rate of energy dissipation (ε) which is the method used to relate morphology to fermenter operating conditions in several studies (Heydarian 1998a; Justen *et al.* 1998; Ammanullah *et al.* 1999).

It has also been shown that the image analysis data can be used to satisfactorily predict biomass concentration in complex broths such as that derived from the oil based medium. This avoids the limitations of on-line gas data becoming non-representative of the biomass concentration when growth is restricted as highlighted by Sarra *et al.* (1996). The use of the total hyphal length (HL) for the calculation of biomass concentration in OBM proved to be a useful tool from mid exponential growth phase onwards.

Finally, the relationship between the mycelial morphology and permeate flux was examined In dead-end filtration permeate flux rates were demonstrated to be related to the morphology of different uni-cellular bacterial species (Nakanishi *et al.* 1987). Using TFF *E. coli* cells were found to align themselves in the direction of flow at the membrane surface (Tanaka *et al.* 1994). In silica bead feed streams Zhang and Song (2000) described the difference in fouling of membranes with variation of particle size, with small particles leading to rapid fouling but higher values of steady state permeate flux.

Evidence that the MF performance could be predicted by the mean main hyphal length (ML – see Figure 5.9) from experiments on fermentation broths grown in 20 L fermentations was presented. Further investigation to increase the sample size for this work using variable tip speeds in 42 L fermentations could not replicate the earlier results and no relationship was found between the steady state permeate flux at cTMP and ML or any other of the measured morphological characteristics. The variation in permeate flux observed from samples taken over the duration of the fermentation could not be attributed to the morphology of *S. erythraea.*

6 Modelling of Fermentation - Microfiltration Interactions

6.1 Microfiltration Modelling

The aim of this section of the work is to take into account the varying fermentation physical parameters to predict the performance and optimum operating conditions of the microfiltration process. The genetic engineering of *S. erythraea* (Section 1.1.3) to form new polyketide products affects the process performance of the fermentation (Mirjalili *et al.* 1999). The medium composition and fermenter operating conditions will then therefore need to be reviewed as each new strain is evaluated. So, rapid methods to assess the effect of these changes on the performance over the whole process sequence are thus required. With many potential new products, development costs are high, so modelling of a process united with accurate scale-down to allow for predictive performance will reduce the amount of required data and enable rapid development at reduced cost and thus shorten product lead times.

Scale-down of MF to allow development of processes at small scale is an invaluable tool in industry, which enables rapid and inexpensive evaluation of changes in organism or fermentation protocols to be made. Recent advances in membrane design have transferred the onus of scaleability onto the vendor rather than the user (van Reis *et al.* 1997a). It is still necessary to verify the ability of systems to predict between scales and in this study the scale-down of *S. erythraea* broths in Millipore Pellicon-2 and Pellicon-Mini cartridges was carried out. The membrane area of these cartridges was 0.5 m^2 and 0.1 m^2 respectively giving a five fold scale difference. From the use of modelling and scale-down, the key

parameters affecting the MF will be identified so that maximum benefit can be gained from the rapid collection of data at small scale.

6.1.1 Model Synthesis

Tangential flow filtration systems operate under two different regimes. One is where the permeate flux is dependant on the transmembrane pressure and the other, a region where the process is independent of pressure. In this chapter a simple model linking operation in both regions is developed and tested. Volumetric crossflow rate, TMP and apparent viscosity are the MF factors that affect the permeate flux at steady state and a model to explain the behaviour of *S. erythraea* fermentations grown in SCM broths harvested by TFF is developed. The mass transfer model described by Porter (1972), in the pressure independent region, is evaluated with respect to SCM broths using the fermentation parameters of biomass concentration and apparent broth viscosity.

The mass transfer model of permeate flux (J) relates the percentage concentration (w/v) of material at the wall due to polarisation (C_w) to the percentage concentration (w/v) of the feed stream (C_b) in terms of a mass transfer coefficient (k). This model is also referred to as the film theory model (Cheryan, 1998) and is described by:

$$J = k\left(\ln\frac{C_w}{C_b}\right) \qquad [6.1]$$

The mass transfer coefficient, k, in flat sheet membrane modules has been correlated to relevant process variables by Porter (1972) as shown by Equation

[6.2], where K_p is a dimensionless constant, Q is the volumetric crossflow rate ($m^3.s^{-1}$), b is the channel height (m), w is the channel width (m), L is the channel length (m), D is the solute diffusion coefficient ($m^2.s^{-1}$) and ν is the kinematic viscosity of the broth ($m^2.s^{-1}$):

$$k = K_P\left(\frac{Q}{bwL}\right)^{0.5}\frac{D^{0.66}}{\nu^{0.17}} \qquad [6.2]$$

For the non-Newtownian *S. erythraea* broth (Section 2.3.3.3), the kinematic viscosity is described as the apparent viscosity (Pa.s) divided by the broth density ($kg.m^{-3}$) as in Equation [6.3].

$$\nu = \frac{\mu_a}{\rho} \qquad [6.3]$$

Since the broth is shear thinning as previously shown in Section 3.2.3 and the viscosity will depend on the shear rate in the membrane module, substituting from Equations [6.3] and [2.2] into [6.2] gives:

$$k = K_P\left(\frac{Q}{bwL}\right)^{0.5}\frac{D^{0.66}}{\left(\frac{K\gamma^{n-1}}{\rho}\right)^{0.17}} \qquad [6.4]$$

Equations [6.1] and [6.4] thus allow prediction of the permeate flux based on knowledge of the broth physical properties, membrane module geometry and operation and a single independent variable (K_p). Experiments to determine K_p are described later in Section 6.1.2.

6.1.1.1 Accounting for the Effects of Volumetric Crossflow and Apparent Viscosity on Permeate Flux

As described in Section 1.4.2, the shear induced at the membrane surface by the passage of the feed stream tangentially to the flow of filtrate, provides the mechanism by which fouling material and the polarisation layer is removed. The liquid crossflow velocity thus not only acts to increase back-transport of material away from the membrane surface but, because the shear rate changes in proportion to the crossflow velocity (and therefore the volumetric crossflow rate), it also alters the apparent viscosity of the broth. In complex non-Newtonian fluids such as filamentous fermentation broths, which for the broths studied here are shear thinning (see Section 2.3.3.3), increased shear rate through increased crossflow leads to decreased apparent broth viscosity. Since permeate flux is inversely proportional to apparent viscosity (Equation [1.8]), increased crossflow will be expected to increased flux through reducing the hydrodynamic resistance to the flow of permeate across the membrane, but also by decreasing the viscosity of the feed stream. In this section the roles of crossflow and apparent viscosity are investigated with respect to their affect on the steady state permeate flux of SCM broths.

Figure 6.1 shows a graph of steady state permeate flux against volumetric crossflow rate for broths harvested from fermentation SCM42L6. As volumetric crossflow rate increases so does the permeate flux. The relationship between the two is also seen to vary during the course of the fermentation time suggesting that other factors such as the biomass concentration and morphology impact on model

parameters such as the viscosity Power Law constants (see Section 2.3.3.3) which will also change over time.

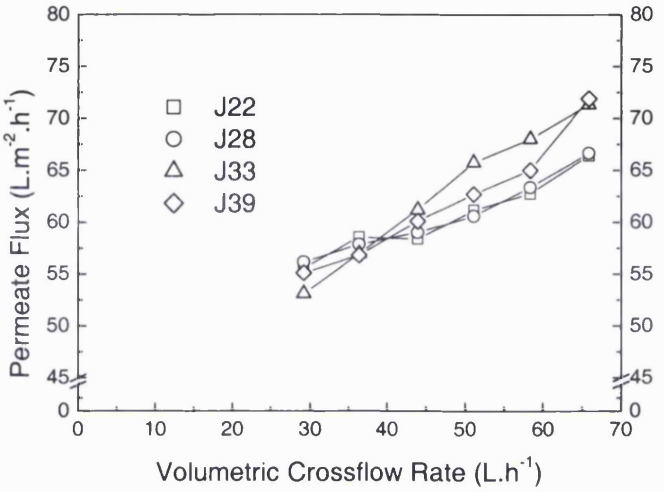

Figure 6.1. Steady state permeate flux against volumetric crossflow rate for fermentation SCM42L6 at times □ - 22 hours, ○ - 28 hours, △ - 33 hours, ◇ - 39 hours. Fermentation carried out as described in Section 2.2.2.3 and microfiltration experiments performed as described in Section 2.3.1.2.

Table 6.1 lists the ordinate intercept and gradient of the data shown in Figure 6.1 along with the errors calculated through linear regression of the data. It is considered that the initial flux and the magnitude of the influence of crossflow velocity (represented by the gradient) is dependant on the solids loading on the membrane and the rheology of the broth.

Time	Intercept ($L.m^2.h^{-1}$)	Intercept Error (±)	Gradient (m^{-2})	Gradient Error (±)
22	47.7	1.59	0.270	0.0324
28	47.6	1.37	0.274	0.0280
33	39.0	1.15	0.501	0.0235
39	41.4	2.37	0.433	0.0482

Table 6.1 Differences in the ordinate intercept and gradient of the data plotted in Figure 6.1 from SCM42L6 at 22, 28, 33 and 39 hours.

Figure 6.2 shows the calculated apparent viscosity (μ_a) of the fermentation broths at the different shear rates experienced at the membrane surface, due to the changing volumetric crossflow rates, and plots them against the steady state permeate flux. As previously observed for plots of permeate flux and volumetric crossflow rate (Figure 6.1), the relationship between μ_a and steady state permeate flux does change over fermentation time. In such systems, however, it is difficult to test the two factors independently as they are so closely linked. The constants (K and n) that model the changing apparent viscosity over different values of volumetric crossflow must therefore be determined when considering the filtration of shear-thinning fermentation broths as they have direct relevance to the MF performance

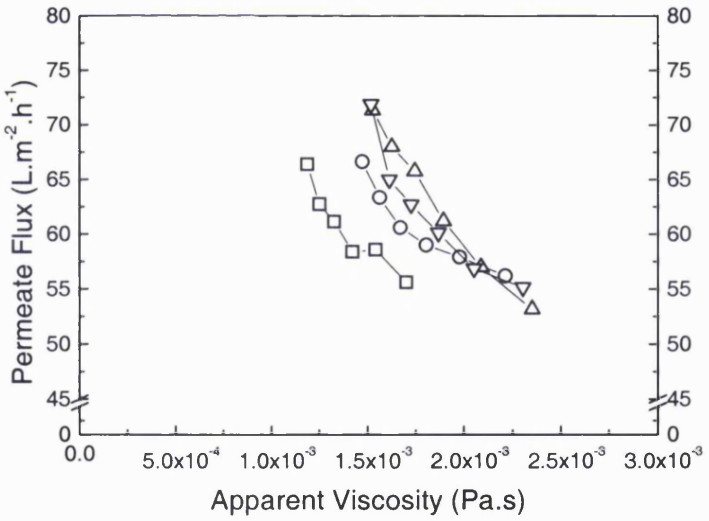

Figure 6.2. Steady state permeate flux against broth apparent viscosity for fermentation SCM42L6 at times □ - 22 hours, ○ - 28 hours, △ - 33 hours, ◊ - 39 hours. Fermentation carried out as described in Section 2.2.2.3 and microfiltration experiments performed as described in Section 2.3.1.2. Apparent viscosity at the membrane surface shear rate was calculated as described in Section 2.3.3.3.

6.1.1.2 Accounting for the Effect of Volumetric Crossflow Rate on the Prediction of Permeate Flux

Porter (1972) reported that the observed experimental values of the power dependence of permeate flux on volumetric crossflow rate, under laminar flow conditions, is often seen to differ from the theoretically derived value of 0.5 (Equation [6.4]). For this reason the relationship between the volumetric crossflow rate and the steady state permeate flux was investigated. The results of the volumetric crossflow experiments described in Section 4.4.1 were plotted on a $\log_{10}$-$\log_{10}$ scale for permeate flux against the volumetric crossflow velocity. The gradient of the regression line is the experimentally derived value of the power to which the (Q/bwL) group in Equation [6.4] is raised.

Figure 6.3 shows an example of this, for data from fermentation SCM42L5 and broth harvested at 37 h and 43 h. This analysis was repeated for broths from fermentation SCM42L6, harvested at times 22 h, 28 h, 33.5 h and 39 h. The mean of the gradient determined in each case was then calculated and used in the model as given in Equation [6.5]. The calculated mean was found to be 0.15 ± 0.3.

$$k = K_P\left(\frac{Q}{bwL}\right)^{0.15}\frac{D^{0.66}}{\left(\frac{K\gamma^{n-1}}{\rho}\right)^{0.17}} \qquad [6.5]$$

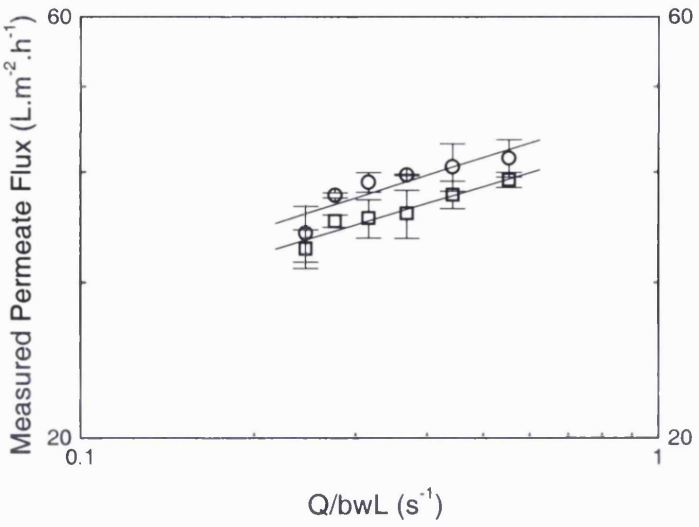

Figure 6.3. Measured permeate flux against Q/bwL plotted on double $\log_{10}$ axes. Data shown is from SCM42L5 at 37 h and 43 h after inoculation, (Section 2.2.2.3) at various volumetric crossflow rates using the Minitan (Section 2.3.1.2).

6.1.1.3 Experimental Determination of Kp

In order to be able to predict the permeate flux, J, values of K_p (for Equation [6.5]) were determined from the MF experiments performed under various operating conditions and ages of broth. Equation [6.1] was first rearranged to calculate the mass transfer coefficient, k, from experimentally measured values of permeate flux and the percentage concentration of biomass in the feed stream (C_b). Using this value of k, and knowledge of the membrane module geometry, operating conditions, apparent viscosity and the solute diffusion coefficient (D), Equation [6.5] is then rearranged. This is then used to calculate the value of K_p.In the following sections the variation of K_p between different fermentations will be described, together with it's use for predicting J over a range of operating conditions.

6.1.1.4 Permeate Flux Predictions Across all Fermentations

The model which was considered device specific with respect to K_P (Brose *et al.* 1996) was first used to predict permeate flux data for MF experiments performed at cTMP for broths harvested from fermentations SCM20L1, 2 and 3 and SCM42L1, 3, 4, 5 and 6. The two sets of fermentation data were considered as different populations since SCM20L1, 2 and 3 broths were examined using only one membrane sheet in the Minitan II module (Section 2.3.1.1) while the broth from the 42 L fermentations were examined using two membrane sheets (Section 2.3.1.2).

The solids concentration at the membrane surface (C_w) was assumed to be 70 % (from Okec 1998). This assumption is used, as explained previously in Section 1.3.3, is made since the value of C_w cannot be determined without altering the outcome of the experiments. The density of the broth was considered to be (1000 $kg.m^{-3}$), the same as water. This assumption is based on experimental determination during SCM20L1 of the density, which was found to be 1013 ± 2 $kg.m^{-3}$ across the duration of the fermentation, a deviation from the assumed value of approximately 1 %. The solute diffusion coefficient was taken as 3.5×10^{-10} $m.s^{-1}$, from values exhibited by molecules of similar size to erythromycin (Atkinson and Mavituna 1991).

The aim of this study was to determine a mean value of K_p that could be used for predictive modelling to within ± 20 %. Values of the mass transfer coefficient (k) were back-calculated from measured values of steady state permeate flux at cTMP as described in Section 6.1.1.3. These were then used to calculate the device specific constant K_P. For each system (one membrane and two membranes), a

mean K_P was then determined, which was then used in Equations [6.1] and [6.5] to calculate the permeate flux at cTMP. A worked example of the calculation procedure is provided in Appendix I. The results of these predictions are shown in Figure 6.4 using values of K_p of 0.324 and 0.654 for data from the 20 L and 42 L fermentations respectively.

Although the relationship is statistically significant and the gradient of the regression line between the measured and predicted permeate flux is 1.00, there is large variation in the data. The mean error was found to be 22.6 ± 3.9 % different to the actual measured values. This was not considered to be accurate enough for modelling the process for microfiltration. The possibility of an unidentified fermentation parameter causing this unpredictability is considered. In order to reduce the error in the model, attention was turned to predicting MF process performance within fermentations. The hypothesis being that values of K_p derived experimentally early in the course of the fermentation could be used to predict the steady state permeate flux at the cTMP at the harvest time.

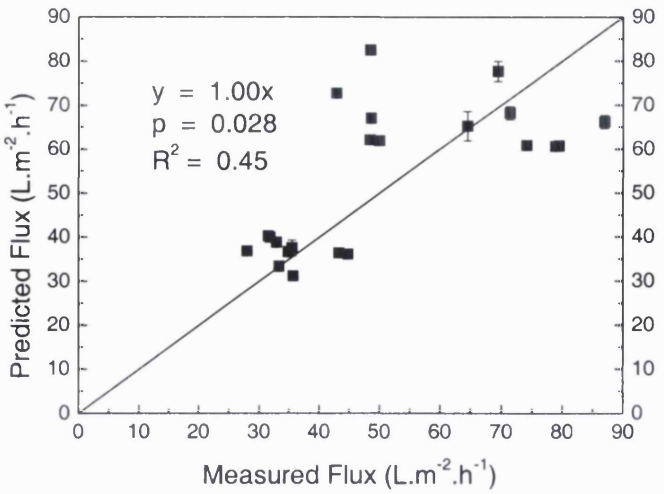

Figure 6.4. Predicted steady state permeate flux against measured steady state permeate flux at cTMP. Predicted values were calculated using Equations [6.5] and [6.1]. Values of K_p used for the two different membrane module configurations are given here. Fermentations were carried out as described in Section 2.2.2 and MF as described in Section 2.3.1.

6.1.1.5 Permeate Flux Predictions Within a Single Fermentation

In the previous section a single value of K_p was used that was a mean of all the K_p values calculated from every time point during the course of all the fermentations performed. Here, the analysis was repeated using a value of K_p calculated from the mean of the K_ps derived from a single fermentation from different times. Separate values of the dimentionless coefficient K_p were therefore required for each fermentation carried out. As shown in Figure 6.5 this allowed much more accurate prediction of the permeate flux within each set of fermentation data. Individual values of K_p are displayed in Table 6.1.

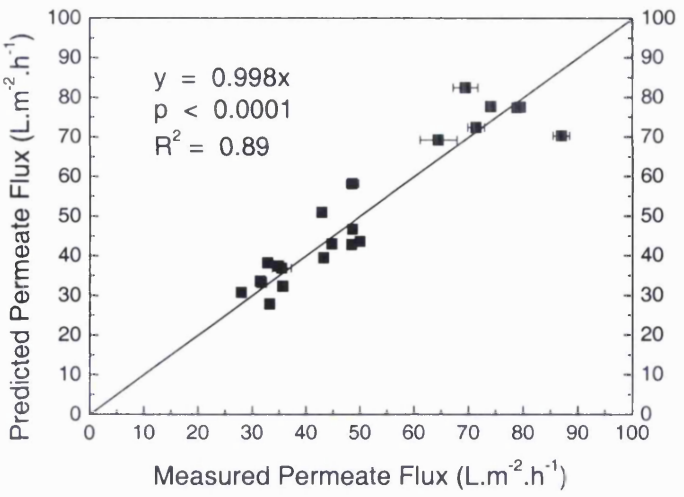

Figure 6.5. Predicted steady state permeate flux against measured steady state permeate flux at cTMP. Predicted values were calculated using Equations [6.5] and [6.1]. Values of K_p used were calculated as the mean of the experimentally derived K_p values from within a fermentation. Fermentations were carried out as described in Section 2.2.2 and MF as described in Section 2.3.1.

Fermentation	Value of K_p
SCM20L1	0.270
SCM20L2	0.330
SCM20L3	0.372
SCM42L1	0.450
SCM42L2	0.816
SCM42L4	0.586
SCM42L5	0.387
SCM42L6	0.593

Table 6.2. Values of K_p derived from experimental values of permeate flux at cTMP for fermentations SCM20L1, SCM20L2, SCM20L3, SCM42L1, SCM42L2, SCM42L4, SCM42L5 and SCM42L6 as described in Section 6.1.1.3.

Here, the variation in the model prediction is generally reduced, giving future predictions of the steady state permeate flux at the cTMP the mean error in the model was 9.5 ± 1.3 %. The disadvantage of this model is that a measurement of flux at cTMP needs to be taken, however it is clear that this can be taken many hours before the point of harvest. It is therefore possible to predict the flux (at

cTMP) during harvest to an accuracy of ~ 10 % by carrying out an optimised MF experiment hours before. Figure 6.6 is an example of the prediction of permeate flux within a fermentation using a value of K_p derived from an experiment carried out from an initial sample of fermentation broth. The numbers next to each data point relate to the time at which the broth was harvested and processed and the predicted value is plotted against the measured value.

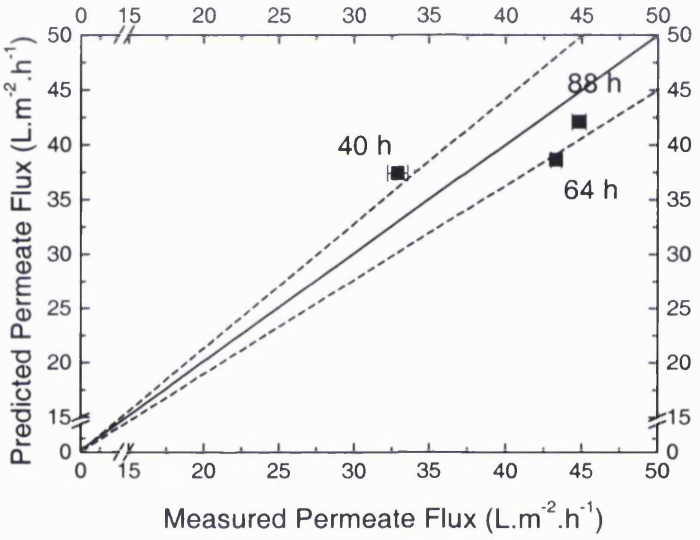

Figure 6.6. Predicted permeate flux against measured permeate flux for values calculated using Equation [6.5]. From fermentation SCM20L2 (Section 2.2.2.3) and MF experiments (Section 2.3.1.2). Predicted values calculated using an experimentally derived value of K_p at 33 h. Dotted line represents 10 % deviation from model.

The predictive capability was then examined for MF operation at different volumetric crossflow rates (Section 2.3.1.2) from fermentations SCM42L5 and SCM42L6. Values of K_P were back-calculated using the measured flux results and Equations [6.5] and [6.1]. A mean value of K_P was then used which was fermentation specific. The results are shown in Figure 6.7. The model adequately

predicts steady state permeate flux at a range of different volumetric crossflow rates and apparent viscosity values.

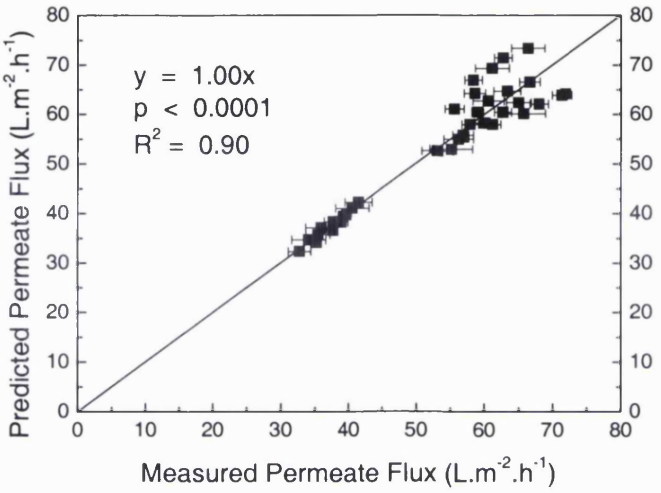

Figure 6.7. Predicted permeate flux against measured permeate flux, predictions were made using Equation [6.5] and data from crossflow experiments, samples from fermentations SCM42L5 and SCM42L6 as described in Section 2.2.2.3 were processed using the Minitan module as described in Section 2.3.1.2.

The steady state permeate flux at cTMP at the harvest time is now known, in Section 6.1.2 a method of determining what the value of this cTMP at the point of harvest is outlined

6.1.2 Adjusting the Model to Account for Transmembrane Pressure

So far permeate flux predictions have only been considered for MF operation at cTMP. In the pressure-dependant region operation of TFF, the steady state permeate flux will be directly proportional to the TMP up to the cTMP value. As described in Section 1.2.2.5, filtration is a pressure driven process and by increasing the driving force, the rate of flow of filtrate is increased. This is limited by the build up of the gel polarisation layer and the compression of the cake.

Beyond this point any increase in TMP will have either no effect or be deleterious to the mass flow across the membrane. It is therefore desirable to operate the process at the cTMP. However, the cTMP involves optimisation tests that exceed cTMP which may result in sub-optimal conditions despite reducing the pressure to below the desired value. It is the aim of this section to describe the relationship between permeate flux and TMP, so that not only can the permeate flux at cTMP be predicted, but also the cTMP itself.

Figure 6.8 is a graph of the percentage change in steady state permeate flux against the corresponding increase in TMP. This figure is obtained from analysis of data from fermentations SCM20L1, 2 and 3 using the Minitan II membrane system fitted with one 60 cm^2 0.2μm Durapore membrane as described in Section 2.3.1. The relationship is described in Equation [6.6], where $J_{initial}$ is the initial or reference steady state permeate flux and $P_{initial}$ is the TMP at which it was measured, J_{new} is the rate of steady state permeate flux at an increased pressure – P_{new}.

$$100\left[\left(\frac{J_{new}}{J_{initial}}\right)-1\right]=0.512\left(P_{new}-P_{initial}\right) \qquad [6.6]$$

To test the predictive capability, Figure 6.9 uses Equation [6.6] and applies the derived constant (of 0.512) to fermentations SCM42L1, 2 and 4 using the Minitan II membrane system fitted with two 60 cm^2 0.2μm Durapore membrane making a total area of 120 cm^2 as described in Section 2.3.1. The predicted flux shows a good correlation with the measured flux rates with a coefficient of variance (R^2) of 0.93. This demonstrates that the relationship described by Equation [6.6] is not affected by the length of the flow path (L).

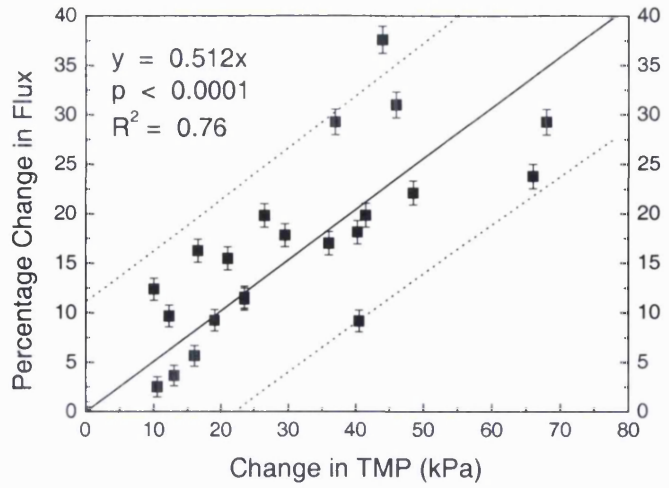

Figure 6.8. Percentage change in permeate flux from the flux at the initial TMP ($J_{initial}$ and $P_{initial}$ respectively) to the flux J_{new} at an increased TMP, P_{new} as described by Equation [6.6]. Broth from fermentations SCM20L1, SCM20L2 and SCM20L3 was used as described in Section 2.2.2.2 and MF optimisation data as described in Section 2.3.1.1.

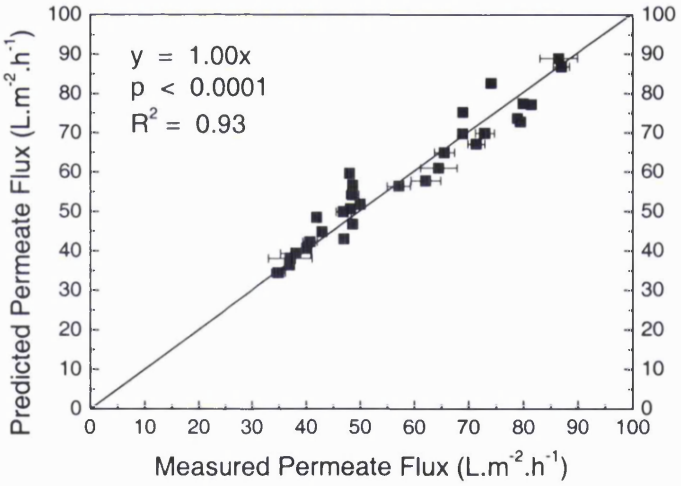

Figure 6.9. Values of predicted against measured permeate flux for fermentations SCM42L1, SCM42L2 and SCM42L4 (Section 2.2.2.3 and Section 2.3.1.2) using the relationship described by Equation [6.6].

6.1.3 Combining Mass Transfer and TMP Models

In this section a method for determining the operating conditions (cTMP) using a rapid filtration experiment and the predicted permeate flux from the mass transfer model. In Figure 6.10 a mean value of K_P from each fermentation is used in the model to predict flux rates at higher values of pressure. A value of steady state permeate flux is first predicted from fermentation data taking into account the membrane module geometry and operating conditions, at the lowest transmembrane pressure. From this, the TMP model (Equation [6.6]) is applied and the predicted flux at higher TMPs is plotted against the actual observed results. From Figure 6.10 it can be seen that the correlation is statistically significant with low variance. So, for every prediction of the future steady state permeate flux, the cTMP at this future time can be determined given an initial unoptimised result at low TMP. So by using a value of K_p derived experimentally earlier in the fermentation using Equation[6.5] the steady state permeate flux at the cTMP (J_{cTMP}) is known. During harvest, a rapid unoptimised MF experiment to obtain a value of steady state permeate flux (J_{low}) at any pressure below the cTMP (P_{low}) is carried out. Rearranging Equation [6.6] gives Equation[6.7] which uses these measurements to calculate the cTMP at the harvest time.

$$P_{low} + \left\{ \frac{100\left[\left(\frac{J_{cTMP}}{J_{low}}\right) - 1\right]}{0.512} \right\} = P_{cTMP} \qquad [6.7]$$

Therefore by performing an optimisation experiment at any point prior to harvest and then a single low TMP microfiltration at time of harvest, the optimum

operating conditions and process performance will be known. The values of K_p used for each fermentation are given in Table 6.1. Figure 6.10 gives the results of fermentations SCM20L1, SCM20L2, SCM20L3 and SCM42L1, SCM42L2 SCM42l4 for permeate flux predicted using a value of K_p derived from each experimental sampling time of the fermenter. For example, SCM20L2 was sampled at 40, 65 and 112 hours, predicted permeate flux is plotted against measured permeate flux for 65 and 112 h using K_p derived from the sample at 40 h, 40 h and 112 using the K_p value from 65 h and 40 h and 65 h using K_p calculated from the result at 112 h. This is repeated for all six fermentations For this data the mean error was found to be 12.4 ± 1.3 %.

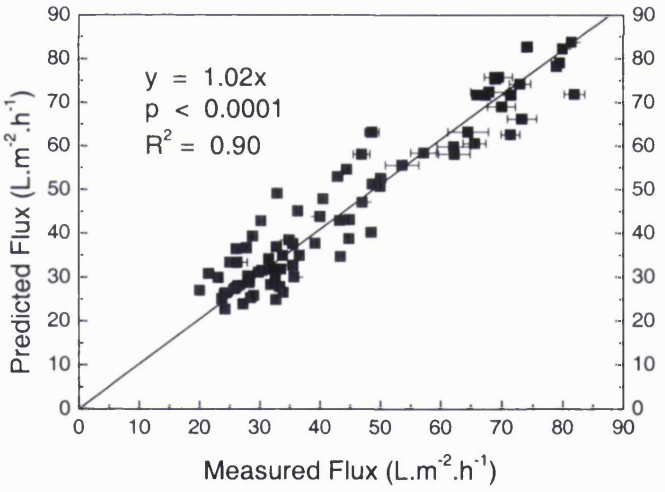

Figure 6.10. Flux and pressure data from base-line reading at low pressures is combined with a mean value of K_P within the fermentation (Table 6.1) to predict the steady state permeate flux using Equation [6.6], as described in Section 6.1.1.3.

Figure 6.11 is a graph of the predicted cTMP against the measure cTMP. As above J_{cTMP} is predicted from an earlier derived value of K_p and the measurements of biomass concentration and viscosity constants K and n at t_{harv} (Equations [6.1] and [6.5]). The P_{cTMP} at t_{harv} is then predicted using this value of permeate flux and measured values of J_{low} at P_{low} at t_{harv} using Equation [6.7]. The predicted values differ from the measured values with a mean error of 20.6 ± 4.3 %. There is a low observed correlation coefficient (R^2 = 0.48) indicating a wide variation of the predicted to the observed TMP values. The largest observed error was 52.9 % indicating that this correlation requires refinement if it is to be used as more than a guideline.

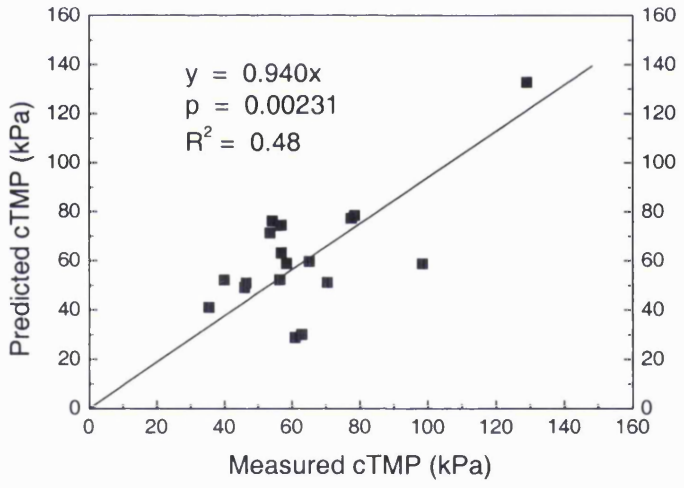

Figure 6.11. Predicted cTMP against measured cTMP for fermentations SCM20L1, SCM20L2, SCM20L3, SCM42L1, SCM42L2, SCM42L4. J_{harv} was calculated from K_p derived from a time prior to t_{harv} and cTMP calculated using J_{harv} and values P_{low} and J_{low} measured at t_{harv}. See Equations [6.1], [6.5] and [6.7].

6.2 Microfiltration Scale-Down

Traditionally, increasing membrane area has often meant increasing the length of the flow path across the membrane surface (Brose *et al.* 1996). Since a given length of pipe, through the actions of friction between the wall and the fluid passing through it, will exhibit a given pressure drop, increasing the pipe length increases the pressure drop. In a tangential flow filtration (TFF) system this would mean possible limitations on the volumetric crossflow rate at production scale since higher crossflows also mean larger pressure drops. This may not be physically possible due to pumping limitations or the mechanical strength of the membrane and supporting material. An altered TMP gradient would also be observed along the flow path with implications for permeate flux and transmission.

It was stated by vanReis *et al.* (1997a) that for linear scaling of TFF system, a constant path length is required. Currently the three main vendors of flat sheet TFF systems supply membrane cassettes of varying area based on this premise. In this study Millipore Pellicon (0.5 m^2) and Pellicon Mini (0.1 m^2) rigs have been used as described in Section 2.3.2, to examine scale-up of the MF process and the prediction of the performance of the larger scale units based on identical operating conditions. The membrane used in both cases was a 0.2 μm pore size Durapore V-screen. These were run concurrently during fermentations SCM42L7, SCM42L8 and SCM42L9 in order to minimise the differences between broth samples.

6.2.1 Comparison of Scale

MF experiments were carried out with a range of fermentation broths over a range of fermentation harvest times (varying biomass concentrations and apparent

viscosities) as previously described. Different transcartridge pressure drops (TCPs which describe volumetric crossflow rates for a given fermentation broth) and TMPs were used between the seven experiments to prove the scaleability over a range of operating conditions. The process conditions were kept identical for the two membrane sizes as described in Section 2.3.2. The results are shown in Figure 6.12. Linear regression of the data shows a good comparison between data from the Pellicon and Pellicon-Mini parallel experiments.

The relationship showed that steady state permeate flux for the 0.5 m^2 Pellicon were approximately 4 % less than those seen with the 0.1m^2 Pellicon-Mini, it is considered that this consistent difference was due to the different pumping rigs employed to run the membranes. The correlation coefficient (R^2) shows that variation about the line of regression is small. End effects are small pressure differences between the observed and actual values due to the pipe-work between the membrane and the pressure transducers. The differences in the pressure drop between the membrane and the pressure transducers / gauges could account for the observed variation in performance. Cumming *et al.* (1999) also reported that geometric differences between the flow channel in the membrane cassette and the flow path through a pressure transducer may not be the same. Since different gauges / transducers are used on different pumping rigs this also gives a possible source of variation.

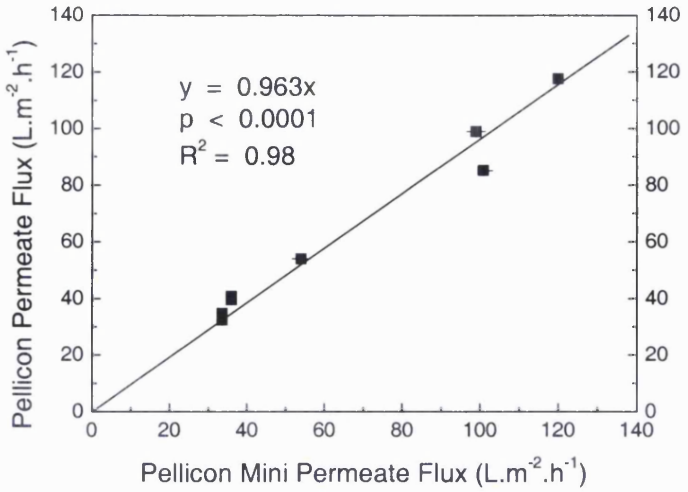

Figure 6.12. A comparison of steady state permeate flux in concurrent runs of fermentation broth (SCM42L7, 8 and 9). The two rigs were run at identical TMPs and TCPs for direct comparison. MF experiments were performed as described in Section 2.3.2.

6.3 Discussion of Modelling and Scale-Down

The model of Porter (1972) was modified on the basis of experimental data, changing the power dependence of flux on volumetric crossflow rate under laminar flow conditions from 0.5 to 0.15. This compares to other studies using micro-organisms in which K_p range from 0.1 to 0.79 (Cheryan 1998). Experimentally derived values of K_p calculated from the mean of single fermentations ranged from 0.270 to 0.816. This compared to values in the literature of 0.664 (Porter 1972) and from 0.216 to 0.373 depending on the device (Brose *et al.* 1996).

It has been possible to predict within fermentations what the future permeate flux at critical transmembrane pressure (cTMP) will be once values for the biomass concentration and the constants responsible for the apparent viscosity are known. It has not been possible to complete a reliable model to explain variation of steady state permeate flux from fermentation to fermentation. This difference is probably

due to one or more unidentified variable(s) that are attributable to the particular fermentation. As described in the Chapter 5 morphological characteristics were tested to discover if this was the cause of the variation, however no link could be established. It is suggested that any future study attempt to discover this/these factors to obtain a complete picture of the process model. It has also been found that a non-device specific constant determines the percentage difference in the flux rate given a difference in TMP. Combining these two relationships allows a prediction of cTMP at t_{harv} from a rapid un-optimised experiment taken at TMP<cTMP at the harvest time (t_{harv}).

Direct linear scale-down based on the Millipore Pellicon and Pellicon-Mini membrane cassettes is possible although engineering of the pumping rig may need to be carefully monitored to minimise the affect of different pipe-work geometries. The transcartridge pressure drop observed during Pellicon experiments at relatively low volumetric flow rates suggested the selection of a membrane with a wider channel geometry would be better suited to such broths.

Figure 6.13 summarises the predictions that this research makes possible during large scale MF operation, given that the production scale rig has the same feed path length as the scale-down equipment.

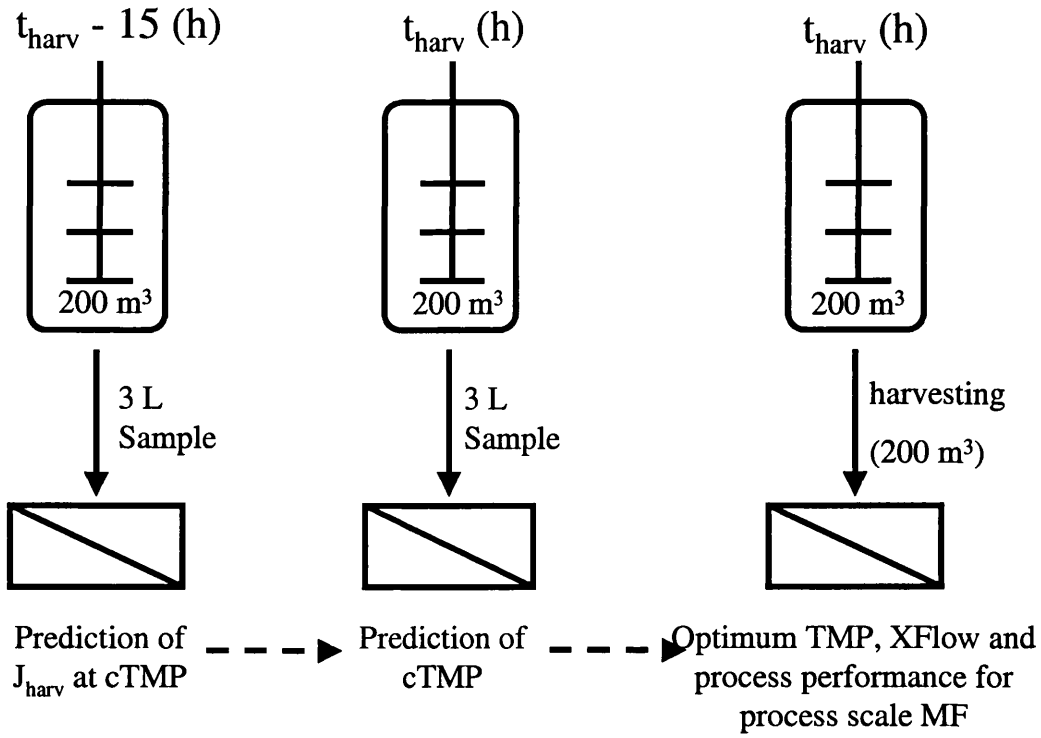

Figure 6.13. A summary of the application of this work to industrial scale fermentation. By carrying out a scale down run at a time prior to harvest, and a scale down run whilst the harvest is commencing, the process parameters and process performance for the large scale MF run are determined.

Figure 6.13 illustrates the usefulness of the work presented in this chapter. At a convenient time during the fermentation, prior to harvest, a small volume sample is taken and used to experimentally determine a value of K_p. From this value, the permeate flux at harvest (t_{harv}) is predicted. Shortly before the harvest time, biomass concentration and the viscosity constants are determined and a small volume is processed at low TMP (P_{low}) to determine J_{low} at t_{harv}, then using Equation [6.7] the cTMP at t_{harv} is then predicted.

7 Global Overview and Future Work

7.1 Summary and Overview

Recent advances in the genetic engineering of *S. erythraea* have led to the possibility of generating a large and diverse range of novel antibiotics (Donadio *et al.* 1991; Donadio *et al*, 1993; Cortes *et al.* 1995). Engineered changes in the sequence of the enzymes in the biosynthetic pathway of erythromycin (Section 1.1.3) give rise to alternative polyketides (the building blocks of erythromycin) and changes in the structure in the lactone ring of the product. Peter Leadley and co-workers at Cambridge University were amongst the pioneers of this technology and early on developed a strain which produces a three ketide product – the tri ketide lactone (TKL) (Cortes *et al.* 1995). Here at UCL, this strain has been used to evaluate how changing the genetics of the organism impacts on it's phenotypic characteristics and how those changes effect the process of erythromycin production and purification.

It has been shown that the specific utilisation rate of rape seed oil by the TKL strain as a carbon and energy source is significantly different than that of the wild type organism (Mirjalili *et al.* 1999). The concentration of the TKL is found to be far less (150 $mg.L^{-1}$) than that of the the wild type product (1089 $mg.L^{-1}$), with a range of closely related analogues also produced in the engineered strain. This could require a change in medium formulation and fine separation techniques for each new recombinant strain. The mechanical stability of the hyphae has also been found to be altered. The wild type strain displays a significantly lower normalised protein release over a range of shear rates than the TKL producer (Postlethwaite

1998). Considering that the production of erythromycin is dependent on the size of the hyphae (Martin and Bushell 1996) and the size of the hyphae in the mycelium is dependent on it's strength and the applied power (Heydarian *et al.* 1999; Bushell *et al.* 1997; Justen *et al.* 1998). Any changes in the mechanical stability of the organism will therefore have a direct effect on the operating conditions of the fermentation and/or product titre. Studies on the solvent extraction of recombinant polyketides have also shown that the partition was of the recombinant products between the aqueous and organic phases during solvent extraction was considerably altered (Vargas-Mora, 1997), thus requiring optimisation of the solvent extraction step for each new antibiotic.

The large number of possible products and strains, each of which may have different phenotypic properties can affect any and all of the unit operations of the manufacturing process. It has been the goal of the Small Molecule Processing Group at UCL to model the operation of polyketide production and purification in order to use these methodologies to rapidly develop the process for the production and purification of TKL. The aim of this particular work has been to understand how factors that influence the fermentation process such as medium composition and operating conditions affect the primary separation of *S. erythraea* biomass from the fermentation broth using tangential flow filtration. In this way changes to the fermentation process that can arise through altered nutritional requirements and growth characteristics of the organism and their effects on the microfiltration can be rapidly predicted. The impact of the performance of the MF step on subsequent DSP operations has also been considered.

Fermentations using traditional oil based media are used industrially to avoid problems associated with the catabolite repression seen in media with smaller molecular weight carbon sources (Wallace *et al.* 1992). Also because of the economic advantages of using such a readily available complex source of nitrogen and trace elements as soya bean flour. With the TKL strain the specific oil utilisation is reduced. So use of an OBM may not be desirable because of the high apparent viscosity (μ_a) of the broth. This causes dissolved oxygen limitations and is not ideal for MF also due to the high μ_a. The long fermentation times encountered are also a disadvantage (OBM 176 ± 15 h SCM 64.2 ± 0.3 h), but this is associated with higher product titres (OBM 617 ± 147 $g.L^{-1}$ SCM 241 ± 95 $g.L^{-1}$). With the use of fed-batch techniques the problems associated with the inhibition of product formation could be avoided. More work is required to assess the impact of different media and different feeding strategies, such as fed batch on the production of novel polyketides. Since the biomass concentrations are similar between the two media broths (SCM 11.9 ± 0.6 $g.L^{-1}$ OBM 11.5 ± 0.9 $g.L^{-1}$), the capability for the production of erythromycin are also similar (Trilli *et al* 1987).

The differences between the microfiltration performance of the two fermentation broths was also found to be marked. Fouling profiles for the two broths are also different, OBM fouled quickly followed by a slow decline, SCM broths are the opposite, in the first part of the curve the flux drops slowly relative to that seen in the OBM, followed by a relatively rapid flux decline as discussed in Section 4.2.1. In both cases however the fouling profiles indicate surface blocking of pores rather than blocking within the pores (Tracy and Davis 1994). Large colloids present in the OBM, such as un-dissolved flour are responsible for the decrease in flux and

the majority of these gather quickly at the membrane surface. Future work should investigate the effects of using high performance tangential flow filtration (HP-TFF), where a permeate metering pump is used to control flux across the membrane. This has been shown to increase the average permeate flow over the whole of the primary separation therefore increasing the process efficiency (vanReis *et al.* 1997b). Based on the fouling profiles of both media it is predicted that HP-TFF will give the most effective improvement in the MF of the SCM broths due to their slower rate of flux decline.

It has also been demonstrated that cross-flushing, where the permeate flux is stopped periodically to allow the retentate flow to reduce reversible fouling and back-flushing, where the permeate flow is reversed to push the cake and gel layer away from the membrane, can improve process efficiency (Kuberkar and Davis 2001). Any improvements by techniques such as this must be balanced against the added complications and costs of the instrumentation and possible membrane damage and reduced life expectancy.

Mass flux of erythromycin across the membrane is approximately the same for both SCM and OBM broths (SCM: $1.47 \pm 0.28 \times 10^{-6}$ kg.m^{-2}.s^{-1}, OBM: $1.38 \pm 0.20 \times 10^{-6}$ kg.m^{-2}.s^{-1}). This is because of the high permeate flux and low product titre of SCM fermentations and the low permeate flux and high product titre of OBM fermentations respectively (Section 4.2.5). In Appendix II it has been discussed how using Dean vortices to enhance shear at the membrane surface benefits the permeate flux of both SCM and OBM broths. Created through careful membrane cartridge design, the enhanced flow device (EFD) was found improve permeate

fluxes between 3.5 and 6.5 times that observed using the Minitan. The variation in enhanced performance depended on the medium composition and the harvest time of the broth.

The critical transmembrane pressure is reached at low TMP values during the MF of OBM broth (usually before any backpressure is imposed using the retentate backpressure valve). Therefore increased TMP has little part to play in the optimisation of the MF of OBM broths (Section 4.2.1). In SCM broths there is a linear relationship between permeate flux and TMP up to the cTMP as expected. This relationship shows the same characteristics in spite of the length of the membrane flow path (it is the same for the Minitan rig with one or two membranes in place) or in spite of the membrane design (the relationship is the same for the EFD rig – Appendix II). This is true as long as the increase is relative to a starting permeate flux and TMP as described by Equation [4.1].

For volumetric crossflow (which is directly proportional to crossflow velocity and shear rate at the membrane surface) there is a proportional relationship with permeate flux, which is due to the associated reduced apparent viscosity at higher shear rates. This is true of both types of broth, but is more apparent in the more viscous OBM fermentations, which is in agreement with published data (Fradin and Field 1999). The optimum operating conditions from the work carried out in this thesis would therefore be to operate the rig at the highest permissible volumetric crossflows in order to reduce the apparent viscosity of the shear thinning feed streams. Provided it is economic to do this, with respect to pumping costs and the additional cooling that may be required at industrial scale. The effect

of increasing crossflow on the cTMP was not evaluated during this study and any future work should include an analysis of the relationship. Care should be taken during such experiments since the long term storage of broth is not possible and the effect of short term broth ageing on microfiltration has also recently been demonstrated (Okamoto *et al.* 2001).

Previously published papers have drawn a relationship between microbial morphology and steady state permeate flux for both dead-end filtration (Nakanishi *et al.* 1987) and crossflow filtration (Nagata *et al.* 1989; Tanaka *et al.* 1994) due to the arrangement of cells in the cake at the membrane surface. Lu and Ju (1989) also described how particle size distributions at the surface of a membrane changed by altering the crossflow velocity. Image analysis was used in Chapter 5 to investigate the relationship between impeller speed, fermentation time, morphology and microfiltration performance. The principal reason for this study was to identify the causes of the variation in steady state permeate flux seen at the critical transmembrane pressure throughout fermentation time and between different SCM fermentations (as indicated in Figure 4.2.2). Unfortunately no relationship between the morphology and steady state permeate flux could be established that affected the permeate flux directly or via the established model.

However image analysis proved to be a useful tool in estimating the biomass concentration of multi-phase fermentation broths where traditional methods for a biomass assay were not possible due to the presence of suspended solids (Section 5.1.3). This prediction had a mean error of 11.1 ± 2.2 % and the relationship is described by Equation [5.2] and displayed in Figure 5.5. Further investigation to

provide a dilution series to enable more accurate measurement at low biomass concentration is suggested and or to take hyphal diameter into account. The possibility of an on-line biomass measurement system as previously described by (Treskatis *et al.* 1997) should also be investigated. No relationship could be determined between impeller speed and the mean values of the morphological characteristics suggesting that shear within the fermenter between the tip speeds of 1.63 and 3.28 $m.s^{-1}$ did not effect growth. Future work should also concentrate on the size distribution of the mycelia (Ammanullah *et al.* 1999) and the effect of the different forms of filamentous organism growth; freely dispersed and clumped mycelia (Sarra *et al.* 1996). The effect of morphology on the production characteristics and concentrations of erythromycin should also be considered as several studies have related morphology to the production of antibiotics. In *S. erythraea.* (Bushell *et al.* 1997) showed improved production in low shear environments due to increased mycelial size and other in organisms. Gehrig *et al.* (1998) demonstrated increased production of the antibiotics Striatals A, B and C in *Cyathus striatus* was increased at lower tip speeds for a given fermenter scale and impeller geometry.

It has been shown that using the models proposed for SCM broths (Equations [6.1] and [6.6]) for predicting permeate flux at cTMP using a mean value of K_p averaged over several fermentations, that the model gives a mean error of 22.6 % with extremes of 0.2 to 69.8 %. When this prediction is used within fermentations using values of K_p determined from sample points at different times during the same fermentation a prediction with a mean error of 9.5 % with extremes of 1.3 to 19.7 % is obtained. This combined with scale-down methods allows a sample to be

taken at any time before the harvest point and with an optimisation run at small scale, the flux at the harvest time at cTMP can be predicted. As long as the biomass concentration and the values of the viscosity constants K and n from the broth at the time of harvest are known.

Using the TMP prediction (Section 6.1.2), combined with the model used within fermentations and given an initial flux measurement at given pressure, the flux at any other pressure less than or equal to the flux at cTMP can be predicted. The mean error of 6.2 % with extremes of 0.4 to 23.1 %. This means that it is possible predict the steady state permeate flux at cTMP for the harvest time and at the harvest time a scale-down rig is used to find the permeate flux at low TMP then from Equation [6.7] the cTMP can also be predicted (Section 6.1.3).

The scale-down techniques used together with the models of gel polarisation and TMP allow the MF process performance and cTMP of SCM broths to be determined relatively quickly within the fermentation time of this process. For OBM fermentation broths this can be determined using scale-down and apparent viscosity measurements. Characterisation of the MF process is then possible in terms of the physical parameters of the broth and operating conditions of the MF. Using flat-sheet membrane modules the process can be predicted for large scale permeate fluxes and operating conditions from lab scale equipment. This will therefore allow rapid process characterisation for any novel polyketide products. Chapters three and four show how the choice of two different media can impact on MF performance. This work highlights the issues related to the choice of media for recombinant strains and the subsequent affect on MF. Chapter 5 demonstrates the

power of image analysis to determine the biomass concentration, however no link could be established for either the impeller speed or the permeate flux during MF. A method was developed at small-scale for the rapid evaluation of MF performance of the large number of recombinant strains that can potentially be produced. This work also showed the data can be used to successfully predict the performance of larger scale operations. Such predictions are useful to provide data for process and cost modelling to allow decisions to be taken on the selection of different strains or process options.

7.2 Future Work

It is advised that any future work on the fermentation would be to try to increase erythromycin titre using fed batch techniques. The use of continuous culture with on-line MF product removal using a chemostat to keep the culture in a nitrogen limited environment with enough carbon source to produce erythromycin. An improved description of how OBM steady state permeate flux relates to the apparent viscosity is required. Using MF operational changes such as HP-TFF, cross-flushing and back-flushing to increase performance should also be developed as well as new membrane designs such as the EFD (Appendix II). The diafiltration of the final concentrated cell slurry, in order to maximise erythromycin recovery has not been covered by this work and is a major time constraint in the industrial process. Any future investigation should aim to identify the best volumetric concentration factor to use and the number of diafiltration volumes.

8 References

Agrawal, A. and Burns, M.A. **1997**. Application of membrane-based preferential transport to whole broth processing. *Biotechnol. Bioeng.* **55**, 581-591.

Alex, T. and Haughney, H **1998**. New membrane-based technologies for the pharmaceutical industry. *In: Filtration in the Biopharmaceutical Industry.* 745-782. Ed. by: Meltzer, T.H. and Jornitz, M.W. Marcel Dekker Inc.

Allen, D.G. and Robinson, C.W. **1990**. Measurement of rheological properties of filamentous fermentation broths. *Chem. Eng. Sci.* **45**, No. 1, 37-48.

Alvarez, M.A., Fu, H., Khosla, C., Hopwood, D.A. and Bailey, J.E. **1996**. Engineered biosynthesis of novel polyketides: properties of *shiE* aromatase/cyclase. *Nature Biotechnol.* **14** 335-338.

Amanullah, A., Blair, R., Nienow, A.W. and Thomas, C.R. **1999**. Effects of agitation intensity on mycelial morphology and protein production in chemostat cultures of recombinant *Aspergillus oryzae. Biotechnol. Bioeng.* **62** 435-446.

Antoniou, C., Mir, L. and de-los-Reyes, G. **1990**. Clarification of antibiotic broths by cross flow microfiltration. *In: Bioprocess Eng. Symp. 1990.* 33-39.

Arnot, T.C., Field, R.W. and Koltuniewicz, A.B. **2000**. Cross-flow and dead-end microfiltration of oily-water emulsions Part II. Mechanisms and modelling of flux decline. *J. Memb. Sci.* **169** 1-15.

Atkinson, B. and Mavituna, F. **1991**. *Biochemical Engineering and Biotechnology Handbook.* 2nd edition Chapter 11, Macmillan, Basingstoke.

Bader, F.G., **1986**. Physiology and Fermentation Development. In: The Bacteria: A Treatise on Structure and Function: Antibiotic producing *Streptomyces.* Academic Press: New York, New York. Vol. 9 p.281-321 Eds. Queener, S.W. and Day, L.E.

Bailey, J.E. and Ollis, D.F. **1996**. Product recovery operations In: *Biochemical engineering fundamentals* 2nd Edition McGraw-Hill Book Company 726-797.

Bentham, A.C. **1990**. The formation, separation and dewatering of aggregated biological materials. Ph.D Thesis, UCL, U.K.

Berthold, W. and Kempken, R. **1994**. Interaction of cell culture with downstream purification: a case study. *Cytotechnol.* **15** 229-242.

Birnbaum, S. and Bailey, J.E. **1990**. Plasmid presence changes the relative levels of many host cell proteins and ribosome components in recombinant *Escherichia coli. Biotechnol. Bioeng.* **37** 736-745.

Björkman, U. **1987**. Properties and principles of mycelial flow: experiments with a tube rheometer. *Biotechnol. Bioeng.* **29**, 114-129.

Bosnjak, M., Stroj, A., Curcic, M., Adamovic, V., Gluncic, Z. and Bravar, D. **1985**. Application of scale-down experiments in the study of kinetics of oxytetracycline biosynthesis. *Biotechnol. Bioeng.* **27** 398-408.

Brose, D., Dosmar, M. Cates, S. and Hutchison, F. **1996**. Studies on the scale-up of crossflow filtration devices. *FDA J. Pharm. Sci. Tech.* **50** 252-260.

Brown, D.E. and Kavanagh, P.R. **1987**. Crossflow separation of cells. *Process Biochem.* **22** 96-115

Brown, G.G., Foust, A.S., Katz, D.L., Schneidewind, R., Whitw, R.R., Wood, W.P., Brown, G.M., Brownell, L.E., Martin, J.J., Williams, G.B., Banchero, J.T. and York, J.L. **1950**. *Unit Operations*, John Wiley.

Brunner, K.H. **1985**. Whole broth solvent extraction. *Discovery-Isol. Microbial-Prod.* 182-194.

Buckland, B.C., Brix, T., Fastert, H., Gbewnonyo, K., Hunt, G. and Jain, D. **1985** Fermentation exhaust gas analysis using mass spectrometry. *Bio\Technology*. 982-988.

Bulmer, M. **1994**. Selective flocculation for the improved recovery of intracellular proteins from bacterial homogenates. Ph.D Thesis, UCL, U.K.

Bu'Lock, J.D. **1974**. Secondary metabolism of microorganisms. *In Industrial Aspects of Microorganisms*. **1** 335-345 Ed. by B. Spencer. Elsevier.

Bushell, M.E. **1983**. Microbiological aspects of the discovery of novel secondary metabolites. *In Topics in Enzyme and Fermentation Biotechnology*. **6** 32-67. Ed by A Wiseman. Blackie.

Bushell, M.E., Dunstan, G.L. and Wilson, G.C. **1997**. Effect of small scale culture vessel type on hyphal fragment size and erythromycin production in *Saccharopolyspora erythraea*. *Biotehnol. Lett.* **19** 849-852.

Cane, D.E., Luo, G., Khosla, C., Kao, C.M. and Katz, L. **1995**. Erythromycin biosynthesis: highly efficient incorporation of polyketide chain elongation

intermediates into 6-deoxyerythronolide B in an engineered *Streptomyces* host. *J. Antibiot.* **48** 647-651.

Caffrey, P., Bevitt, D.J., Staunton, J. and Leadley, P.F. **1992**. The identification of DEBS-1, DEBS-2 and DEBS-3, the multi-enzyme polypeptides of the erythromycin - producing synthase from *Saccharopolyspora erythraea. FEBS Lett.* **304** 39-49.

Carrere, H and Rene, F. **1996**. Industrial multi-stage continuous filtration process: influence of operating parameters. *J. Memb. Sci.* **110** 191-202.

Carrington, R. **1986**. A review of antibiotic isolation techniques. In: *Bioactive Microbial Products* **3** 45-58. Ed by Stowell, J.D., Bailey, P.J. and Winstanley, D.J. Academic Press. London.

Chandavarkar, A.S. and Cooney, C.L. **1989**. Dynamics of flux during microfiltration baused by protein-membrane interactions. *Abstr. Pap. Am. Chem. Soc. 198th Meeting*. MBTD 044.

Chartrain, M., Hunt, G., Horn, L., Kirpekar, A., Mathre, D., Powell, A., Wassel, L., Nielsen, J., Buckland, B. and Greasham, R. **1991**. Biochemical and physiological characterisation of the efrotomycin fermentation. *J. Indus. Micro.* **7** 293-300.

Cheryan, M. **1998**. Ultrafiltration and Microfiltration Handbook. *Technomic Publishing Inc. Pennsylvania, USA.* 113 – 170.

Cheryan, M., Veeranjaneyulu, B. and Schlicher, L.R. **1990**. Reverse-osmosis of milk with thin-film composite membranes. *J. Memb. Sci.* **48** 103-112.

Christy, C. **1998**. Pharmaceutical filtration design, applications and examples. *Lecture at UCL Department of Biochemical Engineering.*

Clark, G.J., Langley, D. and Bushell, M.E. **1995**. Oxygen limitation can induce microbial secondary metabolite formation: investigations with miniture electrodes in shaker and bioreactor culture. *Microbiology.* **141** 663-669.

Conrad, P.B. and Lee, S.S. **1998**. Two-phase bioconversion product recovery by microfiltration 1. Steady state studies. *Biotechnol. Bioeng.* **57** 631-641.

Cortes, J., Wiesmann, K.E.H., Robets, G.A., Brown, J.B., Staunton, J. and Leadley, P.F. **1995**. Repositioning of a domain in a modular polyketide synthase to promote specific chain cleavage. *Science* **268** pp. 1487-1489.

Da Costa, A.R., Fane, A.G., Fell, C.J.D. and Franken, A.C.M. **1991**. Optimal channel spacer design for ultrafiltration. *J. Memb. Sci.* **62** 275-291.

Cumming, I.W., Holdich, R.G. and Ismail, B. **1999**. Prediction of deposit depth and transmembrane pressure during crossflow microfiltration. *J. Memb. Sci.* **154**, 229-237.

Dahlgren, M.E., Powell, A.L., Herber, W.K., Maigetter, R.Z., Greasham, R.L. and George, H.A. **1991**. Development of scale-down techniques for investigation of recombinant *Escherichia coli* fermentations - acid metabolites in shake flasks and stirred vessels. *Biotechnol. Progress.* **9** 580-586.

Danash, H., Gardener, D.C.J. and Oliver, S.G. **1991**. Heritable damage to yeast caused by transformation. *Bio/Technol* **9** 179-182.

Davies, J.L., Baganz, F., Ison, A.P. and Lye, G.J. **2000**. Studies on the interaction of fermentation and microfiltration operations: erythromycin recovery from *Saccharopolyspora erythraea* fermentation broths. *Biotechnol. Bioeng.* **69** 429 - 439

Dittus, F.W. and Boetler, L.M.K. Heat transfer in automobile radiators of the tubular type. **1930**. *Publ. Eng.* **2** 443.

Donadio, S., Staver, M.J., McAlpine, J.B. and Swanson, S.J. **1991**. Modular organisation of genes required for complex polyketide biosynthesis. *Science* **252** 675-679.

Donadio, S., M^{c}Alpine, J.B., Sheldon, P.J., Jackson, M. and Katz, L. **1993**. An erythromycin analog produced by reprogramming of polyketide synthesis. *Proc. Natl. Acad. Sci. USA* **90**. 7119-7123.

Doran, P.M. **1995**. Bioprocess Engineering Principles. 1st Edition *Academic Press.*

Escalante, L., Lopez. H., Mateos, R.C., Lara, L. and Sanchez, S. **1982**. Transient repression of antibiotic formation in *Streptomyces erythreus. J. Gen. Microbiol.* **128** 2011-2015.

Flair, J.R. **1985**. Liquid-gas systems. In: *Perry's Chemical Engineers' Handbook.* Ed by: Perry, R.H. and Green, D. McGraw-Hill.

Fradin, B and Field, R.W. **1999**. Crossflow microfiltration of magnesium hydroxide suspensions: determination of critical fluxes, measurement and modelling of fouling. *Sep. Purif. Technol.* **16**, 25-45.

Freeman, A., Woodley, J.M. and Lilly M.D. **1993**. In situ product removal as a tool for bioprocessing. *Bio/Technology*. **11**, 1007-1012.

Gallagher, P.A. and Danielson, N.D. **1995**. Colorimetric determination of macrolide antibiotics using ferric ion. *Talanta* **42** 1425-1432.

Gardner, A., Gerber, R., Smith, C., McAllister, and Zabriskie, D. **1996**. Use of scale-down models in validation of cell culture processes for production of biopharmaceuticals. *Abstr. Pap. Am. Chem. Soc. 211th Meeting Pt. 1* BIOT 039.

Gehlert, G., Luque, S. and Belfort, G. **1998**. Comparison of ultra- and microfiltration in the presence and absence of secondary flow with polysaccharides, proteins and yeast suspensions. *Biotechnol. Prog.* **14** 931-942.

Gehrig, I., Bart, H.-T., Anke, T. and Gemerdonk, R. **1998.** Influence of morphology and rheology on the production characteristics of the Basidiomycete *Cyathus striatus*. *Biotechnol. Bioeng.* **59** 525-533.

Ghogomu, J.N., Guigui, C., Rouch, J.C., Clifton, M.J. and Aptel, P. **2001**. Hollow-fibre membrane module design: comparison of different curved geometries with Dean vortices. *J. Memb. Sci.* **181**. 71-80.

Goodfellow, M. and Cross, T. **1983**. Classification. In: *The Biology of Actinomycetes*. 7-131

Goodfellow, M., Williams, S.T. and Mordarski, M. **1983**. Introduction to and importance of actinomycetes. In: *The Biology of Actinomycetes*. 1-6.

Gravatt, D.P. and Molnar, T.E. **1986**. Recovery of an antibiotic by ultrafiltration. In: *Membrane Separations in Biotechnology*. **1**, 89-97. Ed by: McGregor, W.C. Dekker, New York.

Gregory, J. **1973**. Rates of flocculation of latex particles by cationic polymers. *J. Coll. Int. Sci. Vol.* **42** 448-492.

Gregory, J. **1976**. The effect of cationic polymers on the colloidal stability of latex particles. *J. Coll. Int. Sci.* **55** 35-44.

Guigui, C., Manno, P., Moulin, P., Clifton, M.J., Rouch, J.C., Aptel, P. and Laine, J.M. **1998**. The use of Dean vortices in coiled hollow-fibre ultrafiltration membranes for water and wastewater treatment. *Desalination*. **1998**. 73-79.

Gyure, D.C. **1992**. Set realistic goals for crossflow filtration. *Chem. Eng. Prog*. **88** 60-66.

Hammer, B.E., Heath, C.A., Mirer, S,D. and Belfort, G. **1990**. Quantitative flow measurement in bioreactors by nuclear magnetic resonance imaging. *Biotechnology*. **8** 327-330.

Hernandez-Pinzon, I. and Bautista, J. **1992**. Product concentration during tangential flow microfiltration. *Biotechnol. Tech*. **6** 511-516.

Hernandez-Pinzon, I., Millan, F. and Bautista, J. **1997**. Streptokinase recovery by CFMF: Study of enzyme denaturation. *Biosci. Biotech. Biochem*. **61** 1240-1243.

Heydarian, M.S., Mirjalili, N. and Ison, A.P. **1999**. Effect of shear on morphology and erythromycin production in *Saccharopolyspora erythraea* culture. *Bioprocess Eng.* **21**, 31-39.

Heydarian, S.M. **1998a**. The influence of agitation on morphology, rheology and erythromycin production in *Saccharopolyspora erythraea* culture. *PhD Thesis*, University College London.

Heydarian, S.M., Ison, A.P. and Mirjalili, N. **1998b**. A rapid and simplified extraction method of erythromycin from fermentation broth with bond elut C18 cartridge for analysis by HPLC. *Biotechnol. Tech.* **12** 155-158.

Heydarian, S.M., Lilly, M.D. and Ison, A.P. **1996**. The effect of culture conditions on the production of erythromycin by *Saccaropolyspora erythraea* in batch culture. *Biotechnol. Lett.* **18** 1181-1186.

Hong, S., Faibish, R.S. and Elimelech, M. **1997**. Kinetics of permeate flux decline in crossflow membrane filtration of colloidal suspensions. *J. Colloid Interface Sci.* **196** 267-277.

Junker, B., Mann, Z., Gailliot, P., Byrne, K. and Wilson, J. **1998**. Use of soybean oil and ammonium sulfate additions to optimise secondary metabolite production. *Biotechnol. Bioeng.* **60** 580-588.

Justen, P., Paul, G.C., Nienow, A.W. and Thomas, C.R. **1998**. Dependence of *Penicillium chrysogenum* growth, morphology, vacuolation and productivity in fed-batch fermentations on impeller type and agitation intensity. *Biotechnol. Bioeng.* **59**. 762-775.

Kao, C.M., Katz, L., and Khosla, C. **1994**. Engineered biosynthesis of a complete macrolactone in a heterologous host. *Science* **265** 509-512.

Karsheva, M., Hristov, J., Penchev, I. and Lossev, V. **1997**. Rheological behaviour of fermentation broths in antibiotic industry. *App. Biochem. Biotech.* **68** 187-206.

Kawakatsu, T, Nakao, S. and Kimura, S. **1993**. Effects of pore size and compressibility of suspended particles and surface pore size of membrane on flux in crossflow filtration. *J. Memb. Sci.* **81** 173-190.

Kluge, T., Rezende, C., Wood, D and Belfort, G. **1999**. Protein transmission during Dean vortex microfiltration of yeast suspensions. *Biotechnol. Bioeng.* **65** 649-658.

Kuenzi, M.T. **1980**. Regulation of cephalosporin synthesis in *Cephalosporium acremonium* by phosphate and glucose. *Arch. Microbiol.* **128** 78-83

Kitcherner, J.A., **1972**. Principles of action of polymeric flocculants. *Br. Polym. J.* **4** 217-229.

Knight, P. **1989**. Downstream processing. *Bio/Technology*. **7**, 780-782.

Kuriyel, R. **1993**. A methodology to calculate the scaling factors for ultrafiltration processes by the use of the osmotic model. *Abstr. Pap. Am. Chem. Soc. 205th Meeting Pt.1* BIOT 116.

Labeda, D.P. **1987**. Transfer of the type strain of *Streptomyces erythraeus* (Waksman 1923) Waksman and Henrici 1948 to the genus *Saccharopolyspora* Lacy and Goodfellow 1975 as *Saccharopolyspora erythraea* sp. nov., and

designation of a neotype strain for *Streptomyces erythraeus*. *I. J. System. Bac.* **37** 19-22.

Large, K.P, Ison, A.P. and Williams, D.J. **1998**. The effect of agitation rate on lipid utilisation and clavulanic acid production in *Streptomyces clavuligerus*. *J. Biotechnol.* **63** 111 – 119.

Larsson, A. **1974**. Various approaches to the separation process for harvesting the products of fermentation in the field of antibiotics. *Biotechnol. Bioeng. Symp. No. 4* 917-931.

Larsson, G. and Enfors, S.-O. **1985**. Influence of oxygen starvation on the respiratory capacity of *Pennicillium crysogenum*. *Appl. Microbiol. Biotechnol.* **21** 228-233.

Leadlay, P.F., Staunton, J, Aparicio, J.F., Brevitt, D.J., Caffrey, P, Cortes, J., Marsden, A. and Roberts, G.A.. **1993**. The erythromycin-producing polyketide synthase. *Biochem. Soc Trans.* **21**, pp. 218-221

Lee, S.S. and Buckland, B.C. **1995**. Microfiltration of recombinant yeast cells using a dynamic vibratory filtration system. *Abstr. Pap. Am. Chem. Soc. 209th Meeting Pt. 2* BTEC 128.

Lee, S.S., Buckland, B.C. and Cheung, C.K. **1996**. Microfiltration of recombinant yeast cells using a vibratory filtration system. *Abstr. Pap. Am. Chem. Soc. 211th Meeting Pt. 1* BIOT 170.

Li, G-Q., Qiu, H-W., Zheng, Z-M., Cai, Z-L. and Yang, S-Z. **1995.** Effect of fluid rheological properties on mass transfer in a bioreactor. *J. Chem. Tech. Biotechnol.* **62** 385-391.

Li, Q.Y., Cui, Z.F. and Pepper, D.S. **1997**. Fractionation of HSA and IgG by gas sparged ultrafiltration. *J. Memb. Sci.* **136** 181-190.

Liew, M.K.H., Fane, A.G. and Rogers, P.L. **1997**. Fouling of microfiltration membranes by broth-free antifoam agents. *Biotech. and Bioeng.* **56** 89-98.

Lilly, M.D., Ison, A. and Shamlou, P.A. **1992**. The influence of the physical environment in fermenters on antibiotic production by microorganisms. *Harnessing-Biotechnol. 21st Century*. 219-222.

Lindquist, G.M. and Stratton, R.A. **1976**. The role of polyelectrolyte charge density and molecular weight on the adsorption and flocculation of colloidal silica with polyethylenimine. *J. Coll. Int. Sci.* **55** 45-49.

Lindstrom, T. and Soremark, C. **1976**. Flocculation of cellulosic dispersions in the presence of divalent metal ions. *J. Coll. Int. Sci.* **55** 69-72.

Locci, R and Sharples, G.P. **1983**. Morphology. In: *The Biology of Actinomycetes*. 164-192.

Lohr, D., Buschulte, T. and Gilles, E. **1989**. Continuous cultivation of *Streptomyces tendae* in different media. *Appl. Microbiol. Biotechnol.* **32** 274-279.

Lu, W.M. and Ju, S.C. **1989**. Selective particle deposition in crossflow filtration. *Sep. Sci. Technol.* **24**.

Luque, S., Mallubhotla, H., Gehlert, G., Kuriyel, R., Dzengeleski, S., Pearl, S. and Belfort, G. **1999**. A new coiled hollow-fiber module design for enhanced microfiltration performance in biotechnology. *Biotechnol. Bioeng.* **65** 247-257.

Maibre, F., Audebert, R. and Quivoron, C. **1984**. Flocculation properties of some water soluble cationic copolymers towards silica suspensions: a semiquantitative interpretation of the role of molecular weight and cationicity through a 'patchwork' model. *J. Coll. Int. Sci.* **97** 120-136.

Mannweiler, K. **1990**. The recovery of biological particles in high speed centrifuges with special reference to feed zone break up effects. *UCL PhD Thesis.*

Mannweiler, K. and Hoare, M. **1992**. The scale down of an industrial disk stack centrifuge. *Bioprocess Eng.* **8** 19-25.

Martin, S.E. and Bushell, M.E. **1996**. Effect of hyphal micromorphology on bioreactor performance of antibiotic-producing *Saccharopolyspora erythraea* cultures. *Microbiology.* **1412** 1783-1788.

Martin, J. and Demain, A. **1980**. Control of antibiotic biosynthesis. *Microbiol. Rev.* **44** 230-251.

Matsumura, M., Imanaka, T., Yoshida, T. and Taguchi, H. **1978.** Effect of glucose and methionide consumption rates on cephalosporin C production by *Cephalosporium acremonium. J. Ferm. Tech.* **56** 345-353.

McDaniel, R., Khosla, E.S., Hopwood, D.A. and Khosla, C. **1995**. Rational design of aromatic polyketide natural products by recombinant assembly of enzymatic subunits. *Nature.* **375** 549-554.

Meindersma, G.W., Augeraud, J. and Vergossen, F.H.P. **1997**. Separation of a biocatalyst with ultrafiltration or filtration after bioconversion. *J. Memb. Sci.* **125** 333-349.

Metz, B., Kossen, N.W.F. and van Suijdam, J.C. **1979** Rheology of mould suspensions. *Advances in Biochemical Engineering.* **2** 103-156.

Meyer, F., Gehmlich, I., Gunthke, R., Gorak, A. and Knorre, W.A. **1998**. Analysis and simulation of complex interactions during dynamic microfiltration of *Escherichia coli* suspensions. *Biotech. Bioeng.* **59** 189-202.

Mirjalili, N., Zormpaidis, V., Leadley, P.F. and Ison, A.P. **1999**. The effect of rape seed oil uptake on the production of erythromycin and triketide lactone by *Saccharopolyspora erythraea.* Biotechnol. Progress. **15** 911-918.

Murrell, N.J. **1998**. Engineering study of the recovery of shear sensitive biological materials by high speed disk stack centrifuge. *UCL PhD Thesis.*

Nagata, N., Herouvis, K.J., Dziewulski, D.M. and Belfort, G. **1989**. Crossflow membrane microfiltration of a bacterial fermentation broth. *Biotechnol. Bioeng.* **34.**

Nakanishi, K., Tadokoro, T. and Matsuno, R. **1987**. On the specific resistance of cakes of micro-organisms. *Chem. Eng. Comm.* **62** 187-201.

Narendranathan, T.J. and Dunnill, P. **1982**. The effect of shear on globular protein during ultrafiltration: Studies of alcohol dehydrogenase. *Biotechnol. Bioeng.* **24** 2103-2107.

Neusil, J. and Hostalek, Z. **1986**. Enzymes of secondary metabolism and the biosynthesis of macrolide antibiotics. *Folia. Microbiol.* **31**. 402-421.

Okamoto, Y., Ohmori, K. and Glatz, C.E. **2001**. Harvest time effects on membrane cake resistance of *Escherichia coli* broth. *J. Memb. Sci.* **190**, 93-106.

Okec, R. **1998**. Model development and simulation of membrane separation systems for the recovery of intracellular protein products from crude biological feedstock. Ph.D Thesis, UCL, U.K.

Oosterhuis, N.M.G. **1983**. Scale-up of bioreactors. *Process Biochem. Suppl. Proc. Conf. Adv. Ferment.* 191-201.

Oosterhuis, N.M.G., Kossen, N.W.F., Olivier, A.P.C. and Schenk, E.S. **1985**. Scale-down and optimisation studies of the gluconic acid fermentation by *Gluconobacter oxydans. Biotechnol. Bioeng.* **27** 711-720.

Ozbek, B. **1997**. Mathematical modeling and simulation studies of scale-down fermentation systems. *Chem. Eng. Technol.* **20** 259-267.

Packer, H.L. and Thomas, C.R. **1990**. Morphological measurements on filamentous micro-organisms by fully automatic image analysis. *Biotech. Bioeng.* **35** 729-742.

Palceck, S.P. and Zydney, A.L. **1994**. Intermolecular electrostatic interactions and their effect on flux and protein deposition during protein filtration. *Biotechnol. Prog.* **10** 207-213.

Paul, G.C. and Thomas, C.R. **1998**. Characterisation of mycelial morphology using image analysis. *Adv. Biochem. Eng. Biotech.* **60** 1-59.

Pickup, K.M., Nolan, R.D. and Bushell, M.E. **1993**. A method for increasing the success rate of duplicating antibiotic activity in agar and liquid culture of *Streptomyces* isolates in new antibiotic screens. *J. Ferm. Bioeng.* **76** 89-93.

Pons, M.N., Drouin, J.F., Louvel, L., Vanhoutte, B., Vivier, H. and Germain, P. **1998**. Physiological investigations by image analysis. *J. Biotechnol.* **65** 3-14.

Porter, M.C. **1972**. Concentration Polarization with membrane ultrafiltration. *Ind. Eng. Chem. Prod. Res. Develop.* **11** 234-248.

Prosser, J.I. and Tough, A.J. **1991**. Growth mechanisms and growth kinetics of filamentous microorganisms. *Crit. Rev. Biotechnol.* **10** 253-274.

Postlethwaite, J. **1999**. Scale-down of Pallsep dynamic microfiltration systems. *MSc. Thesis* University College London.

Queener, S.W. and Day, L.E. **1986** The Bacteria: A Treatise on Structure and Function: Antibiotic producing *Streptomyces.* Academic Press: New York, New York. Vol. 9 p xviii.

Reid, J.L., Rubin, P.C. and Whiting, B. **1992**. Lecture notes on clinical pharmacology. 4th Ed. *Blackwell Scientific Publications.* 108-131.

van Reis, R., Goodrich, E.M., Yson, C.L., Frautschy, L.N., Dzengeleski, S. and Lutz, H. **1997a**. Linear scale ultrafiltration. *Biotechnol. Bioeng.* **55** 737-746.

van Reis, R., Gadam, S., Frautschy, L.N., Orlando, S., Goodrich, E.M., Saksena, S., Kuriyel, R., Simpson, C.M., Pearl, S. and Zydney, A.L. **1997b**. High performance tangential flow filtration. *Biotechnol. Bioeng.* **56** 71-82.

Reismeier, B., Kroner, K.H. and Kula, M.R. **1989**. Tangential-flow filtration of microorganism cell suspension, mathematical model. *J. Biotechnol.* **12** 153-172.

Reuss, M. **1988**. Influence of mechanical stress on the growth of *Rhizopus nigricans* in stirred bioreactors. *Chem. Eng. Technol.* **11** 178-187.

Reuss, M., Debus, D. and Zoll, G. **1982**. *Biochem. Eng.* **83** 233-236.

de-los-Reyes, G. **1990**. Scale-up considerations for tangential flow filtration processes. *J. Cell. Ciochem. Suppl. 14D.*

Riviere, J. **1977**. Industrial applications of microbiology. *Thomson Litho Ltd.* Translated by Moss, M.O. and Smith, J.E. 197-218.

Roels, J.A., Van den Berg, J. and Voncken, R.M. **1974**. The rheology of mycelial broths. *Biotech.Bioeng.* **16** 181-208.

Roth, M., Noack, D. and Reinhardt, G. **1982**. Properties of non-differentiating derivatives of *Streptomyces hygroscopicus*. *J. Gen. Microbiology*. **128** 2687-2691.

Russotti, G, Gokken, K.E. and Wilson, J.J. **1995a**. Development of a pilot-scale microfiltration for the isolation of physostigimine from *Streptomyces grisefuscus* broth. *J. Chem. Technol. Biotechnol.* **63** 37-47.

Russotti, G., Osawa, A.E., Sitrin, R.D., Buckland, B.C., Adams, W.R. and Lee, S.S. **1995b**. Pilot-scale harvest of recombinant yeast employing microfiltration: a case study. *J. Biotechnol.* **42** 235-246.

Sarra, M., Ison, A.P. and Lilly, M.D. **1996**. The relationships between biomass concentration, determined by a capacitance-based probe, rheology and morphology of *Saccharopolyspora erythraea* cultures. *J. Biotech.* **51** 157-165.

Sato, M., Watari, J., Sahara, H. and Kashino, S. **1994**. Instability in electrophoretic karyotype of brewing yeast. *J. Am. Soc. Brew. Chem.* **52** 148-151.

Schafer, A.I., Schwicker, U., Fischer, M.M., Fane, A.G. and Waite, T.D. **2000**. Microfiltration of colloids and natural organic matter. *J. Memb. Sci.* **171** 151-172.

Shapiro, S. and Vinning, L.C. **1983**. Nitrogen metabolism and chloramphenicol production in *Streptomyces venezuelae. Can. J. Microbiol.* **29** 1706-1714.

Shimizu, Y. Uryu, K., Okuno, Y.-I., Ohtubo, S. and Watanabe, A. **1997**. Effect of particle size distributions of activated sludges on cross-flow microfiltration flux for submerged membranes. *J. Ferment. Bioeng.* **83** 583-589.

Shomura, T., Yoshida, J., Amani, S., Kojima, M., Inouye, S. and Niida, T. **1979**. Studies on *Actinomycetales* producing antibiotics only on agar culture. 1. Screening, taxonomy and morphology-productivity relationship of *Streptomyces halstedii* strain Sf-1993. *Journal of Antibiotics.* **32** 427-435.

Shuler, M.L. **1987**. Bioprocess engineering. In: *Encyclopaedia of Physical Science and Technology Vol.2* . Ed by: Meyers, R.A. Academic Press.

Stanier, R.Y., Ingrham, J.L., Wheelis, M.L. and Painter, P.R. **1987**. General Microbilogy. *Macmillan Education Ltd.* 5th Ed. 505-519.

Stowell, J.D. **1987**. The application of oils and fats in antibiotic processes. In: Carbon substrates in biotechnology. Ed. Stowell, J.D. IRL Press 139-159.

Summers, R.G., Ali, A., Shen, B., Wessel, W.A. and Hutchinson, C.R. **1995**. Malonyl coenzyme A: acyl carrier protein acyltransferase of *Streptomyces glaucescens*: a possible link between fatty acid and polyketide biosynthesis. *Biochemistry*. **34**. 9389-9402.

Sweere, A.P.J., van Dalen, J.P., Kishoni, E., Luyben, K.C.A.M., Kossen, N.W.F. and Renger, R.S. **1988**. Theoretical analysis of the baker's yeast production: An experimental verification, liquid mixing, mass transfer, applyed to scale-up. *Bioprocess Eng*. **3** 165-171.

Tada, S., Oshima, S. and Yamane, R. **1996**. Classification of pulsating flow patterns in curved pipes. *J. Biomech Eng*. **118** 311-317.

Tanaka, T, Abe, K., Asakawa, H., Yoshida, H. and Nakanishi, K. **1994**. Filtration characteristics and structure of cake in crossflow filtration of bacterial suspension. *J. Ferment. Bioeng*.**78**.

Taniguchi, M. Kotani, N. and Kobayashi, T. **1987**. High concentration cultivation of lactic acid bacteria in fermenters with crossflow filtration. *J. Ferment. Technology*. **65** 179-184.

Tarleton, E.S. and Wakeman, R.J. **1994**. Understanding flux decline in crossflow microfiltration: Part II. Effects of process parameters. *Trans. IChemE. Part A* **72**.

Tiller, C.L. and O'Melia, C.R. **1993**. Natural organic matter and colloidal stability: models and measurement. *Colloids and Surfaces A: Physiochem. and Eng. Aspects*. **73** 89-102.

Todd, W.J. and Podbielniak, D.B. **1965**. Centrifugal extraction. *Chem. Eng. Progress*. **61** 69.

Tracy, E.M. and Davis, R.H. **1994**. Protein fouling of track-etched polycarbonate microfiltration membranes. *J. Colloid Interface Sci*. **167** 104-116.

Treskatis, S.K., Orgeldinger, V., Wolf, H. and Gilles, E.D. **1997**. Morphological characterisation of filamentous microorganisms in submerged cultures by on-line digital image analysis and pattern recognition. *Biotech and Bioeng*. **53** 191-201.

Trilli, A., Crossley, M.V. and Kontakou, M. **1987** Relation between growth rate and erythromycin production in *Streptomyces erythraeus*. *Biotechnology Letters* **9** 765-770.

Turker, M. and Hubble, J. **1987**. Membrane fouling in a constant flux ultrafiltration cell. *J. Membrane Sci*. **34** 267-281.

Tutunjian, R.S. **1986**. Cell separations with hollow fibre membranes. In: *Comprehensive Biotechnology* **2** 383-409. Ed by: Cooney, C.L. and Humphrey, A.

Vargas-Mora, V. **1997**. Extraction kinetics of erythromycin from whole fermentation broths. *MSc. Thesis* University College London.

Vickroy, T.B., de-Vries, R.L. and Zabriskie, D.W. **1996**. Optimisation of cell culture process development for biopharmaceuticals. *Abstr. Pap. Am. Chem. Soc. 211th Meeting Pt. 1*, BIOT 042.

Wakil, S.J. **1989**. Fatty acid synthase a proficient multi-functional enzyme. *Biochemistry* **28** pp. 4523-4530.

Wallace, K.K., Payne, G.F. and Speedie, M. K. **1992**. *Streptomyces* Bioprocessing: From Secondary Metabolites to Heterologous Proteins. *Frontiers: Bioprocessing II.* 168-180.

Warren, S.J., Keshevarz-Moore, E., Shamlou, P.A. and Lilly, M.D. **1995**. Rheologies and morphologies of three actinomycetes in submerged culture. *Biotech. Bioeng.* **45** 80-85.

Wilde, P.F. and Dexter, R.W. **1972**. Parameters affecting the performance of polyelectrolytes as aids to water clarification. *Br. Polym. J.* **4** 239-250.

Zhang, M. and Song, L. **2000**. Mechanisms and parameters affecting flux decline in crossflow microfiltration and ultrafiltration of colloids. *Environ. Sci. Technol.* **34**, 3767-3773.

Zeman, L.J. and Zydney, A.L. **1996**. Microfiltration and ultrafiltration: principles and applications. *Marcel Dekker Inc.* N.Y.

Appendix I: Calculations

I.1 Reducing Sugar (DNS) Assay Calibration Curve

Figure I.1 is a typical example of a calibration curve for the DNS reducing sugar assay. The assay mixture is calibrated against known concentrations of glucose, from which the glucose concentration of fermentation broth can then be determined.

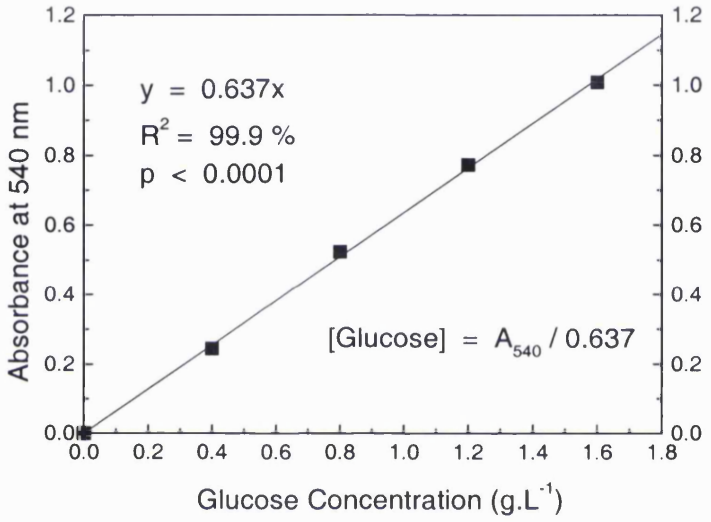

Figure I.1. Example of a typical calibration curve for the DNS reducing sugar assay, as described in Section 2.2.3.1.

I.2 Total Soluble Protein (Bradford) Assay

Figure I.1 is a typical example of a calibration curve for the Coomassie blue protein assay. The assay mixture is calibrated against known concentrations of protein (bovine serum albumin), from which the protein concentration of fermentation broth can then be determined.

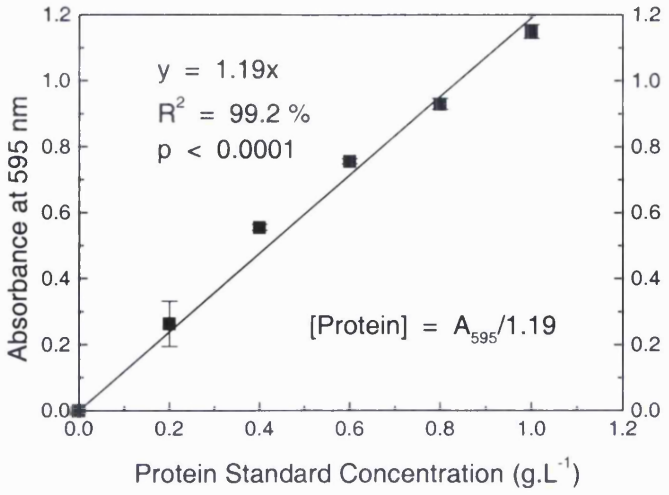

Figure I.2. Example of a typical calibration curve for the Coomassie blue protein assay, as described in Section 2.3.3.1.

I.3 Erythromycin Transmission Assay

Figure I.3 is a typical example of a calibration curve for the erythromycin assay. The assay mixture is calibrated against known concentrations of erythromycin, from which the erythromycin concentration of the broth can then be determined.

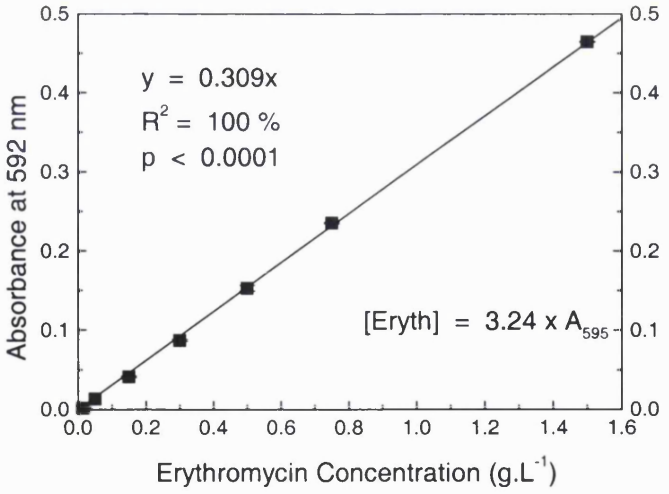

Figure I.3. Example of a typical calibration curve for the erythromycin concentration assay, as described in Section 2.3.3.2.

I.4 Energy Dissipation Rate Calculation

Both fermenters used three, six-bladed Rushton turbine impellers. For the purposes of the calculation the bottom impeller is assumed to be under aeration and the top two impellers are considered to be un-gassed. The gas power was based on the Michel and Miller correlation. Reynolds number (Re) was obtained using:

$$\mathrm{Re} = \frac{\rho N D_i^2}{\mu_a} \qquad [I.1]$$

where ρ is the density of the broth, assumed to be 1000 $kg.m^{-3}$, N is the impeller speed (s^{-1}), D_i is the impeller diameter (m) and μ_a is the apparent viscosity of the broth(Pa.s), calculated by:

$$\mu_a = K(k_s N)^{n-1} \qquad [I.2]$$

where K is the consistency index, n is the flow behaviour index (both dimentionless and derived experimentally as described in Section 2.3.3.3), N is the impeller speed (s^{-1}) and k_s is the impeller shear rate constant, assumed to be 11.4. The power number (N_p) was determined as described by the Reynolds number correlation and the un-gassed power dissipation was calculated using:

$$P_o = \frac{N_p}{\rho N^3 D_i^5} \qquad [I.3]$$

This was then used to calculate the gassed power (P_g):

$$P_g = 0.756\left(\frac{P_o^2 N D_i^3}{Q_g^{0.56}}\right) \qquad [I.4]$$

where Q_g is the gas flow rate ($m^3.s^{-1}$), the total power dissipation (P) is therefore given as:

$$P = P_g + P_o + P_o \qquad [I.6]$$

I.5 Circulation Time Calculation

Circulation time (t_c) was calculated from the method used by Reuss (1988), with the equation:

$$t_c = \frac{0.76\left(\frac{H_L}{T}\right)^{0.6}\left(\frac{T}{D_i}\right)^{2.7}}{N} \qquad [I.7]$$

where H_L is the liquid height in the fermenter (m), T is the diameter of the fermenter, D_I is the impeller diameter.

I.6 K_p Calculation

The K_p value was calculated from experimental values of steady state permeate flux (measured in $m.s^{-1}$) by rearranging Equation [6.1] to:

$$k = \frac{J}{\ln\left(\frac{C_w}{C_b}\right)} \qquad [I.1]$$

where: C_w is the percentage concentration of solids at the membrane surface (w/v), which is assumed to be 70 %. C_b is the percentage concentration of solids in the feed stream. This value of the mass transfer coefficient k, was then used to determine K_p by rearranging Equation [6.5] to:

$$K_p = k\left(\frac{bwL}{Q}\right)^{0.15} \frac{\left(\frac{K\gamma^{n-1}}{\rho}\right)^{0.17}}{D^{0.66}} \qquad [I.2]$$

where b is the membrane module height (3.54 10^{-4} m), w is it's width (0.0572 m) and L is the flow path length (0.111 m with one membrane sheet and 0.222 with two). K is the apparent viscosity Power law consistency index and n is the flow behaviour index (both dimentionless), ρ is the density, assumed to be 1000 $kg.m^{-3}$, D is the diffusion coefficient, assumed to be 3.5 x 10^{-10} $m.s^{-1}$.

Appendix II: Membrane Design

II.1 Introduction to Membrane Design

Tangential flow filtration has long been established as a viable alternative to existing rotary drum vacuum filtration and other dead-end filtration techniques (Gravatt and Molnar 1986; Tutunjian 1986; Meindersma *et al.* 1997). Membranes for TFF are expensive and must therefore offer considerable performance improvement to make them commercially viable. New techniques have been developed in order to improve permeate flow rates, such as dynamic membranes where the shear necessary to reduce fouling and gel layer formation comes from moving the membrane past the feed stream by vibration (Lee and Buckland, 1995), or rotation (Lee *et al.*, 1996). Charged membranes which separate not only on the basis of size, but also electrostatic forces (Palecek and Zydney, 1994) have also been developed as techniques for altering the flow of the liquid past the membrane in such a way as to minimise gel layer formation and fouling. The best example of the latter being the creation of Dean vortices in the membrane module (Hammer *et al.* 1990; Tada *et al.* 1996; Ghogomu *et al.* 2001).

Dynamic membranes suffer from the disadvantages of moving parts where containment is an issue leading to wear, increased heating through power input and safety issues in the event of failure. Dynamic membranes can also impart very high shear rates to the process, thus damaging shear sensitive cells and contaminating broths with intracellular components that can add to the gel layer thus decreasing flux, or increasing the loading on processes downstream of the microfiltration step. Calculation of the shear forces operating inside the system is also difficult and highly complex. Hydrostatic membranes can only be used in

systems where using the differences between charges within the feed stream are beneficial.

Dean vortices have been shown to improve TFF process efficiency in a number of different applications, such as poly-saccharide ultrafiltration and protein transmission during yeast microfiltration (Gehlert *et al.* 1998; Kluge *et al.* 1999; Luque *et al.* 1999). In *Saccharopolyspora erythraea* fermentations, for the recovery of erythromycin, media can be highly complex with up to 3 separate phases of components. Industrial scale media contain undissolved soya bean flour as a complex source of nutrients, rape seed oil as the primary carbon source and aqueous salts as complex sources of trace nutrients. Combined with the mycelial nature of the organism the harvest point (maximum erythromycin concentration) is associated with the beginning of death phase and the release of intracellular components (Heydarian, 1998b), leads to a highly viscous broth which is a challenge for any filtration system. The size and mycelial structure means that the cells are very susceptible to shear damage. Therefore high shear systems would lead to the rapid destruction of the cell walls and associated release of protein, ribonucleic acids and cellular apparatus capable of passing through a microfiltration membrane and causing a chemical and colloidal load on subsequent downstream processes.

In this work two fundamentally different media were investigated to demonstrate the effect of the differences using the existing flat sheet process and the enhanced flow device (EFD), an experimental spirally wound hollow fibre membrane module of 125 cm^2 with 0.1 μm pore size Durapore membrane from Millipore which was

run in concentration mode using the Proflux M-12 TFF rig as described in Section 2.3.2.1. This was compared to a flat sheet system, the Minitan II acrylic membrane holder, fitted with one 60 cm^2 durapore membrane of 0.2 μm pore size as described in Section 2.3.1.1.

II.2 Effect of Membrane Design

II.2.1 Microfiltration and SCM Broths

Table II.1 gives details of the broth used in the EFD at the two sample times, that of maximum biomass concentration and again at maximum erythromycin concentration. It has been recorded previously in a number of studies that secondary metabolite production, such as that of erythromycin, reaches a peak after the cessation of growth (Wallace *et al.* 1992; Larsson and Enfors 1985; Riveriere 1987). Biomass and apparent viscosity (at a shear rate of 71 s^{-1}) decrease after growth stops from 10.63 to 9.62 $g.L^{-1}$ and 0.01808 to 0.1111 Pa.s respectively. The soluble protein concentration doubled from 0.38 $g.L^{-1}$ to 0.73 $g.L^{-1}$ as cellular degradation releases proteins into the extracellular aqueous phase of the broth. Erythromycin concentration increased from 0.12 to 0.16 $g.L^{-1}$.

As can be seen from Figure II.1 A at the point of maximum biomass concentration i.e. when the solids loading is highest, (typically 35 to 40 hours after inoculation) the EFD produces steady state permeate fluxes of approximately 220 $L.m^{-2}.h^{-1}$ compared to 30 to 40 $L.m^{-2}.h^{-1}$ observed using the flat sheet membrane, an improvement of over 600 %. Figure II.1 B and C show the transmission of protein and erythromycin across the membrane at maximum biomass, which do not show a significant difference between the two membrane modules for product transmission

(Minitan – 97.3 %, EFD – 95.6 %; p = 0.324). Protein transmission is statistically lower for the EFD (Minitan – 54.6 %, EFD – 45.7 %, p = 0.028) although the sample size is small. This conveys the additional advantage to the process in that fewer contaminants are passed downstream to the next unit operation.

	Sample at maximum biomass conc. (t = 40h)	**Sample at maximum eryth. conc. (t = 65h)**
Biomass Concentration ($g.L^{-1}$)	10.63±0.27	9.42±0.17
Protein Concentration ($g.L^{-1}$)	0.38±0.03	0.73±0.03
Erythromycin Concentration ($g.L^{-1}$)	0.12±0.01	0.16±0.01
Apparent Viscosity at 100 s^{-1} (Pa.s)	0.01808	0.01111

Table II.1 Composition and rheology of SCM fermentation broths at two time points, samples were taken at the point of maximum biomass and at maximum erythromycin concentration. Fermentations and MF were carried out as described in Sections 2.2.2.3 and 2.3.2.1 respectively.

At the point during the fermentation of maximum erythromycin concentration, 20 to 25 hours after maximum biomass, the experiments were repeated to represent the conditions that would be observed at the normal point of harvest. Figure II.2 A shows the permeate flow rates observed from the EFD and flat sheet membranes. The flux seen using the Minitan has remained approximately the same at between 30 and 40 $L.m^{-2}.h^{-1}$ whereas for the EFD the flux has decreased nearly two fold to between 120 and 130 $L.m^{-2}.h^{-1}$, but still shows an improvement of over 300 % compared to the flat sheet system. Whilst some of the fermentation characteristics between the two time points have become more favourable to microfiltration such as the reduction in solids loading and the reduced viscosity (see Table 4.2), the cell lysis that has produced these effects also releases intracellular components into the broth. This is demonstrated by the increased extracellular soluble protein at 60 hours.

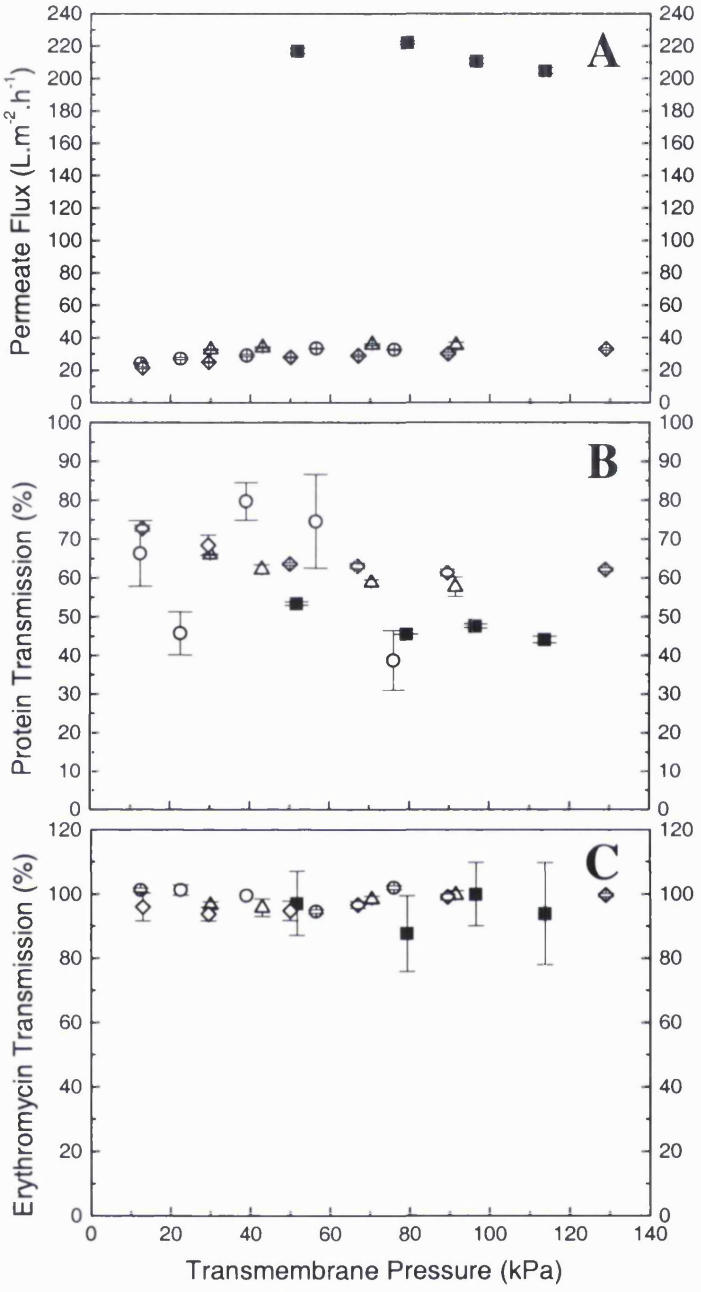

Figure II.1. Performance of flat sheet and EFD membrane modules showing steady state permeate flux (A), protein transmission (B) and erythromycin transmission (C), comparison for the SCM fermentation at maximum biomass concentration in the EFD - ■, and three runs in the Minitan using comparable broth, SCM20L1 - ○, SCM20L2 - △ and SCM20L3 - ◇. Fermentations and MF were carried out as described in Sections 2.2.2.3 and 2.3.2.1 respectively.

The protein, ribonucleic acids and cellular fragments have a deleterious effect on the EFD membrane by promoting gel layer formation at the membrane surface. This appears to have had a greater effect on the EFD, demonstrated by the reduction permeate flux between time points, whilst the flux through the flat sheet membrane was unaffected. These results are summarised and compared to data from the Minitan II flat sheet membrane module in Table II.2. Values for the Minitan are averaged over the fermentations SCM20L1, 2 and 3 with standard deviations calculated from the 3 fementations. EFD values are calculated from the mean and standard deviations of triplicate measurements; as described in Sections 2.2 and 2.3.

	Sample at maximum biomass conc. (t = 40h)		**Sample at maximum eryth conc. (t = 65h)**	
	Minitan	**EFD**	**Minitan**	**EFD**
Feed stream biomass conc. ($g.L^{-1}$)	11.71±0.42	10.63±0.27	10.68±0.13	9.42±0.17
Feed stream protein conc. ($g.L^{-1}$)	0.372±0.167	0.383±0.026	0.781±0.166	0.733±0.033
Mean Flux ($L.m^{-2}.h^{-1}$)	33.97±1.51	222.0±1.0	35.87±7.66	127.7±6.0

Table II.2. Comparison of Minitan and EFD values for biomass concentration, protein concentration and mean steady state permeate flux rates at the critical TMP at the time of maximum biomass and maximum product concentration.

There is no significant change in permeate flux in the flat sheet membranes for a 10 % difference in solids concentration and 110 % increase in protein concentration has no effect. Conversely the drop of over 40 % in permeate flux in the EFD membrane is a significant change with only a 12 % decrease in biomass, but a 90 % increase in total soluble protein concentration. It is possible that suspended particulate matter in the form of biomass is a limiting factor in the Minitan II flat sheet membrane system and surface fouling by the solid phase of the broth is

important to the hydrodynamic resistance to permeate flux. In contrast the EFD, when the biomass concentration in the broth is at a maximum value, the flux is greater than when there is a high concentration of lysed intracelluler components, suggesting that the gel layer formed by these compounds exhibits greater resistance to flow than the suspended solids.

Figure II.2 B gives the protein transmission at the point of maximum erythromycin concentration. The data follows the trend and magnitude of that of the Minitan, transmission decreases with increasing TMP, due to the build up of the gel layer at increased pressure. The transmission is also lower than that seen at the time of maximum biomass concentration, it is possible that this is due to increased protein concentration in the aqueous phase at 60 hours causing an increased gel layer depth which causes rejection of protein at the membrane surface. Erythromycin transmission, shown in Figure II.2 C is again, similar between the two devices and is unaffected by TMP.

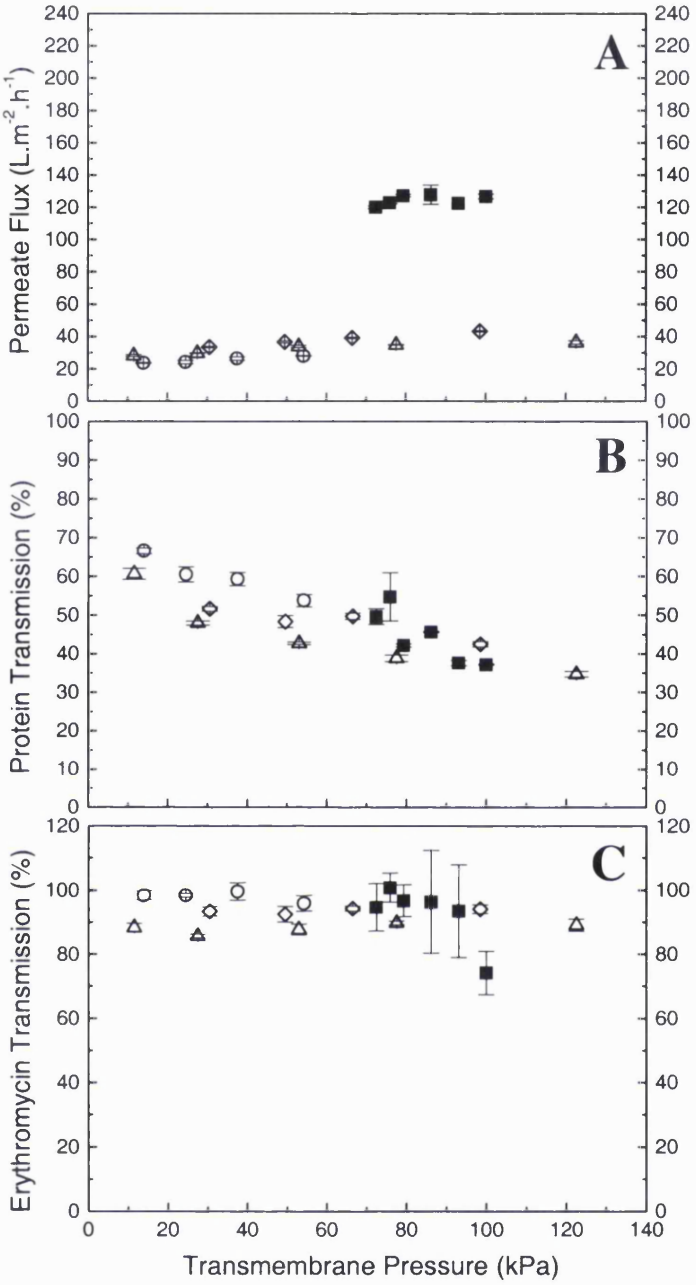

Figure II.2. Performance of flat sheet and EFD membrane modules showing steady state permeate flux (A), protein transmission (B) and erythromycin transmission (C), comparison for the SCM fermentation at maximum erythromycin concentration in the EFD - ■, and three runs in the Minitan using comparable broth, SCM20L1 - ○, SCM20L2 - △ and SCM20L3 - ◇. Fermentations and MF were carried out as described in Sections 2.2.2.3 and 2.3.2.1 respectively.

II.2.1.1 The Effect of Transmembrane Pressure

The relationship between the change in TMP and the percentage change in steady state flux was examined in the enhanced flow device to test the validity of the TMP adjustment model (as described in Section 4.2.2.1) to membranes of fundamentally different design. As can be seen from Figure II.3 there is a good correlation between the measured flux and the flux predicted by measuring permeate flux at low values of TMP and applying Equation [4.2].

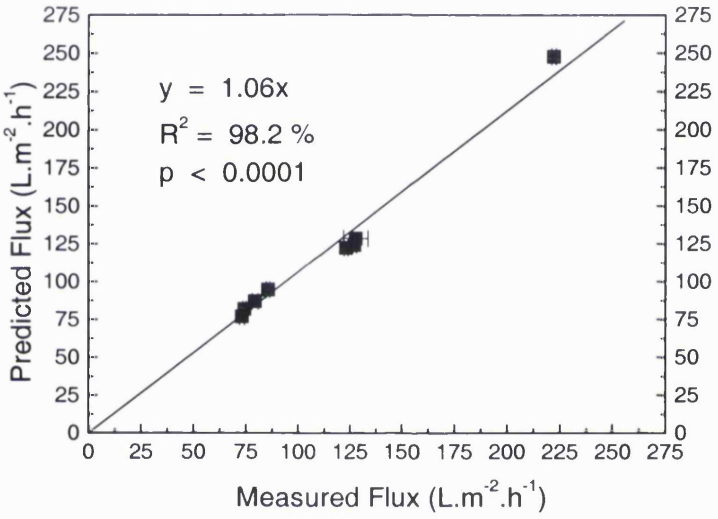

Figure II.3. The correlation between TMP increase and the percentage increase in steady state permeate flux as described by Equation [6.5].

II.2.2 Microfiltration of OBM Broths

Figure II.4 shows the comparison between the EFD and flat sheet membrane modules using a more typical industrial medium. It uses rape seed oil as the carbon source and soya bean flour as a complex source of nitrogen and other nutrients. A large proportion of the flour remains in the solid phase and residual oil is always present throughout the fermentation (Davies *et al.* 2000). The broth presents a

challenge for filtration systems due to its high viscosity and solid loading. The flat sheet membrane provides permeate flow rates of between 10 and 20 $L.m^{-2}.h^{-1}$ and the EFD of 70 to 85 $L.m^{-2}.h^{-1}$, an improvement of over 500 %. Unlike the SCM, the oil based medium showed a different trend in the EFD, improvements in permeate flux with increasing TMP were observed. In the Minitan the pressure dependant region of the process was passed at very low values of TMP, and in both devices in SCM. In the OBM broth flux increased from 71 $L.m^{-2}.h^{-1}$ to 85 $L.m^{-2}.h^{-1}$ over a pressure increase of 62 kPa

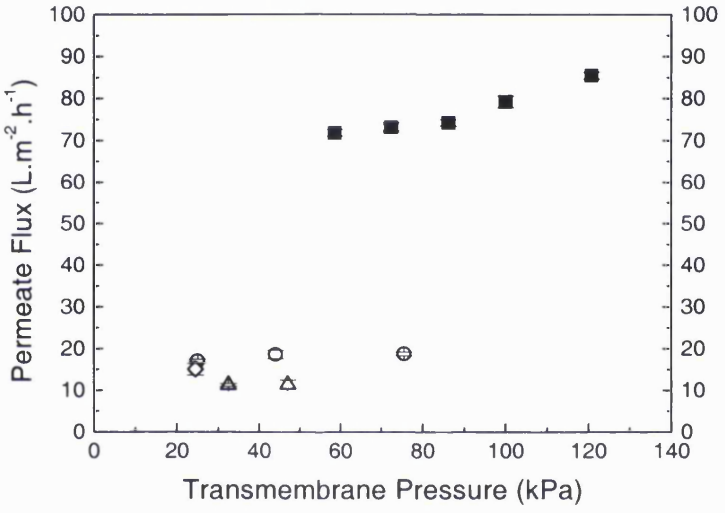

Figure II.4 Performance of flat sheet and EFD membrane modules showing steady state permeate flux comparison for the OBM fermentation for the EFD (OBM20L6) - ■, and three runs in the Minitan using comparable broth, OBM20L1 - ○, OBM20L2 - △ and OBM20L3 - ◊. Fermentations and MF were carried out as described in Sections 2.2.2.3 and 2.3.2.1 respectively.

II.3 Summary of Membrane Design

The enhanced flow device gives between 350 and 650 % increase in flux performance over the Minitan flat sheet membrane module. The improved

performance depends on the time and composition of the fermentation broth. Protein and erythromycin transmission are unaffected by the different membrane configurations. Improvements in performance are seen in two different types of media for the growth of *S erythraea.* The superior permeate flux combined with unaltered process complications warrants the further study of Dean vortex forming devices.